DYNAMIC SIMULATION OF AN INDIRECT PARTIAL OXIDATION REACTOR FOR METHANE CONVERSION TO HYDROGEN

by

Mustafa Karakaya

B.S., Chemical Engineering, Boğaziçi University, 2003

Submitted to the Institute for Graduate Studies in
Science and Engineering in partial fulfillment of
the requirements for the degree of
Master of Science

Graduate Program in Chemical Engineering
Boğaziçi University

2006

DYNAMIC SIMULATION OF AN INDIRECT PARTIAL OXIDATION REACTOR FOR METHANE CONVERSION TO HYDROGEN

APPROVED BY:

Prof. Zeynep İlsen Önsan ……………………
(Thesis Supervisor)

Assoc. Prof. Ahmet Erhan Aksoylu ……………………
(Thesis Co–Supervisor)

Asst. Prof. Ahmet Kerim Avcı ……………………

Asst. Prof. Hasan Bedir ……………………

Prof. Mehmet C. Çamurdan ……………………

DATE OF APPROVAL: ………………………

dedicated to my family,
grandmother
and Katja

ACKNOWLEDGEMENTS

I would like to express my gratitude to my supervisors, Professor Zeynep İlsen Önsan and Associate Professor Ahmet Erhan Aksoylu, whose expertise, understanding and patience added greatly to my graduate experience. It was under their tutelage that I developed a focus and became interested in catalysis. I would like to thank both of them for the assistance and “occupational therapy” they provided at all levels in the course of the project. Each of them became more of a friend or a mentor, than a professor. Not even these few paragraphs would have come to life had I not the luck to work with them.

A very special thanks goes out to Assistant Professor Ahmet Kerim Avcı, or whom I am used to calling “Ahmet Abi”, for his suggestions on the framework of the project and devoting his leisure time to seeking answers to my never–ending questions. I must also acknowledge Associate Professor Ramazan Yıldırım for his everlasting help and encouragement. I would like to thank my roomie Erdem Günay, M.S., for his friendship and for providing remote assistance.

I am incapable of giving coherent, clear, or effective expressions to my feelings about my family. All I can say is that I am greatly indebted to these patient people for the support they provided me through my entire life. And a short note to my grandmother: Rest in peace; may the eternal and celestial serenity find you...

How you are going to respond to this, my dear Katja, I do not know; you might wag your tail or whine with sorrow, but I am sure of one thing: You and I are one and a whole!

In conclusion, I recognize that this research would not have been possible without the financial support provided by TÜBİTAK–MAG (Türkiye Bilimsel ve Teknolojik Araştırma Kurumu – Mühendislik Araştırma Grubu) through project **104M163** and Boğaziçi University Research Fund through project **DPT–03K120250**.

ABSTRACT

DYNAMIC SIMULATION OF AN INDIRECT PARTIAL OXIDATION REACTOR FOR METHANE CONVERSION TO HYDROGEN

The steady and dynamic behavior of a catalytic indirect partial oxidation (combined total oxidation/steam reforming) reactor for the conversion of methane to hydrogen is investigated using computer–based modeling/simulation techniques. A one–dimensional pseudohomogeneous reactor model is employed for the description of autothermal conversion of methane over a physical mixture of Pt/δ–Al_2O_3 and Ni/MgO–Al_2O_3 catalysts. Steady–state and dynamic simulation of the bench–scale reactor is carried out for a set of different feed conditions. Transients during the start–up of the autothermal reforming process are analyzed, and the steady values of the system variables such as temperature and product flow rates are compared with those obtained from the steady–state simulations. The dynamic response of the reactor which is initially at steady state to a disturbance in the feed is also analyzed. The response to a step change that involves an increase in the inlet oxygen flow rate is the elevation of temperature, which in turn leads to higher product yields. If the disturbance involves an increase in the steam flow rate, the temperature and product yields decrease in time to a local minimum, and from that moment onwards, they gradually increase to the subsequent steady state. The size of an indirect partial oxidation reactor for producing 1.5 kW–fuel–cell–grade hydrogen is determined by steady–state simulations and trial–and–error for different feed conditions.

ÖZET

METAN GAZININ DOLAYLI KISMİ OKSİDASYON REAKTÖRÜNDE HİDROJENE DÖNÜŞÜMÜNÜN DİNAMİK BENZETİMİ

Metan gazının katalitik dolaylı kısmi oksidasyon (toplam oksidasyon + buhar reformlama) reaktöründe hidrojene dönüşümü bilgisayar destekli modelleme/benzetim yöntemleriyle kararlı durumda ve dinamik olarak incelenmiştir. Metanın harmanlanmış Pt/δ–Al_2O_3 ve Ni/MgO–Al_2O_3 katalizörlerinin üzerinde ototermal dönüşümü bir boyutlu türdeş reaktör modeliyle gösterilmiştir. Deneysel bir reaktörün farklı giriş şartlarında kararlı durum ve dinamik benzetimleri yapılmıştır. Ototermal reformlama sürecinin başlamasından kararlı duruma varıncaya kadarki geçişli durumu incelenmiş ve sıcaklık ve ürün debisi gibi değişkenlerin kararlı hali kararlı durum benzetimlerinden elde edilen sonuçlarla karşılaştırılmıştır. Ayrıca kararlı duruma ulaşmış reaktörün giriş şartlarında ortaya çıkan ani bir değişime zaman içinde verdiği tepki de incelenmiştir. Buna göre, girişte, metan debisi sabit kalmak kaydıyla, oksijenin debisinin artması sıcaklığın, dolayısıyla ürün eldesinin artmasına yol açmıştır. Buhar debisinin artması durumunda ise, sıcaklık ve ürün elde değerlerinin bir müddet sonra en küçük değerlerine gerilediği, bu durumdan itibaren de aşamalı olarak artarak sonraki kararlı duruma geldikleri görülmüştür. Son olarak, 1,5 kilowattlık PEM tipi yakıt piline yetecek miktarda hidrojen eldesi için gerekli dolaylı kısmi oksidasyon reaktörünün ebat hesabı farklı giriş şartlarında kararlı durum benzetimleri ve deneme yanılma yöntemiyle yapılmıştır.

TABLE OF CONTENTS

LIST OF FIGURES

LIST OF TABLES

LIST OF SYMBOLS/ABBREVIATIONS

A_c	Cross–sectional area of reactor	cm^2
c_j	Concentration of species j	kmol cm^{-3}
c_{pj}	Heat capacity of species j	J $gmol^{-1}$ K^{-1}
d_r	Reactor diameter	cm
E_i	Activation energy of reaction i	kJ $kmol^{-1}$
F_j	Flow rate of species j	kmol s^{-1}
F_{j0}	Initial flow rate of species j at $t = 0$	kmol s^{-1}
F_j^{in}	Inlet flow rate, boundary condition at $z = 0$	kmol s^{-1}
F_T	Total flow rate	kmol s^{-1}
F_T^{in}	Total inlet flow rate	kmol s^{-1}
i	Reaction index	–
j	Species index	–
k_i	Rate coefficient for reaction i	kmol $kgcat^{-1}$ h^{-1}
k_{oi}	Intrinsic reaction rate of reaction i	kmol $kgcat^{-1}$ h^{-1}
K_j	Adsorption constant for species j (reforming)	bar^{-1}
K_{eq}^{I}, K_{eq}^{II}, K_{eq}^{III}	Equilibrium constants for SR reactions	bar^2, bar^2, –
$K_{CH_4}^{c}$	Adsorption constant for methane (oxidation)	bar^{-1}
$K_{O_2}^{c}$	Adsorption constant for oxygen (oxidation)	bar^{-1}
L	Reactor length	cm
m, M	Number of nodes and intervals in the spatial grid	–
n, N	Number of nodes and intervals in the temporal grid	–
p_j	Partial pressure of species j	bar
p_T	Total pressure	bar
p_T^{in}	Total inlet pressure	bar
r_i	Rate of reaction i	kmol $kgcat^{-1}$ s^{-1}
R_j	Total rate of formation or depletion of species j	kmol $kgcat^{-1}$ s^{-1}
t	Simulation clock	s

T	Temperature	K
T_0	Initial temperature at $t = 0$	K
T^{in}	Inlet temperature, boundary condition at $z = 0$	K
T_{exit}^{SS}	Exit temperature at steady state	K
v	Volumetric flow rate	$cm^3\ s^{-1}$
v^{in}	Inlet volumetric flow rate	$cm^3\ s^{-1}$
$x_{CH_4}^{SS}$	Methane conversion at steady state	–
W_T	Catalyst weight	g
$y_{H_2}^{SS}$	Hydrogen yield at steady state	–
y_{CO}^{SS}	Carbon monoxide yield at steady state	–
z	Axial coordinate	cm

α	Reaction order with respect to CH_4	–
β	Reaction order with respect to O_2	–
α_j	Constant in the heat capacity equation	$J\ gmol^{-1}\ K^{-1}$
β_j	Constant in the heat capacity equation	$J\ gmol^{-1}\ K^{-2}$
γ_j	Constant in the heat capacity equation	$J\ gmol^{-1}\ K^{-3}$
δ_j	Constant in the heat capacity equation	$J\ gmol^{-1}\ K^{-4}$
ΔH_{fj}^{0}	Standard heat of formation of species j	$kJ\ gmol^{-1}$
ΔH_i	Heat of reaction i at T	$kJ\ gmol^{-1}$
ΔH_j	Heat of adsorption of species j (reforming)	$kJ\ kmol^{-1}$
$\Delta H_{CH_4}^{c}$	Heat of adsorption of methane (oxidation)	$kJ\ kmol^{-1}$
$\Delta H_{O_2}^{c}$	Heat of adsorption of oxygen (oxidation)	$kJ\ kmol^{-1}$
Δt	Time step	s
Δz	Grid size	cm
ε_{bed}	Bed void fraction	–
ρ_B	Bulk catalyst density	$kgcat\ m^{-3}$

AFC	Alkaline fuel cell
ATR	Autothermal reforming
CFL	Courant–Friedrichs–Levy
CPO	Catalytic partial oxidation
GHSV	Gas hourly space velocity
HTS	High–temperature shift
IPOX	Indirect partial oxidation
LNG	Liquefied natural gas
LPG	Liquefied petroleum gas
LTS	Low–temperature shift
MCFC	Molten carbonate fuel cell
NK	Numaguchi and Kikuchi
PAFC	Phosphoric acid fuel cell
PEMFC	Polymer electrolyte/Proton exchange membrane fuel cell
ppm	Parts per million
SOFC	Solid oxide fuel cell
SR	Steam reforming
STP	Standard temperature and pressure
TOF	Turnover frequency
TOX	Total oxidation
XF	Xu and Froment
WGS	Water–gas shift

1. INTRODUCTION

The long–expected increase in quantity of hazardous emissions and the parallel growth of environmental awareness have, through the imposition of stringent legislative regulations by the state, forced the automobile industry to find innovative solutions for the development of engines that are energy–efficient and produce lower quantities of pollutants. The use of catalytic converters and particle recovery systems were realized in the early 80s and implemented in vehicles, which resulted in significant decrease of toxic emissions such as CO, NO_x and unburned hydrocarbons. However, continuous increase in the number of vehicles, which is forecast to double to 800 million within the next 20 years (Golunski, 1998), has led the automobile manufacturers to the search for development of vehicles that have zero on–road emission. Fuel–cell–powered vehicles have become promising candidates for achieving this goal.

Fuel cells have been recognized to have significant advantages over their conventional counterparts, such as the internal combustion engine (ICE) and the diesel engine, in clean and efficient power generation. Zero emission can be achieved if pure hydrogen is used as the fuel. Comparably longer service life, presence of fewer moving parts and the electrochemical conversion of the fuel without the need for a heat generation step are attractive features that make fuel cells a significant candidate for replacing the existing energy conversion systems in automobiles. Apart from their potential use in powering vehicles, fuel cells which are available in various types, find widespread use in stationary applications, ranging from small systems located in remote areas and residences in urban areas to large central power stations (Avcı, 2003).

The choice of the type of fuel cell and the fuel depends closely on the application it will be used in. Central power plant owners are investigating the use of Phosphoric Acid Fuel Cells (PAFCs), Molten Carbonate Fuel Cells (MCFCs), and Solid Oxide Fuel Cells (SOFCs), since there are no restrictions as to the size or the weight of the fuel cells or the fuel processor, the only requirement being the durability of the system. While the higher temperature fuel cells, MCFC and SOFC, are being demonstrated for power plants, the

Proton Exchange/Polymer Electrolyte Membrane Fuel Cell (PEMFC) predominates among the smaller power generators being developed for small–scale Combined–Heat–and–Power (CHP) units. On the other hand, automobile manufacturers have decided that the PEMFC, fuelled by hydrogen seems to have the best potential to replace the ICE for propulsion power, due to its compactness, ability to start up quickly, dynamic response and cost. The lack of a hydrogen refueling infrastructure and the low–energy density of today's hydrogen storage technology are, however, the major problems encountered in generating propulsion power from PEM fuel cells. The alternative is to carry readily available liquid fuels (primary fuels) that have high–energy densities and to convert them to a hydrogen–rich gas via an on–board fuel processor, on an as–needed basis. Furthermore, the fuel processor, which is now a part of the fuel cell engine (fuel processor/fuel cell assembly), must also meet the requirements of size and weight, be able to start up very quickly, and be dynamically responsive to changing power demands, which impose a varying fuel processing rate (Ahmet and Krumpelt, 2001). The fuel processor/fuel cell assembly is an integrated system consisting of several reactors, heat exchangers, evaporators, a control unit, peripherals and finally the fuel cell.

Processes using primary fuels to make fuel–cell hydrogen involve chemical conversion in reactors of different kinds such as fixed–bed, membrane and monolithic (Avcı *et al.*, 2000; de Smet *et al.*, 2001; Ma and Trimm, 1996; Springmann *et al.*, 2004). One route for hydrogen production is indirect partial oxidation (IPOX), which is a combination of catalytic combustion of the fuel and the simultaneous or subsequent steam reforming of the remaining fuel. Steam reforming reacts water vapor with the primary fuel, forming carbon monoxide, carbon dioxide, and hydrogen. Steam reforming (SR) is always endothermic, so energy must be supplied for this reaction. In the partial oxidation (POX) reaction, the primary fuel reacts with oxygen for complete combustion, and heat is liberated. Endothermic steam reforming reactions are facilitated by the heat released during POX. Coupling of the exothermic partial oxidation and endothermic reforming reactions are named autothermal reforming (ATR) or autothermal hydrogen production (Brown, 2001).

The reformate is yet to be processed for fuel–cell grade hydrogen. In the subsequent water–gas shift (WGS) reaction in a separate reactor, the reformate is enriched in hydrogen, and the carbon monoxide (CO) content is significantly lowered since the latter is a catalyst inhibitor. In the preferential oxidation of CO in the presence of hydrogen, small amounts of CO can be removed from the process stream before feeding it to a PEM fuel cell.

This study is a preliminary to the project of designing fuel processor/fuel cell assemblies for mobile and small–scale stationary applications. The fuel processor/fuel cell assembly can be modelled accurately for steady–state operation, which is well suited for stationary applications, but transient operation arising from the nature of a mobile application such as automobile start–up or change in propulsion power demand calls for the development of a dynamic model. It can then be possible to implement accurate control and coordination of the assembly based on its dynamic behavior.

The object is to investigate, using mathematical models, the steady and dynamic behavior of a catalytic indirect partial oxidation reactor for the conversion of methane to hydrogen. The simplest of the reactor models, namely the one–dimensional pseudohomogeneous model, is used for the simulations. Theoretical kinetic models are employed for predicting the reaction rates. A parametric study is conducted by varying the feed conditions to realize their effects on hydrogen yield and maximum reactor temperature. The latter is essential since catalyst sintering may occur at the hotspot location any time in the reactor from start–up to steady state.

A literature survey on fuel cell technology and catalytic oxidation and steam reforming of methane is presented in Chapter 2. The mathematical models employed for simulation of the IPOX reactor are given in Chapter 3. Simulation results are presented and discussed in Chapter 4. Chapter 5 includes the conclusions that can be drawn from this study and the recommendations for future work.

2. LITERATURE SURVEY

2.1. Fuel Cell Technology and Fuel Conversion

2.1.1. Fuel Cell Operation

Energy conversion in fuel cells is direct and simple compared to the sequence of chemical and mechanical steps in heat engines. A fuel cell consists of an anode, an electrolyte, and a cathode (Vielstich and Iwasita, 1997). On the anode, the fuel is oxidized electrochemically to positively charged ions. On the cathode, oxygen molecules are reduced to oxide or hydroxide ions. The electrolyte serves to transport either the positively charged or negatively charged ions from anode to cathode or cathode to anode. Figure 2.1 is a schematic representation of the reactions in a fuel cell operating on hydrogen and air with a hydrogen–ion–conducting electrolyte. The hydrogen flows over the anode, where the molecules are separated into ions and electrons. The ions migrate through the ionically conducting but electronically insulating electrolyte to the cathode, and the electrons flow through the outer circuit energizing an electric load. The electrons combine eventually with oxygen molecules flowing over the surface of the cathode and hydrogen ions migrating across the electrolyte, forming water, which leaves the fuel cell in the depleted air stream.

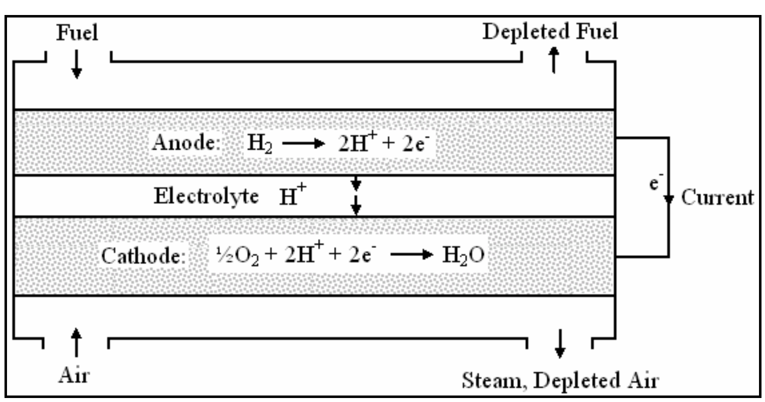

Figure 2.1. Fuel cell schematic

The anodes and cathodes in a fuel cell stack have to be good electronic conductors and must have electrocatalytic properties to facilitate the anodic and cathodic reactions. In addition, the anodes and cathodes must be porous to allow the fuel and oxidant gases to diffuse to the reaction sites, yet they must be mechanically strong enough to support the weight of the fuel cell stacks. The electrolyte must be chemically stable in hydrogen and oxygen. Five classes of electrolytes have been found to meet these requirements: potassium hydroxide, phosphoric acid, perflourinated sulfonic acid resins, molten carbonates, and oxide–ion–conducting ceramics. Consequently, five types of fuel cells based on these electrolytes have been developed (Perry and Green, 1997; Ralph and Hards, 1998).

An individual fuel cell will generate an electrical potential of about 1 V or less, and a current that is proportional to the external load demand. For practical applications, the voltage of an individual fuel cell is obviously too small, and cells are therefore stacked up as shown in Figure 2.2. Anode/electrolyte/cathode assemblies are electrically connected in series by inserting a bipolar plate between the cathode of one cell and the anode of the next. The bipolar plate must be impervious to the fuel and oxidant gases, chemically stable under reducing and oxidizing conditions, and an excellent electronic conductor. In addition, it is often used to distribute the gases to the anode and cathode surfaces through flow channels cut or molded into it (Perry and Green, 1997; Dhathathreyan, 1999).

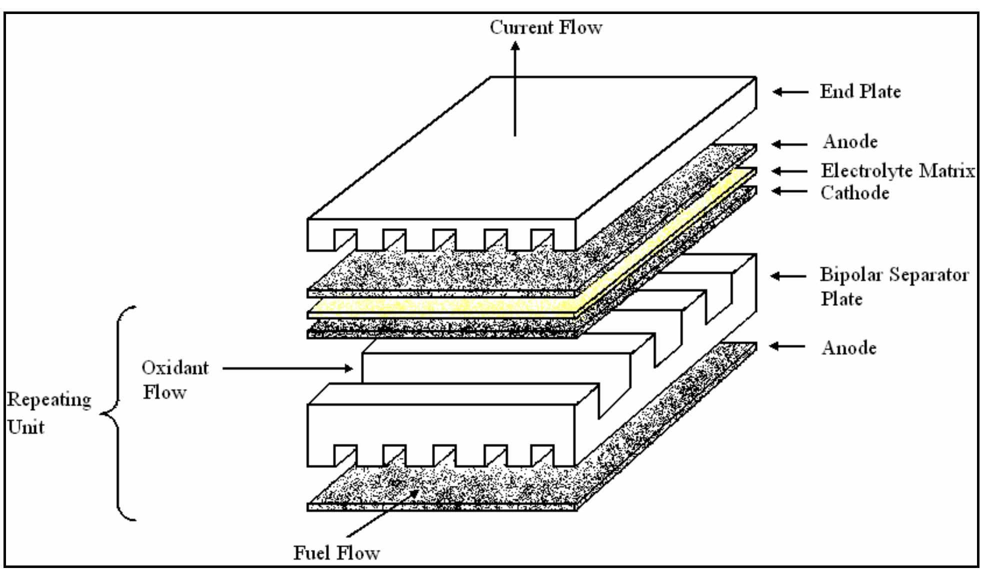

Figure 2.2. Stacking of individual fuel cells (Perry and Green, 1997)

The number of fuel cells that are stacked is determined by the desired electrical potential. For 110–volt systems it can be about 200 cells. Since a typical fuel cell is about 5 millimeters thick, a 200–cell stack assembly is about 2 meters tall.

Because fuel cells generate an amount of excess heat consistent with their thermodynamic efficiency, they must be cooled. In low–temperature fuel cells, the cooling medium is generally water or oil, which flows through cooling plates interspaced throughout the stack. In high–temperature cells, heat is removed by the reactant air stream and also by the endothermic fuel reforming reactions in the stack (Perry and Green, 1997).

2.1.2. Types and Applications of Fuel Cells

The five major types of fuel cells are listed in Table 2.1. Each has unique chemical features. The Alkaline Fuel Cell (AFC) has high power density and has proven itself as a reliable power source in the U.S. space program, but the alkaline electrolyte reacts with carbon dioxide, which is present in reformed hydrocarbon fuels and air. The Polymer Electrolyte/Proton Exchange Membrane Fuel Cell (PEMFC) and the Phosphoric Acid Fuel Cell (PAFC) are compatible with carbon dioxide, but both are sensitive to carbon monoxide, which is adsorbed onto the platinum catalyst and renders it inactive. Therefore, these three types of fuel cells require pure hydrogen as fuel; and if the hydrogen has been obtained by reforming a fuel such as natural gas, the hydrogen–rich fuel stream must be purified before being introduced into the fuel cell (Perry and Green, 1997; Ralph, 1999). The Molten Carbonate Fuel Cell (MCFC) and the Solid Oxide Fuel Cell (SOFC) can tolerate carbon monoxide and can operate on hydrocarbon fuels with minimal fuel processing, but they operate at elevated temperatures.

The operating temperature also affects the fuel cell operating potential. A high operating temperature accelerates reaction rates but lowers the thermodynamic equilibrium potential. These effects balance one another, and, in practice, the operating point of any fuel cell is usually between 0.7 and 0.8 V. The cell reactions for the five types of fuel cells are summarized in Table 2.2. It is important to note that in cells with acidic electrolytes

(PAFC and PEMFC) the product water evolves on the air electrode, but in the alkaline ones it is generated on the fuel electrode (Perry and Green, 1997).

Table 2.1. Fuel cell characteristics (Perry and Green, 1997)

Type of Fuel Cell	Electrolyte	Operating Temperature °C	Coolant Medium
Alkaline	KOH	90	Water
Polymer	$CF_3(CF_2)_nOCF_2SO_3^-$	80	Water
Phosphoric Acid	H_3PO_4	200	Steam/Water
Molten Carbonate	$Li_2CO_3–K_2CO_3$	650	Air
Solid Oxide	$Zr_{0.92}Y_{0.08}O_{1.96}$	1000	Air

Table 2.2. Fuel cell reaction electrochemistry

Type of Fuel Cell	Conducting Ion	Anode Reaction	Cathode Reaction
Alkaline	OH^-	$H_2 + 2OH^- \rightarrow 2H_2O + 2e^-$	$\frac{1}{2}O_2 + H_2O + 2e^- \rightarrow 2OH^-$
Polymer	H^+	$H_2 \rightarrow 2H^+ + 2e^-$	$\frac{1}{2}O_2 + 2H^+ + 2e^- \rightarrow H_2O$
Phosphoric Acid	H^+	$H_2 \rightarrow 2H^+ + 2e^-$	$\frac{1}{2}O_2 + 2H^+ + 2e^- \rightarrow H_2O$
Molten Carbonate	CO_3^{2-}	$H_2 + CO_3^{2-} \rightarrow H_2O + CO_2 + 2e^-$	$\frac{1}{2}O_2 + CO_2 + 2e^- \rightarrow CO_3^{2-}$
Solid Oxide	O^{2-}	$H_2 + O^{2-} \rightarrow H_2O + 2e^-$	$\frac{1}{2}O_2 + 2e^- \rightarrow O^{2-}$

Due to its high power density, ability to start up quickly and deliver about 40 per cent of its nominal power at room temperature, the Polymer Electrolyte/Proton Exchange Membrane Fuel Cell (PEMFC) is a candidate to replace internal combustion engines in transport applications. Methanol, ethanol, hydrogen, natural gas, dimethyl ether and common transportation fuels such as gasoline are being considered as fuel. All but hydrogen require a reforming step to provide hydrogen for the fuel cell (Perry and Green, 1997; Ahmed and Krumpelt, 2001; Brown, 2001; Joensen and Rostrup–Nielsen, 2002). The ultimate goal is the design of a fuel processor/fuel cell assembly for mobile and small–scale stationary applications, and it is decided that the PEMFC is the most suitable choice for this purpose, so, unless otherwise specified, all the information and data to be presented here and calculations to be performed in this work pertain to this type of fuel cell.

In a PEMFC, the electrolyte is a perfluorosulfonic acid ionomer, commercially available under the trade name of Nafion™. It is in the form of a membrane about 0.17 mm thick, and the electrodes are bonded directly onto the surface. The electrodes contain platinum or platinum alloys dispersed on carbon powder or fibers. The bipolar plates are made of graphite or metal. Typical platinum catalyst loadings needed to support the anodic and cathodic reactions are currently 1 to 2 mg/cm^2 of active cell area. Owing to the cost of platinum, substantial effort has been made to reduce the catalyst loading, and some fuel cells have operated at a catalyst loading of 0.25 mg/cm^2 (Gamburzev, 1999; Starz, 1999; Stevens et al., 2003; Sasikumar *et al*., 2004; Gasteiger *et al*. 2004).

The PEMFC does not tolerate more than 5–10 ppm carbon monoxide. The platinum catalysts on the electrodes are extremely sensitive to this poisonous gas. The acidic ionomers of the electrolyte, on the other hand, can tolerate carbon dioxide in the fuel and air stream (Joensen and Rostrup–Nielsen, 2002). To be ionically conducting, the fluorocarbon ionomer must be "wet": i.e., under equilibrium conditions, it will contain about 20 per cent water. The PEMFC thus requires low operating temperatures (< 373 K) in order to avoid deterioration of the polymer membranes (Perry and Green, 1997).

2.1.3. On–Board Fuel Conversion Processes

Conversion of liquid or gaseous fuels into hydrogen for fuel cells, commonly referred to as fuel processing, most often involves either hydrocarbons, like methane, propane or alcohols, e.g. methanol and ethanol. The conversion of fuels to hydrogen, or hydrogen–rich product streams may be carried out by two basically different types of processes. One is endothermic steam reforming in which the hydrocarbon or alcohol is reacted catalytically with steam. The heat required is supplied either by combustion of part of the feed, by burning combustible off–gases or by a combination of both. The other type of process is exothermic partial oxidation, where the feed reacts directly with air at a balanced oxygen–to–fuel ratio. In either of the processes, thermal integration is the key to achieve high overall efficiencies (Ahmed and Krumpelt, 2001; Avcı, 2003).

Steam reforming of either natural gas as in Reaction (2.1) or liquid hydrocarbons like heptane as in Reaction (2.2) on Ni–based catalysts is the well–known route to hydrogen:

$$CH_4 + H_2O \longleftrightarrow CO + 3H_2, \qquad \Delta H^0_{298} = 206.2\ \mathrm{kJ/gmol} \tag{2.1}$$

$$C_7H_{16} + 7H_2O \longleftrightarrow 7CO + 15H_2, \qquad \Delta H^0_{298} = 1{,}175\ \mathrm{kJ/gmol} \tag{2.2}$$

For small–scale applications, steam reforming of methanol as in Reaction (2.3) may be an attractive alternative (Joensen and Rostrup–Nielsen, 2002):

$$CH_3OH + H_2O \longleftrightarrow CO_2 + 3H_2, \qquad \Delta H^0_{298} = 49.6\ \mathrm{kJ/gmol} \tag{2.3}$$

The water–gas shift (WGS) reaction, Reaction (2.4), takes place independently and increases the hydrogen produced while lowering the undesired carbon monoxide:

$$CO + H_2O \longleftrightarrow CO_2 + H_2, \qquad \Delta H^0_{298} = -41.2\ \mathrm{kJ/gmol} \tag{2.4}$$

The reformers are well suited for long periods of steady–state operation and can deliver relatively high quantities of hydrogen (> 70% on a dry basis). The carbon monoxide and carbon dioxide are removed from the reformate gas stream by a variety of reactions and scrubbing techniques such as additional water–gas shift reaction, methanation, CO_2 absorption, pressure swing adsorption and preferential oxidation (Ahmed and Krumpelt, 2001). The primary steam reforming (SR) reaction is strongly endothermic, and reactor designs are limited by heat transfer, rather than by reaction kinetics. Consequently, the reactors are designed to promote heat exchange and tend to be large. Indirect heat transfer across a wall makes conventional steam reformers less attractive for the rapid and dynamic response needed in mobile applications (Ahmed and Krumpelt, 2001).

Direct partial oxidation, or catalytic partial oxidation (CPO), represented by Reaction (2.5), is another route to hydrogen:

$$CH_4 + \tfrac{1}{2}O_2 \longrightarrow CO + 2H_2, \qquad \Delta H^0_{298} = -35.7\ \mathrm{kJ/gmol} \tag{2.5}$$

It has been shown that at temperatures as high as 1373 K and under extremely short residence times as low as $10^{-4} - 10^{-2}$ s, methane may be partially oxidized forming H_2 and CO as the main products (Hickman and Schmidt, 1992). CPO is kinetically controlled due to the short contact times and to the oxidation reactions being much faster than the steam reforming and shift reactions. The process characteristics, temperature and concentration profiles, and eventually the entire product distribution are determined by heat and mass transfer resistances which dominate over kinetics (Witt and Schmidt, 1996; Basile *et al.*, 1998).

Another promising method of hydrogen production is Indirect Partial Oxidation (IPOX), which is the combination of total oxidation of the fuel, represented by Reaction (2.6), SR and WGS (Trimm and Önsan, 2001; Avcı *et al.*, 2001a). Oxidation can be catalytic (flameless) or non–catalytic, but the stoichiometry for the conversion is the same either way:

$$CH_4 + 2O_2 \longrightarrow CO_2 + 2H_2O, \qquad \Delta H^0_{298} = -802.3\ \mathrm{kJ/gmol} \tag{2.6}$$

The heat required to initiate and sustain SR can be supplied by the exothermic oxidation. The water produced by oxidation is not sufficient to drive SR and WGS, so further water injection is needed. Also, in order to minimize coke formation during SR (Trimm, 1999) and for temperature control (Avcı *et al.*, 2000), extra water is required. When water is fed together with the fuel and air, the process is also called autothermal reforming (ATR)

(Ahmed and Krumpelt, 2001). Thermal integration due to the combination of exothermic and endothermic reactions, high space velocity and preset H_2/CO ratio regulated by the inlet fuel−to−oxygen and oxygen−to−water ratios are the main features of ATR (Freni, *et al.*, 2000).

Compared to catalytic partial oxidation and autothermal reforming, steam reforming yields the highest hydrogen concentration in the product. For mobile applications, however, the CPO and ATR processes are more attractive because their response to changes in demand is more robust and the hardware can be more compact (Ahmed and Krumpelt, 2001). Further, the advantages offered by the CPO process may be offset by the competing total oxidation reactions which significantly enhance process exothermicity (Joensen and Rostrup–Nielsen, 2002). Similar carbon monoxide and hydrogen selectivities as for CPO can also be obtained by ATR (Aasberg–Petersen *et al.*, 2001; Trimm and Önsan, 2001; Avcı *et al.*, 2001a). Therefore, the ATR pathway to hydrogen production is investigated in detail in this work.

2.1.4. Fuels and CO Removal Techniques

2.1.4.1. Fuels: The choice of the fuel for conversion to hydrogen varies with the application. In mobile applications it may be a liquid fuel such as methanol or gasoline. In stationary systems natural gas or propane (LPG) can be the fuel. Ethanol or biomass–derived materials can also be used depending on the availability and extent of renewability. During reforming of diesel, coke deposition on the catalyst is likely to occur, so it is not suitable for on–board conversion (Jamal and Wyszynski, 1994).

Table 2.3 shows the temperature ranges in which steam reforming of different fuels takes place. Low–temperature reforming of methanol, represented by Reaction (2.3), in addition to its being in liquid form at ambient temperatures, is an attractive feature. Commercially available methanol possesses essentially no sulfur, as it can be removed at an early stage of manufacture (Brown, 2001).

Table 2.3. Reactor temperature ranges for steam reforming of different fuels (Brown, 2001)

Fuel	Temperature Range (K)
Methane	1000 – 1100
Methanol	500 – 560
Ethanol	~ 800 – 1000
Multi–carbon Hydrocarbons	1000 – 1150

Table 2.4. Carbon monoxide contents after reforming of different fuels (Brown, 2001)

Fuel	CO in Product Stream Before WGS (mol%)
Methane	11.2
Methanol	0.8
Ethanol	10 – 14
Multi–carbon Hydrocarbons	20.0

Approximate carbon monoxide concentrations in reformate streams obtained by SR of different fuels are presented in Table 2.4. Methanol reforming does not generate significant amounts of carbon monoxide, as opposed to the other fuels.

The primary fuel for prototype fuel–cell–driven automobiles currently appears to be methanol. However, there are serious problems associated with practical usage of methanol for generating fuel–cell–grade hydrogen. Synthesis gas, produced by methane SR, is the feedstock for methanol production. Current methanol supply can only meet the requirements of a limited number of fuel–cell powered automobiles, if the latter becomes available for widespread use (Thomas *et al*., 2000). A reliable distribution network yet needs to be established. Methanol's toxicity, combined with its solubility in water is a serious environmental threat in case of a leakage and major spill (Brown, 2001).

Like methanol, gasoline offers advantages in terms of high energy density and easy fuel handling; but, unlike methanol, it has an existing refueling infrastructure. Furthermore, gasoline is directly obtained by refining crude oil, not requiring a synthesis step as does methanol. However, coke formation at the reforming conditions may occur due to the presence of aromatic hydrocarbons in the mixture (Rostrup–Nielsen, 1984). Also, sulfur content above 30 ppm may cause catalyst deactivation (Thomas, *et al*., 2000; Urban, *et al*., 2001). Nevertheless, difficulties associated with its conversion can be overcome by novel technologies, so all major car manufacturers are developing prototypes resting on gasoline–based fuel cell systems (Springmann *et al*., 2004).

Liquefied Petroleum Gas (LPG) is another fuel that can be stored in liquid form in pressurized vessels. LPG is a byproduct in crude oil refining and is a mixture of propane and *n*–butane whose relative amounts depend on oil well location. Being a widely available and relatively cheap fuel with high energy density, LPG can be used as the primary fuel in small–scale stationary and mobile fuel cell applications (Ahmed and Krumpelt, 2001).

Ethanol can be converted to hydrogen more easily than gasoline. It is termed a “renewable source” since it can be produced from sugar cane or corn via fermentation. Although complete gasification of the alcohol is necessary for SR (Mariño, *et al*., 2001), ethanol is potentially a primary fuel for on–board conversion. Literature on kinetics of ethanol steam reforming is scarce but investigations are in progress. Some groups have been carrying out thermodynamic analyses and testing catalysts (Garcia and Laborde, 1991; Ioannides, 2001; Mariño, *et al*., 2001; Örücü *et al*., 2005).

Natural gas, among many potential sources, is considered to be one of the ideal fuels for fuel–cell–grade hydrogen. Almost half the world’s hydrogen feedstock is thought to be fixed in natural gas reserves (Armor, 1999). Besides its abundance, natural gas has the lowest carbon dioxide emissions. It is mainly composed of 75 – 85 per cent methane, the rest being ethane, propane and trace carbon dioxide (Dicks, 1996). Thus the ratio of hydrogen atoms to carbon atoms is close to 4 : 1, which makes natural gas cleaner than any other hydrocarbon. Apart from being environmentally benign, it is available through well–established distribution networks, either through pipelines in gaseous form or through shipping in the form of liquefied natural gas (LNG). Like gasoline and LPG, its composition varies from feedstock to feedstock.

Even though processing natural gas possesses many advantages, there are hindrances to its usage as a primary fuel for on–board conversion. It is a gas at ambient temperature and pressure, which requires bulky and costly pressurized cylinders for on–board storage. Also, methane molecule is very stable and considerable energy input is needed to initiate a reaction. Once it is triggered, higher temperatures are still required to sustain the reaction(s). The most common method, steam reforming of natural gas, which is endothermic, is well suited for steady–state operation and can deliver a relatively high concentration of hydrogen, but it suffers from a poor transient operation. Therefore, natural gas is not a suitable fuel for on–board conversion. Processing of natural gas for stationary (residential and commercial) applications and on–site hydrogen production, however, seems to be the promising solution. Commercialization of direct hydrogen storage technologies in the coming years is thought to pronounce the significance of on–site hydrogen production from natural gas (Dicks, 1996). Methane processing for on–board hydrogen production is investigated in this preliminary work unless otherwise specified.

2.1.4.2. CO Removal Techniques: Carbon monoxide content in a hydrogen–rich product stream from the reformer or IPOX reactor is usually 2 – 6 mole per cent, which is 10^6 times higher than the tolerable limit below which a PEM fuel cell can safely operate. Therefore, before the stream is fed to the fuel cell, carbon monoxide must be removed catalytically.

Majority of the CO can be removed by the WGS process, Reaction (2.4). The shift reaction can be carried out at two different temperature ranges and is hence named accordingly: high–temperature shift (HTS) taking place in the range 623 – 673 K, and low–temperature shift (LTS) in the range 453 – 523 K. Iron supported on chromium oxides is used to catalyze the HTS, and the LTS is catalyzed by copper on zinc oxide support (Amadeo and Laborde, 1995). Therefore, either or both of the HTS and LTS reactors can be placed downstream of the fuel processor to remove CO. However, neither configuration can achieve sufficient CO elimination, so additional removal techniques need to be applied.

Among several methods such as methanation of CO and the use of hydrogen diffusion membranes (Trimm and Önsan, 2001), preferential oxidation of CO to CO_2 seems to be the optimal choice (Özkara and Aksoylu, 2003; İnce *et al*., 2005), since during methanation a significant amount of CO_2 may be converted along with CO, resulting in considerable hydrogen loss. Across Pd–based diffusion membranes, on the other hand, temperature and pressure differentials may be high and the overall efficiency may be significantly reduced. Simultaneously carrying out water–gas shift and preferential oxidation reactions by feeding oxygen into the shift reactor is also being investigated (Utaka *et al*., 2000).

2.2. Total Oxidation of Methane

Catalytic combustion of hydrocarbons, because of its claims of near–zero pollutant emissions and a wide range of applications, is receiving increased attention as a candidate for replacing a number of gas–phase combustion processes in the future. It is already being employed in such applications as stationary gas turbine combustors (Dalla Beta and Rostrup–Nielsen, 1999), fuel cells (Finnerty *et al*., 2000), domestic and industrial process heaters (Seo et al., 1999). Many important chemicals may also be produced by catalytic partial oxidation of fuel–rich hydrocarbon–air mixtures (Trimm, 1983). Homogeneous combustion of hydrocarbons requires very high temperatures, leading to the formation of unwanted nitrogen oxides (NO_x).

Steam reforming of a hydrocarbon fuel is the well–known route to hydrogen for fuel cells. The heat input to the endothermic reaction can be supplied by means of an electric heater at the expense of a reduction in overall efficiency. Another and more feasible possibility is catalytically combusting part of the fuel to generate the necessary heat (Trimm and Önsan, 2001), represented by Reaction (2.6):

$$CH_4 + 2O_2 \longrightarrow CO_2 + 2H_2O, \qquad \Delta H^0_{298} = -802.3\,\mathrm{kJ/gmol} \tag{2.6}$$

Combination of total oxidation and steam reforming, also called indirect partial oxidation, is a thermally self–sustaining process. However, initiation of total oxidation of hydrocarbons cannot be achieved at ambient conditions since high temperatures are required. On the contrary, hydrogen and methanol are reported to have been oxidized at room temperaure over a precious metal catalyst such as platinum (Jiang, 1992; Jiang *et al*., 1995; Ma *et al*., 1996), and they can be used for triggering oxidation.

2.2.1. Catalysts

Unlike hydrogen and methanol, methane can be made to react at rigorous conditions since it is the most stable hydrocarbon. Precious metals that are relatively stable at high temperatures are used as the active phase of the oxidation catalysts. It is confirmed that platinum, palladium or a combination of both are suitable for combustion of hydrocarbons (Trimm, 1983). While the ignition (light–off) temperature of methane oxidation is the lowest on palladium–based catalysts (Aryafar and Zaera, 1997; Burch *et al*., 1999; Ciuparu and Pfefferle, 2001; Lee *et al*., 1999), platinum–based (Ma *et*. *al*., 1996; Trimm and Lam, 1980; Veser and Schmidt, 1996) and rhodium–based (Burch *et al*., 1999) catalysts are also being utilized. Light–off temperature is usually defined as the temperature at which approximately 10 per cent of the hydrocarbon has been oxidized, and is an indication of the activity of the oxidation catalyst. On the basis of their activity, precious metals can be classified in the order Pd > Pt > Rh (Aryafar and Zaera, 1997; Burch *et al*., 1999).

The activity of oxidation catalysts is found to depend on metal particle size. Methane oxidation is a structure–sensitive reaction on supported Pd and Pt, with turnover frequencies (TOF) decreasing with increasing metal dispersion. Oxidation kinetics of light hydrocarbons over $Pt/\gamma–Al_2O_3$ is influenced by platinum concentration and particle size. Rate of oxidation is enhanced with an increase in Pt particle size, and with an increase in Pt concentration, TOF changed by one order of magnitude (Ma, 1995).

Table 2.5. Light–off temperatures of methane oxidation

at different CH_4/O_2 ratios (Ma *et al*., 1996)

CH_4/O_2	T_L (K)
0.27	724
0.9	641
2.53	623
5.04	589

Understanding of catalyst ignition in all oxidation processes involving methane is important for process safety and start–up of partial and complete oxidation systems (Bui *et al*., 1997). It is observed that an increase in methane inlet composition results in a decrease in light–off temperature of Pt–based catalysts (Veser and Schmidt, 1996). However, the coupling of gas–phase and surface chemistry and transport phenomena hinders better understanding of mechanisms controlling ignition. Table 2.5 shows the light–off temperatures of methane oxidation over Pt/Al_2O_3 at different methane–to–oxygen ratios (Ma *et al*., 1996).

2.2.2. Kinetics of Methane Oxidation

There is a vast of amount of literature on kinetic studies conducted on hydrocarbon oxidation. Because of the absence of a universally accepted rate law and absence of agreement on the range of operating conditions, however, the subject receives considerable attention. Power–law rate expressions are usually valid in a narrow range of operating temperatures and hydrocarbon–to–oxygen ratios, but still some generalizations can be made. In general, the reaction orders with respect to the hydrocarbon are found to be positive, whereas oxygen is seen to have an effect as to decrease the rate of oxidation over Pt–based catalysts (Avcı, 2003). However, this negative dependency with respect to oxygen becomes less pronounced when the hydrocarbon–to–oxygen ratio is over–stoichiometric, and even positive orders may be observed (Ma *et al*., 1996). A plausible explanation to this is that even though the heat of adsorption for oxygen is less, and hence it has a higher sticking probability, Pt surface becomes poisoned by excessive hydrocarbon molecules (Veser *et al.*, 1999).

Use of bimetallic, bifunctional catalysts can be an innovative solution to the heat transfer problem arising in autothermal reforming of hydrocarbons. The heat released upon oxidation of the fuel can be transmitted with much higher efficiency to the reforming sites via oxides of the catalyst support, which act as micro–exchangers, in addition to transport via bulk fluid (Avcı, 2003; Ma and Trimm, 1996). In an experimental work conducted with bimetallic Pt–NiO/δ–Al_2O_3 catalyst (Opoku–Gyamfi and Adesina, 1999), positive and negative dependencies of the oxidation rate on methane and oxygen concentrations, respectively, are seen to be in agreement with the generalizations made above, despite the non–monotonic behavior of oxygen. The use of a bimetallic catalyst is found to introduce a synergistic effect, which is attributed to the interaction of the two metal centers to form completely new active sites. The difference between the activation energy calculated for the bimetallic catalyst (80.88 kJ/gmol) and composition–weighted average of individual activation energies of the monometallic Pt and NiO catalysts (103.56 kJ/gmol) verifies the phenomenon. Kinetic parameters for two power–law rate expressions are presented in Table 2.6.

Table 2.6. Kinetic parameters for the oxidation of methane based on a power rate law expression

Catalyst/ Support	Fuel Regime	Reaction Order		k (gmol/h kPa$^{\alpha+\beta}$)	Activation Energy (kJ/gmol)	Reference
		CH_4 (α)	O_2 (β)			
Pt/ δ–Al_2O_3	CH_4–rich	0.95	–0.17	$1.20 \cdot 10^4\ m_{cat}^{-2}$	88.5	Ma *et al.*, 1996
Pt–NiO/ δ–Al_2O_3	CH_4–rich	1.22	–0.38	$6.73 \cdot 10^{-3}\ g_{cat}^{-1}$	80.9	Opoku–Gyamfi and Adesina, 1999

Table 2.7. Langmuir–Hinshelwood type rate expressions for methane oxidation over a series of Pt–based catalysts

Catalyst/Support	Temperature Range (K)	Rate Expression	Reference
Pt/Al_2O_3 (porous)	< 813	$-r = \dfrac{k_1 p_{CH_4} p_{O_2}^{1/2}}{1+K_1 p_{O_2}^{1/2}} + \dfrac{k_2 p_{CH_4} p_{O_2}}{1+K_2 p_{O_2}}$ (2.7)	Trimm and Lam, 1980
Pt/Al_2O_3 (porous)	> 813	$-r = \dfrac{k_1 p_{CH_4} p_{O_2}}{\left(1+K_1 p_{CH_4} + K_2 p_{O_2}\right)^2} + \dfrac{k_2 p_{CH_4} p_{O_2}^{1/2}}{1+K_1 p_{CH_4} + K_2 p_{O_2}}$ (2.8)	Trimm and Lam, 1980
Pt/Al_2O_3 (non–porous)	> 823	$-r = \dfrac{k_1 p_{CH_4} p_{O_2}}{\left(1+K_1 p_{CH_4} + K_2 p_{O_2}\right)^2}$ (2.9)	Trimm and Lam, 1980
$Pt/\delta{-}Al_2O_3$	663 – 723	$-r = \dfrac{k_1 K_1 p_{CH_4} \sqrt{K_2 p_{O_2}}}{\left(1+K_1 p_{CH_4} + \sqrt{K_2 p_{O_2}}\right)^2}$ (2.10)	Ma *et al.*, 1996

Kinetics of methane oxidation over Pt–based catalysts can also be expressed by theoretical Langmuir–Hinshelwood type expressions (Trimm and Lam, 1980; Ma *et al.*, 1996). Table 2.7 presents this type of kinetic expressions proposed for a series of Pt–based catalysts at different temperatures. The first term of the rate Equation (2.8) accounts for the reaction between molecularly adsorbed methane and oxygen, while the second term describes the Eley–Rideal reaction between molecularly adsorbed methane and oxygen in the gas phase. The rate coefficients and adsorption constants are estimated at a fixed temperature of 830 K using a nonlinear regression method. The rate coefficients k_1 and k_2 in Equation (2.8) are considered to be dependent on temperature according to an Arrhenius–type equation (Trimm and Lam, 1980).

2.3. Steam Reforming of Methane

2.3.1. Description of the Process

Reforming means rearrangement of atoms. Catalytic steam reforming of hydrocarbons is the well–known route to hydrogen for fuel cells. Industrial–scale steam reforming is also the most economical way to produce hydrogen (Armor, 1999). A good overview of the process is given in the literature (Rostrup–Nielsen, 1984; Rostrup–Nielsen and Alstrup, 1999; Aasberg–Petersen *et al.*, 2001). The process involves, in the presence of steam, catalytic conversion of hydrocarbons, usually natural gas, to a mixture of hydrogen, carbon monoxide, carbon dioxide and methane. The generic reactions for hydrocarbon steam reforming are

$$C_mH_n + mH_2O \longleftrightarrow mCO + (m + n/2)H_2, \qquad \Delta H^0_{298} > 0 \qquad (2.11)$$

$$C_mH_n + (2m)H_2O \longleftrightarrow mCO_2 + (2m + n/2)H_2, \qquad \Delta H^0_{298} > 0 \qquad (2.12)$$

The hydrocarbon is directly steam–reformed to carbon dioxide by the other primary Reaction (2.12), which runs in parallel with Reaction (2.11). Methane steam reforming (MSR) is specifically achieved through

$$CH_4 + H_2O \longleftrightarrow CO + 3H_2, \qquad \Delta H^0_{298} = 206.2\ \mathrm{kJ/gmol} \qquad (2.1)$$

$$CH_4 + 2H_2O \longleftrightarrow CO_2 + 4H_2, \qquad \Delta H^0_{298} = 165\ \mathrm{kJ/gmol} \qquad (2.13)$$

An important side reaction, water–gas shift (WGS), takes place simultaneously with the SR reactions and favors the formation of carbon dioxide at lower temperatures. It is particularly crucial in fuel cell applications since part of the undesired carbon monoxide is converted to hydrogen:

$$CO + H_2O \longleftrightarrow CO_2 + H_2, \qquad \Delta H^0_{298} = -41.2\,\text{kJ/gmol} \qquad (2.4)$$

Methanation becomes significant at low temperatures, the reverse of Reactions (2.1) and (2.13):

$$CO + 3H_2 \longleftrightarrow CH_4 + H_2O, \qquad \Delta H^0_{298} = -206.2\,\text{kJ/gmol} \qquad (2.14)$$

$$CO_2 + 4H_2 \longleftrightarrow CH_4 + 2H_2O, \qquad \Delta H^0_{298} = -165\,\text{kJ/gmol} \qquad (2.15)$$

Steam reforming is thermodynamically favored at high temperatures, typically greater than 1073 K, and at low pressures. However, in industrial practice, the reactions are carried out at pressures greater than 20 atm (Armor, 1999). The overall process is highly endothermic, and considerable heat should be supplied from the surroundings. Primary reformers usually contain between 40 and 400 tubes, typically 6 to 12 meters long, 70 to 160 mm in diameter and 10 to 20 mm in wall thickness (Rostrup–Nielsen, 1984). Reactor tubes usually contain cylindrical catalyst particles, nickel dispersed on alumina. Heat transfer from external burners to the catalyst bed is the most important operating factor with respect to product distribution and optimal reactor performance (Kvamsdal *et al*., 1999).

The major difficulties associated with SR arise from the presence of steam and the requirement of operation at high temperatures. Steam, at high temperatures, accelerates catalyst sintering and enables active site–support interactions. Moreover, coke formation is favored at high temperatures and low H_2O/CH_4 ratios (Ma, 1995).

2.3.2. Catalysts

Catalytic steam reforming in practice is almost invariably conducted on Ni–based catalysts as the metal is sufficiently active and can be obtained easily at a low price. However, as already mentioned, carbon formation over these catalysts is facilitated under steam reforming conditions. Coke deposition over Ni is usually overcome by keeping steam–to–carbon ratios above stoichiometric values; for methane, ratios between 2.5 and 3 are recommended (Rostrup–Nielsen, 1984).

Precious metals such as Rh and Ru are known to be more active and selective than Ni, and can safely operate without coke deposition. The major hindrance to their commercial use is their high price. The activity of various catalysts for MSR is reported as follows (Rostrup–Nielsen and Bak Hansen, 1993):

$$\text{Ru, Rh} > \text{Ir} > \text{Pd, Ni, Pt} > \text{Re} > \text{Co}$$

Minimizing coke formation over nickel–based catalysts is also investigated. Doping of catalysts with small amounts of tin, antimony and silver results in significant reduction of coke formation rate in MSR (Trimm, 1999). Addition of SnO_2 and WO_3 as well as oxides of K, Na, Mg, Ca and Ba also helps in suppressing coking over nickel (Borowiecki *et al*., 1997; Horiuchi *et al*., 1996). The effect of doping is such that methane adsorption is prevented, and hence its decomposition on the surface. Apart from doping, high activities in MSR are reported even at low steam–to–carbon ratios ($H_2O/CH_4 \sim 1$) when catalysts with low nickel content such as $Ni_{0.03}Mg_{0.97}O$ are used (Yamazaki *et al*. 1996). An extensive review of the methods to overcome the coke formation problem can be found in the work of Ma (1995).

The effect of catalyst support on MSR activity also deserves attention. It is revealed that activity of nickel supported on titania (TiO_2) is greater than nickel on other catalyst supports (Bradford and Vannice, 1996):

$$Ni/TiO_2 > Ni/C > Ni/SiO_2 > Ni/MgO$$

Similarly, nickel on alumina (Ni/Al_2O_3) is shown to be more active and stable than nickel on silica (Ni/SiO_2) (Takano *et al*., 1994).

2.3.3. Kinetics of Steam Reforming of Methane

A review and compilation of kinetics and mechanism of MSR can be found in the work of Rostup–Nielsen (1984). In general, the reaction rate expressions exhibit first order kinetics with respect to methane partial pressure. However, depending on the partial pressure of steam, the overall reaction orders attain negative or positive values; even zero–order reaction rates can be observed (Elnashaie *et al*., 1990). The results displayed by the comprehensive model proposed by Xu and Froment (1989a,b) indeed contradicted their previously reported counterparts. The discrepancies, however, are attributed to the non–monotonic dependency of the reaction rate on partial pressure of steam (Elnashaie *et al*., 1990).

Xu and Froment (1989a) investigated the intrinsic kinetics of MSR using a Ni/MgO–Al_2O_3 catalyst. To avoid reoxidation of the Ni catalyst by steam, the experiments were conducted with hydrogen in the feed. Langmuir–Hinshelwood type rate equations for SR towards CO and CO_2, Reactions (2.1) and (2.13), as well as for WGS, Reaction (2.4), were constructed using the elementary–step kinetic model proposed, as presented in Table 2.8. The three rate equations are seen to be inversely proportional to the partial pressure of hydrogen, which will consequently give infinite reaction rates. Since the feed generally contains some hydrogen, simulation of a reactor will not suffer from this problem. Also, Xu and Froment (1989a) worked in a relatively lower temperature range; for obtaining the model they employed temperatures between 773 and 848 K and pressures between 3 and 15 bar. During the indirect partial oxidation process, however, high catalyst temperatures will occur due to the exothermic total oxidation reaction.

To simulate MSR at elevated tempeatures, the kinetic model proposed by Numaguchi and Kikuchi (1988) can be used, for it was derived at higher catalyst temperatures up to 1160 K and higher pressures up to 25 bar. Based on a rate–determining

Table 2.8. Rate equations for methane steam reforming

Reaction	Rate Equation	Reference
$CH_4 + H_2O \rightarrow CO + 3H_2$	$r = \dfrac{k_1 / p_{H_2}^{2.5} \left(p_{CH_4} p_{H_2O} - p_{H_2}^{3} p_{CO} / K_{eq}^{I} \right)}{DEN^2}$ (2.16)	Xu and Froment (1989a)
$CH_4 + 2H_2O \leftrightarrow CO_2 + 4H_2$	$r = \dfrac{k_2 / p_{H_2}^{3.5} \left(p_{CH_4} p_{H_2O}^{2} - p_{H_2}^{4} p_{CO_2} / K_{eq}^{II} \right)}{DEN^2}$ (2.17)	
$CO + H_2O \leftrightarrow CO_2 + H_2$	$r = \dfrac{k_3 / p_{H_2} \left(p_{CO} p_{H_2O} - p_{H_2} p_{CO_2} / K_{eq}^{III} \right)}{DEN^2}$ (2.18)	
$CH_4 + H_2O \leftrightarrow CO + 3H_2$	$r = \dfrac{k_1 \left(p_{CH_4} - p_{H_2}^{3} p_{CO} / K_{eq}^{I} \right)}{p_{H_2O}^{0.596}}$ (2.19)	Numaguchi and Kikuchi (1988)
$CO + H_2O \leftrightarrow CO_2 + H_2$	$r = k_2 \left(p_{CO} - p_{H_2} p_{CO_2} / K_{eq}^{III} \right)$ (2.20)	

$$DEN = \left(1 + K_{CO} p_{CO} + K_{H_2} p_{H_2} + K_{CH_4} p_{CH_4} + K_{H_2O} p_{H_2O} / p_{H_2} \right)$$

surface reaction, Langmuir–Hinshelwood type rate equations for SR towards CO were proposed, presented also in Table 2.8. Reaction (2.13), which shows MSR towards CO_2 was not taken into account in the model of Numaguchi and Kikuchi. The catalyst properties used by Xu and Froment (1989a) and Numaguchi and Kikuchi (1988) for performing SR experiments are shown in Table 2.9. The Ni–content of the Numaguchi–Kikuchi catalyst is lower than that of the catalyst used by Xu and Froment. The Ni–surface areas, however, are more or less identical and allow a reasonable comparison of both kinetic models.

Table 2.9. Catalyst specifications

	Xu and Froment (1989a)	Numaguchi and Kikuchi (1988)
Catalyst	$Ni/MgAl_2O_4$	Ni/Al_2O_3
Metal Content (wt%)	15.2	8.7
Metal Surface Area (m^2/g)	4.1	3.6
Density (kg/m^3)	1,870	1,970

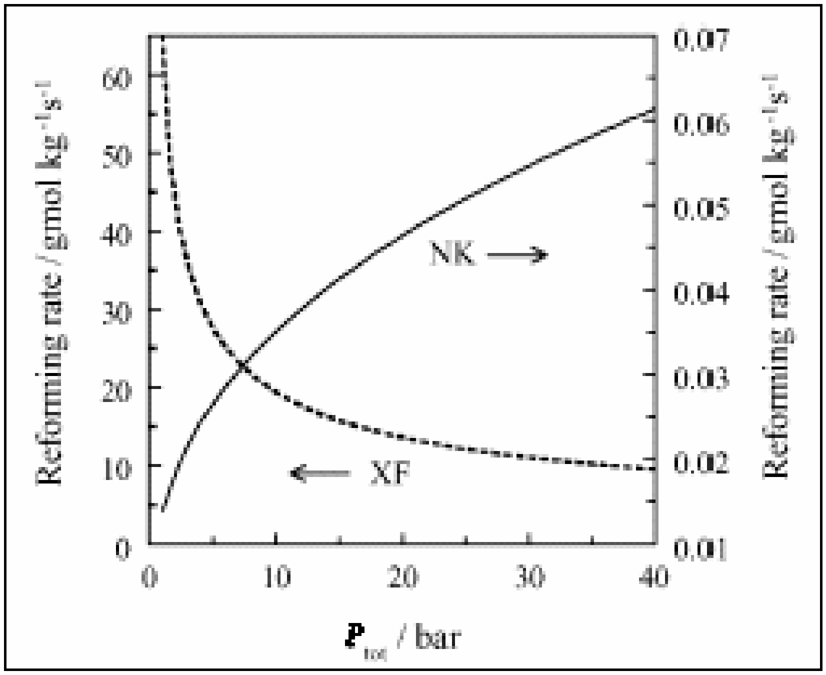

Figure 2.3. Methane steam reforming rates calculated by XF and NK kinetic models versus total pressure (de Smet *et al*., 2001)

The differences between the applied rate equations for steam reforming were examined by de Smet and coworkers (2001) by calculating the corresponding reforming rates as a function of total operating pressure. The catalyst was at 800 K and the feed consisted of methane, oxygen, steam and some hydrogen whose composition was as follows: $CH_4/O_2/H_2O/H_2$: 33.3/16.7/49.9/0.1. As indicated in Figure 2.3, the reforming rate decreases considerably at increasing total pressure in the case of the model of Xu and Froment, whereas the rate increases in the case of the rate equation proposed by Numaguchi and Kikuchi. The difference between the calculated reforming rates is attributed to the negative partial pressure reaction order with respect to hydrogen in the model of Xu and Froment. In the presence of significant amounts of hydrogen, the difference between the calculated rates is less pronounced. Different temperature and concentration profiles will thus be obtained when the proposed rate equations are applied at different operating pressures.

2.4. The Partial Oxidation Process

Steam reforming of hydrocarbons is the route to maximum hydrogen production, yet it suffers from the endothermicity of the reactions involved and the sluggish kinetics. Partial oxidation, on the other hand, is much faster, requires smaller amounts of catalyst and is energetically self–sustaining once started, all of which make it a candidate for supplying propulsion power in automobiles. Partial oxidation is known to occur via two pathways:

- Indirect partial oxidation (IPOX) in which total oxidation and steam reforming reactions are coupled.
- Direct partial oxidation in which the hydrocarbon is converted into synthesis gas in a single–step process.

2.4.1. Indirect Partial Oxidation

Indirect partial oxidation is basically a combination of the total oxidation and steam reforming reactions. What makes it distinct among the conversion routes is its autothermicity such that heat released by the oxidation of the fuel is harnessed by the endothermic steam reforming reactions. Thus, exogenous heat supply will not be necessary once the process is dynamically stable. This aspect of autothermal conversion is already realized in industrial practice in which non–catalytic (homogeneous) combustion is used to supply heat for catalytic methane steam reforming (Pena *et al.*, 1996). Problem of coke formation can partially be eliminated during homogeneous combustion by steam injection, but operation at elevated temperatures (> 2000 K) brings about more serious problems such as material degradation (Bharadwaj and Schmidt, 1995).

The mechanism of catalytic partial oxidation is yet not well understood. The operating conditions and nature of the catalysts are reported to influence the mechanism. Boucouvalas and coworkers (1996) observed that, over Ru/TiO_2 catalyst, significant formation of CO and H_2 took place subsequent to total oxidation at lower flow rates, whereas direct formation of the former was facilitated at higher flow rates. An excellent review on how partial oxidation is affected by the types of catalyst and support and of ways to minimize coke formation can be found in the work of Avcı (2003).

Besides altering catalyst properties, using promoted supports and modifying operating conditions, coke formation over nickel–based catalysts can be minimized by injection of steam. A steam–to–carbon ratio around 2.5 is shown to minimize carbon formation (Rostrup–Nielsen, 1984). Methane partial oxidation in the presence of steam has been investigated over Pt– and Ni–based catalysts placed in various configurations (Ma and Trimm, 1996). Pt– and Ni–based catalysts are known to promote oxidation and steam reforming, respectively, as mentioned in Chapters 2.3 and 2.4. The fixed–bed configurations were named dual–bed, mixed–bed and uniform–bed in accordance with the relative positions of the bulk catalysts or active metals. The dual–bed consisted of Pt–based catalyst placed upstream, and Ni–based catalyst downstream, so that under oxygen–deficient conditions, total oxidation of the fuel took place prior to steam reforming, which was triggered on Ni by harnessing the heat released. The mixed–bed was basically a physical mixture of the two catalysts, and the reactions were thought to take place simultaneously. The uniform–bed (bimetallic) configuration involved the existence of two metals on the same support. They found that, at the same feed properties, experiments conducted with different bed configurations gave different conversion and selectivity results. The bimetallic catalyst bed exhibited the best performance, with 92 per cent methane conversion and about 80 per cent product yield at around 900 K and feed composition of $CH_4/H_2O/O_2$: 25/59/16. The results indicate that heat and mass transfer between the oxidation and reforming sites are enhanced at the microscopic level.

2.4.2. Direct Partial Oxidation

In contrast with indirect partial oxidation, synthesis gas can be obtained from methane in a single–step process via direct partial oxidation:

$$CH_4 + \frac{1}{2}O_2 \longrightarrow CO + 2H_2, \qquad \Delta H^0_{298} = -35.7\ \text{kJ/gmol} \tag{2.5}$$

The advantage of the process is that synthesis gas in its ideal composition, i.e. H_2:CO = 2:1, is produced without the need for steam. However, for fuel cell applications post–processing of the effluent is necessary since carbon monoxide is a poison for PEM fuel cells.

Direct partial oxidation of methane to synthesis gas over Rh and Pt catalysts was investigated by Schmidt and coworkers (Hickman and Schmidt, 1993; Bharadwaj and Schmidt, 1995). It was concluded that while Rh was selective to synthesis gas, Pt catalyzed olefin formation. Also, product composition was close to the equilibrium value at elevated temperatures usually exceeding 1273 K, at contact times on the order of milliseconds, at metal loadings greater than 10 per cent and at near–stoichiometric feed mixtures. Mass transfer resistances were also reported to affect product distribution. The possibility of direct partial oxidation of methane over Ru/TiO_2 at lower temperatures has been reported as well (Boucouvalas *et al.*, 1996). Jin and coworkers (2000) investigated the mechanism of catalytic partial oxidation of methane to synthesis gas over Ni/Al_2O_3 catalyst. They observed that the partial oxidation reaction principally took place over a thin layer of the catalyst bed and that total oxygen and over 90 per cent of methane were converted in the main reaction zone. High methane conversion of 88.4 per cent and CO selectivity of about 96 per cent were obtained even on 1 mm of catalyst bed and at very high space velocities.

Compared with indirect partial oxidation, direct partial oxidation poses some operational challenges during on–board conversion. The process requires high temperatures, millisecond contact times and feed mixtures near the explosive limit, all of which are hindrances to practical applications involving frequent start–ups/shutdowns. However, direct partial oxidation coupled with water injection and low−temperature water−gas shift was simulated and higher hydrogen yields compared with indirect partial oxidation were obtained (Avcı *et al.*, 2001a; Avcı *et al.*, 2002; Avcı *et al.*, 2003). Being dynamically responsive and more feasible a process, direct partial oxidation needs to be further considered for use in mobile applications.

2.5. Simulation of Reactors for Producing Hydrogen

In order to theoretically analyze catalytic hydrogen production via methane conversion, a reactor model taking into account mass balances for reactive and inert components and an energy balance needs to be developed and solved by means of appropriate mathematical methods. Not only does the model in terms of describing gas and solid behavior and gas–solid interactions vary from the simplest to the most comprehensive, but it also describes the steady–state or transient behavior of the system, whichever is pertinent to the application. As mentioned earlier, a steady–state model can be used to simulate an industrial reactor or to make comparisons between primary fuels while a transient model will be more appropriate for simulation of a reactor to be used in mobile applications where frequent start–ups and changes in demand are involved. In this section, related works in the literature on simulation of fixed–bed reactor operation for producing hydrogen via methane conversion are reviewed.

2.5.1. Steam Reforming of Methane

Most of the work and data in literature on conventional steam reforming of hydrocarbons apply to industrial–scale hydrogen production. The most important operating factor is the rate of heat transfer to the catalyst bed from external burners, which affects the product distribution and optimal reactor performance (Kvamsdal *et al*., 1999).

Xu and Froment (1989b) performed the steady–state simulation of an industrial methane steam reformer using their kinetic model shown in Table 2.9. Their heterogeneous model was comprised of the one–dimensional component mass and energy balances in the fluid phase and the catalyst particle. The effectiveness factors for the ring–shaped industrial catalysts were calculated on the basis of the active volume–equivalent slab. The temperature of the external burner wall was generated from a coupled simulation of the fire box and the reactor. They obtained the partial pressure and temperature profiles along the reactor. Intrinsic reaction rates and effectiveness factors in the reformer were also calculated.

Simulations of industrial–scale steam reforming usually differ in the way the furnace is modelled. In one of these modelling studies, Grevskott and coworkers (2001) investigated the radiation and convection heat transfer from the furnace to the reforming tubes. In the catalytic tube, they solved the conservation equations for the components and the energy balance, while in the furnace, conservation equation for energy including radiation was solved. When the design was such that heating was provided through burners attached to the wall of the furnace, the mode of heat transfer was radiation. However, feeding hot gas into the furnace from the opposite end resulted in lateral energy transfer through convection. The results showed that in the convective heat transfer mode, extent of methane conversion is closely related to pressure and velocity fields in the furnace.

Even though indirect heat transfer across the walls makes conventional steam reformers less attractive for use in mobile applications, efficient coupling of exothermic and endothermic reactions still needs to be considered. A countercurrent wall reactor concept for the autothermal coupling of high–temperature endothermic and exothermic reactions was discussed as a case study in order to demonstrate the importance of individual solutions (Kolios *et al*., 2004). The proposed reactor model featured the countercurrent heat exchange of two process streams as a prerequisite for efficient heat recovery. Depositing the reforming and combustion catalysts on opposite surfaces of the separating wall was thought to promote the direct thermal coupling of heat source and sinks. One–dimensional pseudohomogeneous reactor models were developed for both the exothermic and endothermic reaction zones, and by means of appropriate mathematical techniques, optimal temperature and conversion profiles of the reforming and combustion reactions were obtained. As an alternative to the countercurrent mode, the cocurrent mode in which combustion and reforming were initiated at the same end was also investigated.

Quinta Ferreira and coworkers (1992) also dealt with the steady–state operation of an industrial methane steam reformer employing large–pore catalysts in which convection as well as diffusion was taken into account. They built a complete two–dimensional heterogeneous model with diffusion and convection inside the solid particles, and a first–order kinetic model with respect to methane was used to calculate the rate of reaction. Consequently, large–pore catalysts were seen to have higher efficiencies, thus enhancing reaction rates and allowing a reduction in wall temperatures.

In order to perform a complete analysis of a steam reformer, the behavior under transient conditions, such as start–up, shutdown, change of operating conditions and feed disturbances in addition to behavior at steady–state should be investigated. Hence, dynamic simulation is required. Kvamsdal and coworkers (1999) developed a pseudohomogeneous two–dimensional dispersion model of the tubular side and a simple staged mixed flow model of the furnace of an industrial reformer. The reaction kinetics proposed by Xu and Froment (1989a) was included in the model. They studied the dynamic behavior of the reformer under two different scenarios, namely, suddenly stopping the feed flow of steam and stopping the feed flow of gas (CH_4, H_2, CO and CO_2). They also carried out an optimization study to find a value of the feed flow which maximized the methane conversion.

Presence of CO_2 in reforming product streams requires an additional separation step. It can be beneficial to couple reaction and separation within one single unit, which can lead to higher or sometimes complete conversion and purer product. Methane steam reforming in an adsorptive reactor is a typical example (Xiu *et al*., 2003). In an adsorptive reactor packed with an admixture of reforming catalyst and adsorbent for selectively removing CO_2 from the reaction zone, steam reforming is enhanced and the hydrogen–enriched product gas with traces of CO_2 can be directly produced. Once the adsorbent is saturated with CO_2, the regeneration of the adsorbent is performed by *in situ* pressure–swing adsorption. Xiu and coworkers (2003) analyzed the adsorption–enhanced reforming of methane by building a transient two–dimensional heterogeneous model taking into account component mass balances, an overall mass balance, an energy balance, and nonlinear adsorption equilibrium isotherm coupled with steam reforming reactions. The results showed that intraparticle diffusion resistances should be taken into account. In certain periods of reactor operation, the reforming rate was enhanced by adsorption.

A similar theoretical and experimental work on methane steam reforming coupled with simultaneous CO_2 removal was carried out by Lee and coworkers (2004). A one–dimensional pseudohomogeneous dynamic model was developed to describe both the CaO carbonation–enhanced reforming reaction at non–isothermal, non–adiabatic and non–isobaric operating conditions assuming that the rate of CaO carbonation in a local zone of the packed bed is governed by kinetic limitation or by mass transfer limitation of the reactant CO_2. After experimental verification of the model, a parametric study was conducted so as to realize the effects of feed temperature, pressure and composition. The range of operating conditions for the *in situ* CaO carbonation–enhanced reforming was also investigated.

2.5.2. Autothermal Reforming of Methane

In the context of this work, autothermal reforming (ATR) for hydrogen production is understood to be the combination of total catalytic combustion and steam reforming taking place in the same reaction zone with heat and mass transfer at the microscale. However, some authors use the term ATR for the coupling of the exothermic and endothermic reactions in a countercurrent (or cocurrent) wall reactor (Frauhammer *et al*., 1999; Kolios *et al*., 2000; Kolios *et al*., 2001; Kolios *et al*., 2002; Kolios *et al*., 2004; Springmann *et al*., 2003; Springmann *et al*., 2004).

Ma and Trimm (1996) experimentally investigated alternative catalyst bed configurations for the autothermal conversion of methane to hydrogen. In accordance with the relative positions of the bulk catalysts or active metals, the fixed–bed configurations were named dual–bed, mixed–bed and uniform–bed. The dual–bed consisted of oxidation catalyst placed upstream, and steam reforming catalyst downstream so that heat released by total oxidation triggered the reforming reaction. The same sequence of reactions was thought to hold in the mixed–bed configuration which was a physical mixture of the two catalysts. The uniform–bed (bimetallic) configuration involved the existence of two metals impregnated on the same support. While the mixed–bed configuration exhibited superior performance over the dual–bed, optimal performance was obtained when both metals were located on the same support. Autothermal reforming of methane in dual– and mixed–bed configurations was simulated by Avcı and coworkers (2000) at the experimental conditions and system parameters given by Ma and Trimm (1996) using a one–dimensional, pseudohomogeneous steady–state model. Despite the simplicity of the model involved, the simulation results showed general agreement with the experimental results. They also employed a one–dimensional, heterogeneous steady–state model for simulation of the same bench–scale reactor and an industrial–scale autothermal reforming reactor (Avcı *et al.*, 2001b). As expected, intraparticle diffusion limitations, especially in the Pt–based catalyst bed, were significant in the industrial–scale reactor.

An adiabatic fixed–bed indirect partial oxidation (IPOX) reactor for a 10–kW fuel cell application was simulated by de Smet and coworkers (2001) using a steady–state one–dimensional heterogeneous reactor model. External concentration and temperature gradients as well as intraparticle concentration gradients were taken into account. In order to investigate the influence of the reforming kinetics on the simulation results, two intrinsic models were considered: the reforming model proposed by Xu and Froment (1989a) and the model derived by Numaguchi and Kikuchi (1988). The kinetics of methane combustion were taken from Trimm and Lam (1980). Since the latter model was derived for supported Pt catalysts, the corresponding parameters were adjusted for Ni. Application of the two reforming models resulted in significantly different catalyst temperature profiles. A maximum was not observed when the model of Numaguchi and Kikuchi was used.

Hoang and Chan (2004) used a transient, two–dimensional heterogeneous model for the simulation of a Ni–based IPOX reactor. The model included the total oxidation kinetics proposed by Ma and coworkers (1996) and the methane steam reforming kinetics given by Xu and Froment (1989a). They conducted a parametric study to investigate the influence of carbon–to–oxygen and steam–to–carbon ratios, and the space velocity of the feed gas. Carbon–to–oxygen and steam–to–carbon ratios of 1.36 and 1, respectively, and space velocity of 20,000 h^{-1} were seen to be the optimal settings.

2.5.3. Catalytic Partial Oxidation of Methane

De Groote and Froment (1996) performed the simulation of the catalytic partial oxidation of methane on a Ni–based catalyst. The steam reforming reactions were considered to be parallel or more or less consecutive to total combustion, depending on the degree of reduction of the catalyst. The net rates of coke formation was included in the simulation as well. They used a steady–state one–dimensional, heterogeneous model. Since the reactor was chosen to be adiabatic, concentration and temperature gradients were thought to occur only in the axial direction. The only mode of transport in axial direction was the overall flow itself, and this was considered to be of the plug–flow type. Intraparticle diffusion limitations were expressed in terms of effectiveness factors. The effect of presence of CO_2 and steam in the feed mixture was investigated. It appeared from the simulations that the temperatures during the partial oxidation of methane to synthesis gas were within acceptable bounds when air was used or when steam or carbon dioxide were added to the feed. In partial oxidation of methane with oxygen, a maximum temperature of about 1500 °C was predicted. When steam was added, the amount of coking became negligible. CO_2 also reduced the amount of carbon formation, but increased the area on which coke deposited.

The reaction mechanism of direct catalytic partial oxidation of methane to synthesis gas over a platinum catalyst at high temperature and short contact times was studied with a detailed monolith reactor and reaction model (Veser and Frauhammer, 2000; Veser *et al.*, 2000). A one–dimensional heterogeneous reactor model with dispersion was used which also accounted for the surface reactions. The mechanism described all possible surface reaction intermediates for the considered partial and total oxidation routes with the exception of species appearing during methane decomposition since no experimental data are available for these intermediate steps. The simulations demonstrated a transition from an oxygen–covered surface at ignition to a carbon–covered surface under reaction conditions. This transition was accompanied by a switch of the primary reaction pathway from total to partial oxidation. Corresponding to this temporal development during ignition, the spatial reactor profiles under steady–state conditions showed a small oxygen–covered zone near the reactor entrance in which the surplus of surface oxygen led to total oxidation of the reactants and thus to a noticeable loss in reaction selectivity.

Behind this zone, a high carbon coverage built up on the catalyst surface, and the reaction switched to very selective synthesis gas formation. Based on these observations, a countercurrent heat–exchange reactor concept was suggested by the authors.

3. DYNAMIC MODELING AND SIMULATION OF AUTOTHERMAL METHANE CONVERSION

The mathematical models developed and numerical methods employed for the simulation of autothermal hydrogen production are presented in this chapter. A one−dimensional pseudohomogeneous model is used to describe fixed−bed reactor operation along with Langmuir−Hinshelwood−Hougen−Watson−type rate laws to estimate oxidation and steam reforming rates. The reactions and rate expressions already mentioned in Chapter 2 are renumbered here for convenience.

3.1. Introduction

Conversion of different fuels for hydrogen production needs to be quantitatively investigated to ensure optimal fuel cell operation. Avcı (2003) has considered hydrogen generation from methane and other fuels such as propane and methanol by indirect partial oxidation and the one−step direct partial oxidation. He has performed the simulation of the complete fuel processor/fuel cell assembly and obtained the hydrogen yield as a function of the amount of water and fuel fed into the system. In order to perform an in−depth analysis of the process regarding the start−up and its response to changes, however, a transient simulation is necessary. For this purpose, a dynamic model of the indirect partial oxidation reactor for methane conversion is developed and solved by using appropriate numerical methods. Also, the feed conditions are varied in order to determine their effects on the hydrogen yield and maximum reactor temperature.

3.2. The Modeling Procedure

Methane can be converted to hydrogen on a bimetallic Pt–Ni catalyst (Ma and Trimm, 1996) by indirect partial oxidation, the combination of total oxidation (TOX), steam reforming (SR) and water–gas shift (WGS) reactions:

$$CH_4 + 2O_2 \longrightarrow CO_2 + 2H_2O, \qquad \Delta H^0_{298} = -802.3\,\mathrm{kJ/gmol} \tag{3.1}$$

$$CH_4 + H_2O \longleftrightarrow CO + 3H_2, \qquad \Delta H^0_{298} = 206.2\,\mathrm{kJ/gmol} \tag{3.2}$$

$$CH_4 + 2H_2O \longleftrightarrow CO_2 + 4H_2, \qquad \Delta H^0_{298} = 165\,\mathrm{kJ/gmol} \tag{3.3}$$

$$CO + H_2O \longleftrightarrow CO_2 + H_2, \qquad \Delta H^0_{298} = -41.2\,\mathrm{kJ/gmol} \tag{3.4}$$

This process, carried out in an adiabatically operating fixed–bed reactor, is autothermal; that is, heat and part of the steam released by the exothermic total oxidation are harnessed by the endothermic steam reforming. The bimetallic catalyst is functional at temperatures up to 1100 K, above which deactivation is significant due to thermal sintering.

The first step in indirect partial oxidation is the initiation of catalytic combustion, also called surface ignition. Once triggered, the process involving oxidation and steam reforming sustains itself. However, the light–off temperature at which ignition takes place depends on the type of fuel being used and the inlet fuel/oxygen ratio. The light–off temperature is defined as the value at which 10 per cent of the oxidation conversion of the fuel is obtained (Ma *et al.*, 1996). Light–off temperature of methane oxidation at different carbon/oxygen ratios were given in Table 2.5.

3.2.1. Fixed–Bed Reactor Models

In fuel processor/fuel cell operation which involves partial oxidation, water–gas shift and preferential oxidation of carbon monoxide, fixed–bed reactors are employed. The gas–phase reactants are continuously fed into the reactor along which gas–solid reactions take place. The exit stream consists of products, unconverted reactants and inerts.

The reactor model is the combination of conservation equations of mass, energy and momentum, and the appropriate boundary conditions for the reaction system of interest. The reactor models can be grouped in two broad categories: pseudohomogeneous and heterogeneous. Pseudohomogeneous models do not account explicitly for the presence of the catalyst while heterogeneous models lead to separate conservation equations for fluid and catalyst. Within each category, the models are further classified in an order of growing complexity. The basic pseudohomogeneous one–dimensional model only considers transport by plug flow in the axial direction (nonmixing in the direction of flow). The two–dimensional model, on the other hand, accounts for radial gradients. The heterogeneous one–dimensional model considers only transport by plug flow again, but also accounts for interfacial gradients, that is, distinguishes between conditions in the fluid and on the solid. The next heterogeneous model considers both the interfacial and intraparticle gradients. Finally, the two–dimensional heterogeneous model accounts for radial gradients in the fluid phase as well as interfacial and intraparticle gradients (Froment and Bischoff, 1990).

One last classification of the models is according to their dependence on time. Steady–state models do not consider temporal variations of the conditions in contrast with dynamic models. The necessity of and the theory behind dynamic modeling of chemical reactors are covered in depth elsewhere (Elnashaie, 1996). For purposes stated previously, a dynamic reactor model is employed for the simulation of the indirect partial oxidation reactor in the present work. The results of the dynamic simulation are compared with those obtained by the quasi–steady–state model.

In order to gain insight into the transient operating characteristics of the reactor, the simplest of all models, that is, the pseudohomogeneous one–dimensional model is the choice, yet at the cost of accuracy of its outcome. Autothermal hydrogen production is considered to take place adiabatically so that the absence of heat transfer across the walls greatly eliminates radial concentration and temperature gradients. Therefore, inclusion of a second dimension is redundant.

3.2.2. Model Equations for the Steady and Dynamic Operation of the IPOX Reactor

Ma and Trimm (1996) experimentally investigated partial oxidation of methane in the presence of steam over Pt– and Ni–based catalysts placed in different configurations (Section 2.4.1). In this work, the configuration of interest is the mixed–bed which is the physical mixture of the two catalysts so that the occurrence of the oxidation and reforming reactions is simultaneous.

3.2.2.1. Steady–State Operation. The working equations for the steady–state one–dimensional pseudohomogeneous model are as follows:

$$\frac{dF_j}{dz} = A_c \rho_B R_j \tag{3.5}$$

$$\frac{dT}{dz} = \frac{A_c \rho_B \sum_{i=1}^{4} \left(-\Delta H_i r_i\right)}{\sum_{j=1}^{7} F_j c_{pj}} \tag{3.6}$$

$$\text{at } z = 0, \quad F_j = F_j^{in}; \quad T = T^{in} \qquad (j = 1, 2, ..., 7) \tag{3.7}$$

In Equations (3.5)–(3.7), i is the reaction index and j designates the component. Reactions (3.1)–(3.4) and seven components, namely CH_4, H_2O, CO, CO_2, H_2, O_2 and N_2

are involved in indirect partial oxidation. A_c is the cross–sectional area of the reactor tube (m^2), c_{pj} the temperature–dependent gas–phase heat capacity of component j (J $gmol^{-1}$ K^{-1}), ρ_B the bulk catalyst density (kgcat m^{-3}_{reactor}), F_j the molar flow rate of component j (kmol s^{-1}), ΔH_i the heat of reaction i at temperature T (J $gmol^{-1}$), $-r_i$ the rate of reaction i (gmol $kgcat^{-1}$ h^{-1}), R_j the total rate of consumption or generation of component j (gmol $kgcat^{-1}$ h^{-1}), F_j^{in} the inlet flow rate of component j ($\text{kmol}\,\text{s}^{-1}$), and T^{in} the temperature of the feed. The parameters required to evaluate the temperature–dependent heat capacities are reported in Appendix A.

The rate of total oxidation is calculated using the rate law proposed by Ma and coworkers (1996):

$$-r = \frac{k_1 K^c_{\mathrm{CH_4}} p_{\mathrm{CH_4}} \sqrt{K^c_{\mathrm{O_2}} p_{\mathrm{O_2}}}}{\left(1 + K^c_{\mathrm{CH_4}} p_{\mathrm{CH_4}} + \sqrt{K^c_{\mathrm{O_2}} p_{\mathrm{O_2}}}\right)^2} \tag{3.8}$$

In Equation (3.8), k_1 is the rate constant (kmol $kgcat^{-1}$ h^{-1}), $K^c_{\mathrm{CH_4}}$ and $K^c_{\mathrm{O_2}}$ are the adsorption constants for methane and oxygen (bar^{-1}), respectively, and $p_{\mathrm{CH_4}}$ and $p_{\mathrm{O_2}}$ are the partial pressures of the indexed species (bar). The temperature dependence of the constants is expressed by an equation of the Arrhenius type whose parameters are given in Table 3.1. These parameters are estimated by the method of least squares using the experimental data reported in the work of Ma and coworkers (1996).

The rate of methane steam reforming is estimated using two different rate laws, namely that of Xu and Froment (1989a) and of Numaguchi and Kikuchi (1988). The latter excludes steam reforming to CO_2 represented by Reaction (3.3); but, in contrast with the rate law proposed by Xu and Froment, it does not suffer from a singularity arising from the presence of the hydrogen partial pressure in the denominator. Tables 3.2 and 3.3 give the rate laws pertinent to Reactions (3.2)–(3.4), and the parameters for the Arrhenius–type equation to calculate the rate constants, adsorption/desorption and reaction equilibrium constants, respectively. Even though the reaction equilibrium constants K^i_{eq} (i = 2, 3, 4) may also be evaluated using the van’t Hoff relation (Avcı, 2003), the practical approximations proposed by Xu and Froment (1989a) are chosen instead.

Table 3.1. Parameters for calculation of the rate and adsorption constants in Equation (3.8)

	k_{oi} (kmol kgcat^{-1} h^{-1})	E_1 (kJ kmol^{-1})
$k_1 = k_{1o} \exp\left(-\dfrac{E_1}{RT}\right)$	135.587	$-34{,}153$
	$K^c_{\mathrm{CH_4},o}$ (bar^{-1})	$\Delta H^c_{\mathrm{CH_4}}$ (kJ kmol^{-1})
$K^c_{\mathrm{CH_4}} = K^c_{\mathrm{CH_4},o} \exp\left(-\dfrac{\Delta H^c_{\mathrm{CH_4}}}{RT}\right)$	3×10^{17}	$-231{,}680$
	$K^c_{\mathrm{O_2},o}$ (bar^{-1})	$\Delta H^c_{\mathrm{O_2}}$ (kJ kmol^{-1})
$K^c_{\mathrm{O_2}} = K^c_{\mathrm{O_2},o} \exp\left(-\dfrac{\Delta H^c_{\mathrm{O_2}}}{RT}\right)$	2×10^{23}	$-306{,}191$

Table 3.2. Rate equations for methane steam reforming

Reaction	Rate Equation	Reference
(3.2)	$-r_2 = \dfrac{k_2 / p^{2.5}_{\mathrm{H_2}} \left(p_{\mathrm{CH_4}} p_{\mathrm{H_2O}} - p^3_{\mathrm{H_2}} p_{\mathrm{CO}} / K^{\mathrm{I}}_{\mathrm{eq}}\right)}{DEN^2}$ (3.9)	Xu and Froment (1989a)
(3.3)	$-r_3 = \dfrac{k_3 / p^{3.5}_{\mathrm{H_2}} \left(p_{\mathrm{CH_4}} p^2_{\mathrm{H_2O}} - p^4_{\mathrm{H_2}} p_{\mathrm{CO_2}} / K^{\mathrm{II}}_{\mathrm{eq}}\right)}{DEN^2}$ (3.10)	
(3.4)	$-r_4 = \dfrac{k_4 / p_{\mathrm{H_2}} \left(p_{\mathrm{CO}} p_{\mathrm{H_2O}} - p_{\mathrm{H_2}} p_{\mathrm{CO_2}} / K^{\mathrm{III}}_{\mathrm{eq}}\right)}{DEN^2}$ (3.11)	
(3.2)	$-r_2 = \dfrac{k_1 \left(p_{\mathrm{CH_4}} - p^3_{\mathrm{H_2}} p_{\mathrm{CO}} / K^{\mathrm{I}}_{\mathrm{eq}}\right)}{p^{0.596}_{\mathrm{H_2O}}}$ (3.12)	Numaguchi and Kikuchi (1988)
(3.4)	$-r_4 = k_4 \left(p_{\mathrm{CO}} - p_{\mathrm{H_2}} p_{\mathrm{CO_2}} / K^{\mathrm{III}}_{\mathrm{eq}}\right)$ (3.13)	

$$DEN = \left(1 + K_{\mathrm{CO}} p_{\mathrm{CO}} + K_{\mathrm{H_2}} p_{\mathrm{H_2}} + K_{\mathrm{CH_4}} p_{\mathrm{CH_4}} + K_{\mathrm{H_2O}} p_{\mathrm{H_2O}} / p_{\mathrm{H_2}}\right)$$

Table 3.3. Parameters for calculation of the rate and adsorption constants in Equations (3.9)–(3.13)

Xu and Froment (1989a)			Numaguchi and Kikuchi (1988)	
Reaction	k_{oi} (gmol kgcat^{-1} s^{-1})	E_i (kJ kmol^{-1})	k_{oi} (gmol kgcat^{-1} s^{-1})	E_i (kJ kmol^{-1})
(3.2)	1.17×10^{15} bar$^{-0.5}$	240,100	2.62×10^{5} bar$^{-0.404}$	106,900
(3.3)	2.83×10^{14} bar$^{-0.5}$	243,900		
(3.4)	5.43×10^{5} bar^{-1}	67,130	2.45×10^{2} bar^{-1}	54,500
Species	K_{oj} (bar^{-1})	ΔH_j (kJ kmol^{-1})	Equilibrium Constants	
CH_4	6.65×10^{-4}	–38,280	$K_{eq}^{I} = 4.707\times10^{12}\exp\left(-\frac{224{,}000}{RT}\right)$ bar^2	
H_2O	1.77×10^{5}	88,680	$K_{eq}^{III} = .1.142\times10^{-2}\exp\left(-\frac{37{,}300}{RT}\right)$	
CO	8.23×10^{-5}	–70,650	$K_{eq}^{II} = K_{eq}^{I}K_{eq}^{III}$ bar^2	
H_2	6.12×10^{-9}	–82,900		

3.2.2.2. Dynamic Operation. The equations for the steady–state model also hold for the dynamic model with the addition of the time–dependent concentration and temperature terms which lead to a system of hyperbolic partial differential equations (PDE):

$$\varepsilon_{bed}\frac{\partial c_j}{\partial t} = -\frac{1}{A_c}\frac{\partial F_j}{\partial z} + \rho_B R_j \tag{3.14}$$

$$\varepsilon_{bed}\sum_{j=1}^{7}\left(c_j c_{pj}\right)\frac{\partial T}{\partial t} = -\frac{\sum_{j=1}^{7}\left(F_j c_{pj}\right)}{A_c}\frac{\partial T}{\partial z} + \rho_B\sum_{i=1}^{4}\left(-\Delta H_i\right)r_i \tag{3.15}$$

$$\text{at } t = 0, \quad F_j = F_{j0}; \quad T = T_0 \tag{3.16}$$

$$z = 0, \quad F_j = F_j^{in}; \quad T = T^{in} \tag{3.17}$$

The variables and their units in Equations (3.14)–(3.17) are the same as those for the steady–state model. In addition, ε_{bed} denotes bed void fraction, c_j the concentration of component j (kmol cm^{-3}), F_{j0} the initial flow rate of component j (kmol s^{-1}) and T_0 the initial reactor temperature (K).

Effect of volume change in gas–phase plug–flow reactors is usually neglected when the difference between the amounts of reactants and products is small. However, Reactions (3.2) and (3.3) reveal that volume change needs to be included in the model since three and four moles of hydrogen are respectively produced from one mole of methane. The steady–state model captures this effect implicitly while an extra equation is necessary in the dynamic model. This arises from the relation $F_j = c_j v$, which is used for conversion from concentration to flow rate in Equations (3.14) and (3.15) during the simulation. Volume change with reaction is evaluated by the following relation (Fogler, 1999):

$$v = v^{in}\left(\frac{F_T}{F_T^{in}}\right)\frac{p_T^{in}}{p_T}\left(\frac{T}{T^{in}}\right) \tag{3.18}$$

where v is the volumetric flow rate anywhere in the reactor at any time, F_T and T the total flow rate and temperature anywhere in the bed at any time. Differentiating Equation (3.18) with respect to the spatial coordinate z and neglecting pressure drop, one obtains

$$\frac{dv}{dz} = \frac{v^{in}}{F_T^{in}T^{in}}\left[T\frac{dF_T}{dz} + F_T\frac{dT}{dz}\right] \tag{3.19}$$

The time dependence of v is handled implicity through the dependence of F_T and T by Equations (3.14) and (3.15) with which Equation (3.19) is coupled at each time step.

3.3. Numerical Methods

The differential mole and energy balances, Equations (3.5)–(3.7), comprising the steady–state model form a system of ordinary differential equations (ODE) that are solved using a non–stiff, low–order ODE solver, the "ode23" function of the MATLAB^{TM} numerical computation software.

The system of hyperbolic partial differential equations (3.14)–(3.17) and the ordinary differential equation (3.19), modeling the dynamic operation of the reactor, are solved using a finite difference scheme. If the one–dimensional domain is divided into M intervals with M + 1 nodes, and the temporal and spatial derivatives are approximated by central differences, the following explicit scheme is obtained:

$$\frac{\left(c_j\right)_m^{n+1}-\frac{1}{2}\left[\left(c_j\right)_{m+1}^n-\left(c_j\right)_{m-1}^n\right]}{\Delta t}=-\frac{1}{\varepsilon_{bed}A_c}\frac{\left(F_j\right)_{m+1}^n-\left(F_j\right)_{m-1}^n}{2\Delta z}+\frac{\rho_B\left(R_j\right)_m^n}{\varepsilon_{bed}} \qquad (3.20)$$

$$j=1,2,\ldots,7, \qquad m=1,2,\ldots M$$

$$\frac{T_m^{n+1}-\frac{1}{2}\left[T_{m+1}^n-T_{m-1}^n\right]}{\Delta t}=-\frac{1}{\varepsilon_{bed}\left(\sum_{j=1}^{7}\left(c_jc_{pj}\right)\right)_m^n A_c}\frac{T_{m+1}^n-T_{m-1}^n}{2\Delta z}+\frac{\rho_B\sum_{i=1}^{4}\left(-\Delta H_i\right)r_i}{\varepsilon_{bed}\left(\sum_{j=1}^{7}\left(c_jc_{pj}\right)\right)_m^n} \qquad (3.21)$$

Δt is the time step (seconds) and Δz the grid size (cm). At each time step, the value of the variables are calculated at every m, and these are used as input for the next time stepping. This is the so–called Lax–Friedrichs finite difference scheme which is first–order accurate (Strikwerda, 1989; LeVeque, 2002). In order to ensure stability during time stepping, the variables at time n are approximated as the average of their values at (m – 1)th and (m + 1)th nodes instead of simple forward differencing, i.e. $\left(C_j\right)_m^{n+1}-\left(C_j\right)_m^n$ or $T_m^{n+1}-T_m^n$. Furthermore, according to the Courant–Friedrichs–Levy (CFL) criterion (Strikwerda, 1989; LeVeque, 2002), the system retains its stability as long as

$$\left(\frac{1}{\varepsilon_{bed} A_c}\right)\frac{\Delta t}{\Delta x} \leq 1 \tag{3.22}$$

The Dirichlet boundary conditions are given by Equation (3.17). At the end of the reactor domain, a hypothetical node (M + 1) must be included for computation, so an artificial boundary condition is needed which is of the Neumann type that specifies the derivative of the function:

$$\frac{\partial f}{\partial z} = 0 \qquad \text{at} \quad z = L \tag{3.23}$$

A computer code consisting of several subroutines for evaluation of the reaction rates, heat capacities and heat of reactions is prepared, and the Lax–Friedrichs scheme for the solution of the system of partial differential equations is implemented in MATLAB$^{\text{TM}}$ software and run on the Hewlett–Packard xw6200 Workstation.

4. RESULTS AND DISCUSSION

4.1. Simulation of Autothermal Hydrogen Production from Methane

An autothermal, dual catalyst, fixed–bed reaction system proposed for hydrogen production from methane is mathematically investigated using different feed ratios. The fixed–bed consists of the physical mixture of the oxidation and reforming catalysts, Pt/δ–Al_2O_3 and Ni/MgO–Al_2O_3 (Ma and Trimm, 1996). Steady–state reactor operation at different feed ratios is analyzed via a series of simulations by using the one–dimensional pseudohomogeneous fixed–bed reactor model.

Dynamic reactor operation at different feed ratios is also analyzed. Start–up behavior of autothermal reforming subject to conditions similar to those of steady–state operation is investigated by a series of dynamic simulations in order to capture occurrences such as an excessive temperature rise that hinders safe and practical operation and which remains hidden in the course of a steady–state simulation. The response of the reactor to a disturbance in the feed which is initially at steady state is also analyzed.

The operating conditions and reactor data used in the steady–state and dynamic simulations are given in Table 4.1. Operating conditions and data pertinent to dynamic simulations only are presented separately. The amount of methane fed is kept constant at each run. The reaction system and the reactor model were explained in detail in Sections 3.2.1 and 3.2.2, respectively.

Table 4.1. Operating conditions and reactor data

T^{in} (K)	800	W_T (kg)	5×10^{-4}
F_{CH_4} (kmol s^{-1})	4.65×10^{-8}	d_r (m)	1.3×10^{-3}
p_T (atm)	2.9	ρ_B (kg m^{-3})	1167.3

4.1.1. Bench–Scale Reactor Simulations

<u>4.1.1.1. Steady–State Simulations.</u> Apart from carbon–to–oxygen and steam–to–carbon ratios, another reactor operating parameter is the gas hourly space velocity (GHSV), defined as the amount of gas flowing in the reactor (m^3 gas/m^3 reactor–h) at standard temperature and pressure. By adjusting the GHSV, the amount of methane fed into the reactor is kept constant. The space velocities reported in the experimental study of Ma and Trimm (1996) are adapted for the simulation task. In all cases, the feed mixture is comprised of methane, air and steam. The presence of hydrogen partial pressure in the model of Xu and Froment (1989a) necessitates that a small amount of hydrogen be also fed. A value of 10^{-20} is assigned as the hydrogen inlet flow rate in the simulations, thus keeping the real–life assumption intact that the feed does not contain hydrogen.

The feed conditions used as input parameters, outcome of the simulations, namely, oxidation and reforming conversion of methane, product yields at the reactor exit and maximum temperature in the reactor are given in Table 4.2. The reactor simulation is conducted at each feed condition using the rate laws of both XF (Xu and Froment, 1989a) and NK (Numaguchi and Kikuchi, 1988).

The flow rates, mole fraction and temperature profiles along the length of the reactor are shown in Figures 4.1 to 4.12.

The results in Table 4.2 and Figures 4.1, 4.2, 4.5 and 4.6 show that at constant steam–to–methane ratio, a decrease in the methane–to–oxygen ratio should be expected to lead to an increase in the hydrogen yield and to elevated maximum bed temperatures. Increasing the molar flow rate of oxygen in the feed will result in combustion of more methane, hence more heat will be released by total oxidation. Higher bed temperatures will enhance endothermic steam reforming reactions and result in higher hydrogen yields. The results obtained by using two different rate laws for steam reforming (XF and NK) are in general agreement except in predicting the carbon monoxide yield.

Table 4.2. Bench–scale simulation outputs in mixed–bed scheme

Feed conditions (Ma and Trimm, 1996)			x_{CH_4} †		y_{H_2} ‡		y_{CO} ‡		T_{max} (K)	
CH_4/O_2	H_2O/CH_4	GHSV (h^{-1})	XF	NK	XF	NK	XF	NK	XF	NK
2.24	1.17	37,600	86.17	82.60	197.06	202.06	58.36	44.91	999.51	998.56
1.89	1.17	41,100	96.92	95.60	210.93	225.80	70.93	53.71	1064.39	1069.44
1.89	1.56	44,500	97.23	91.97	217.98	218.19	65.10	50.49	1052.60	1046.22
1.89	2.34	51,300	97.62	86.02	229.44	203.25	55.21	46.00	1032.24	1024.82

† Methane conversion: Moles of methane reacted/100 moles of methane fed

‡ Product yield: Moles of product obtained/100 moles of methane fed

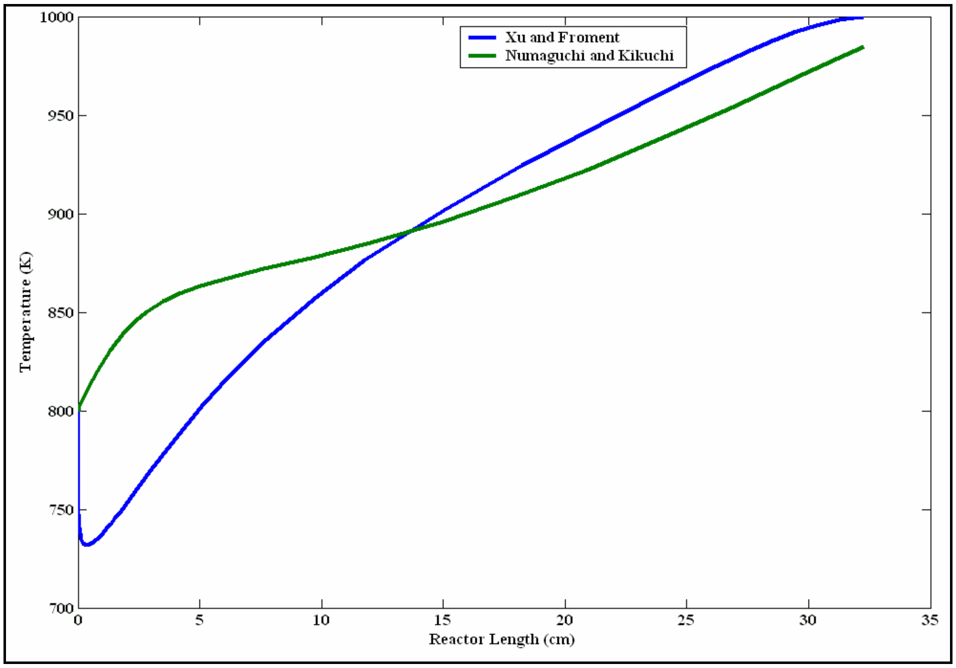

Figure 4.1. Temperature profiles (CH_4/O_2 = 2.24, H_2O/CH_4 = 1.17)

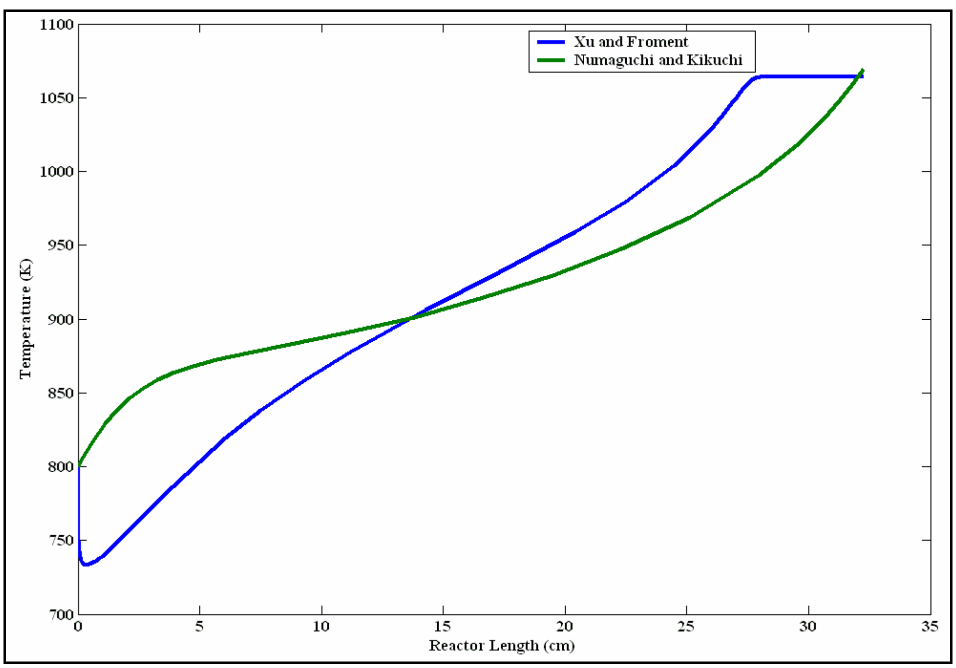

Figure 4.2. Temperature profiles (CH_4/O_2 = 1.89, H_2O/CH_4 = 1.17)

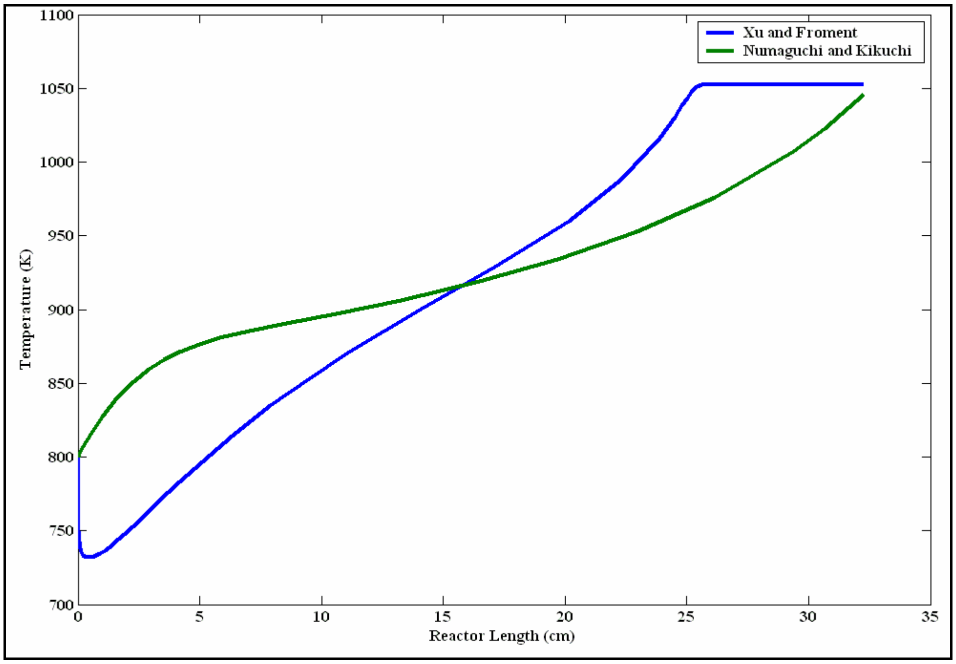

Figure 4.3. Temperature profiles (CH_4/O_2 = 1.89, H_2O/CH_4 = 1.56)

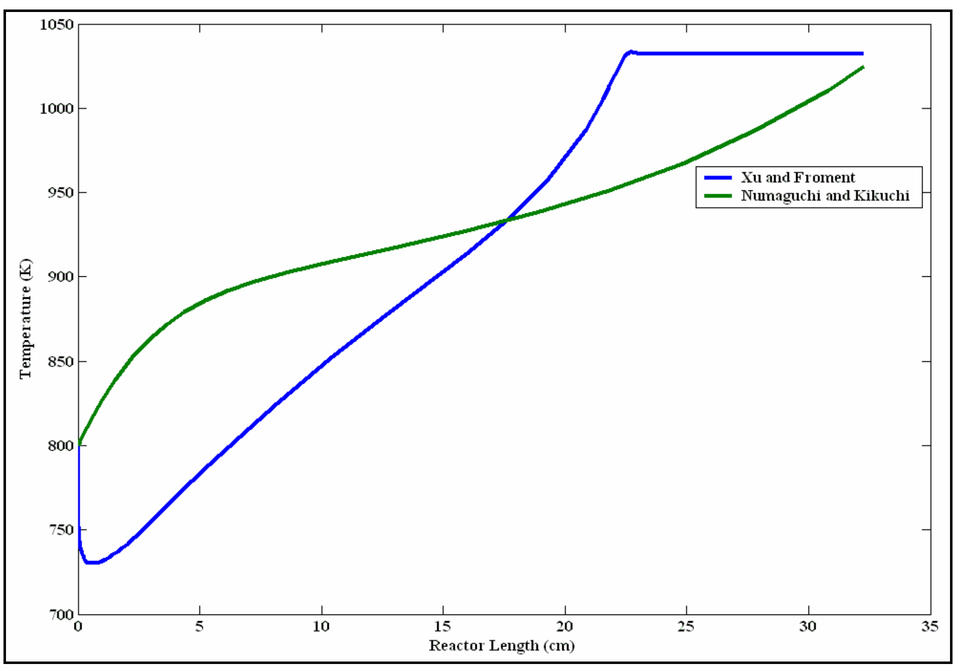

Figure 4.4. Temperature profiles (CH_4/O_2 = 1.89, H_2O/CH_4 = 2.34)

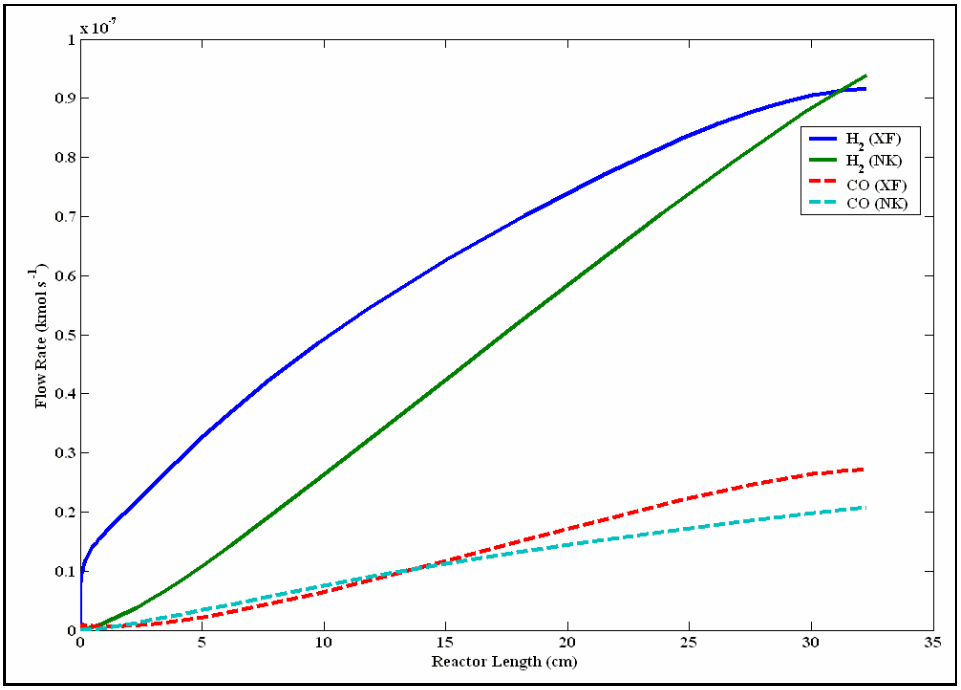

Figure 4.5. Variation of H_2 and CO flow rates along the length of the reactor ($CH_4/O_2 = 2.24$, $H_2O/CH_4 = 1.17$)

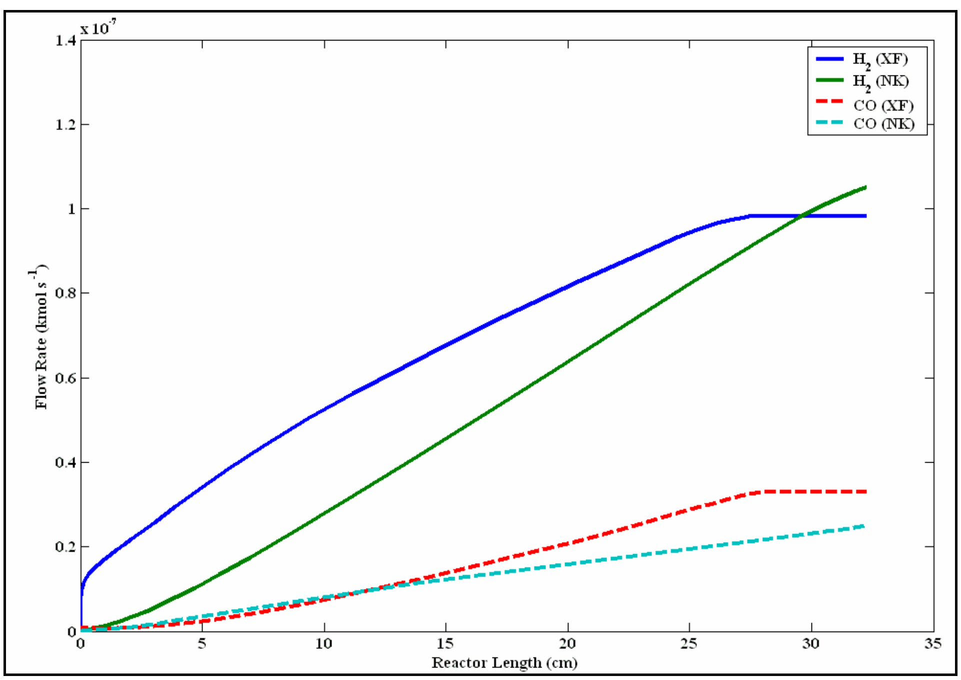

Figure 4.6. Variation of H_2 and CO flow rates along the length of the reactor ($CH_4/O_2 = 1.89$, $H_2O/CH_4 = 1.17$)

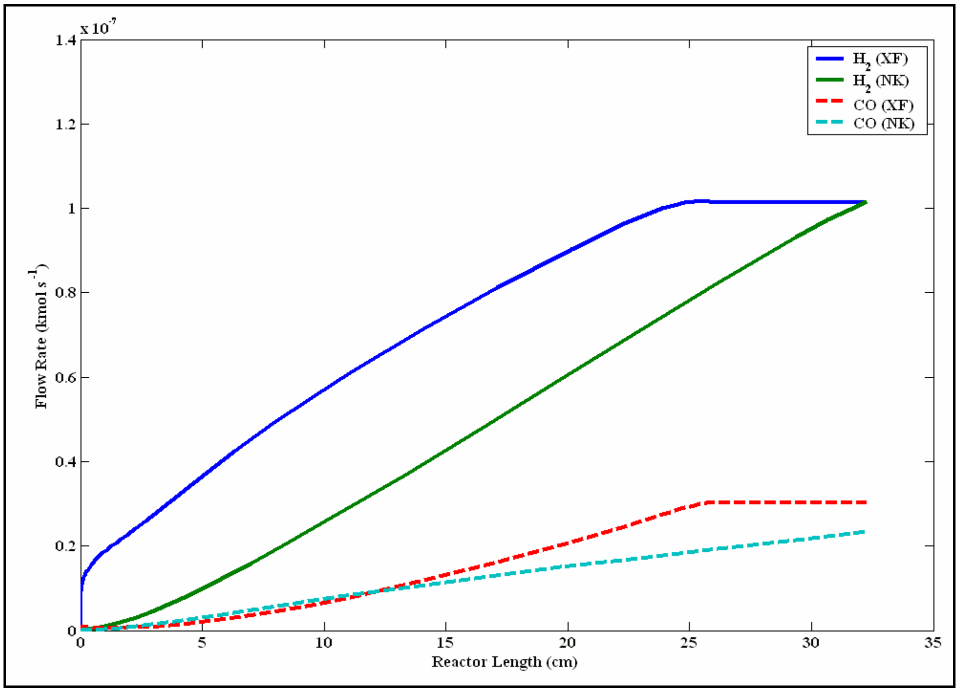

Figure 4.7. Variation of H_2 and CO flow rates along the length of the reactor ($CH_4/O_2 = 1.89$, $H_2O/CH_4 = 1.56$)

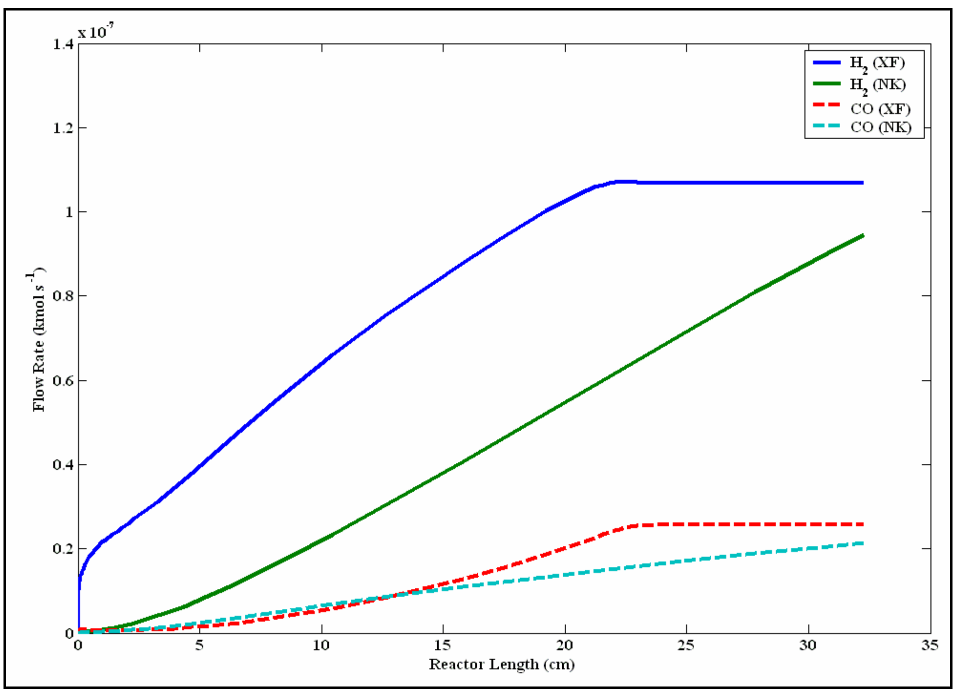

Figure 4.8. Variation of H_2 and CO flow rates along the length of the reactor ($CH_4/O_2 = 1.89$, $H_2O/CH_4 = 2.34$)

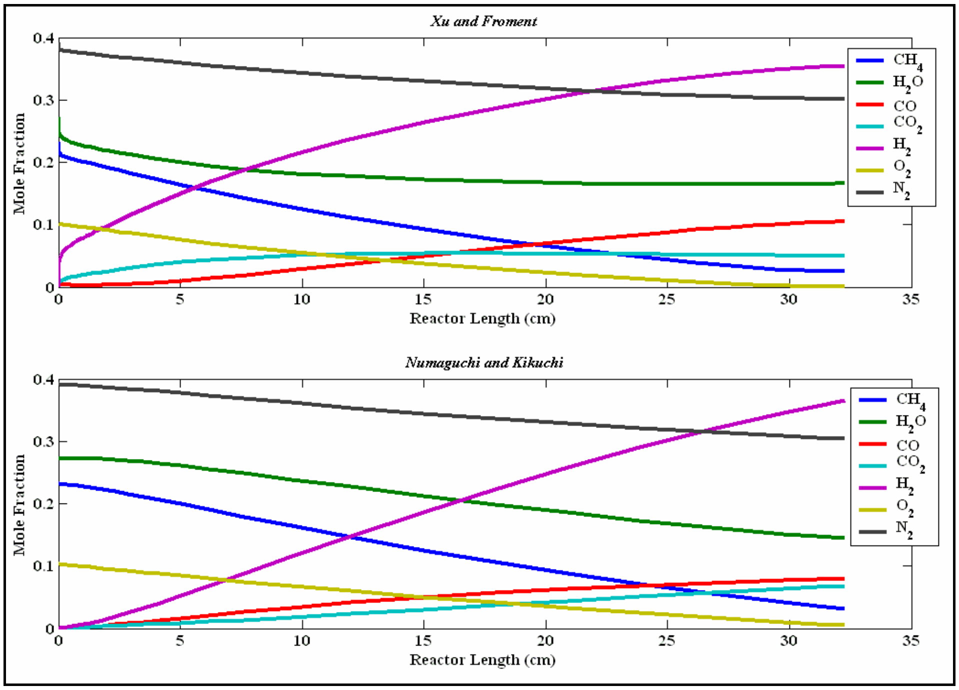

Figure 4.9. Mole fraction profiles ($CH_4/O_2 = 2.24$, $H_2O/CH_4 = 1.17$)

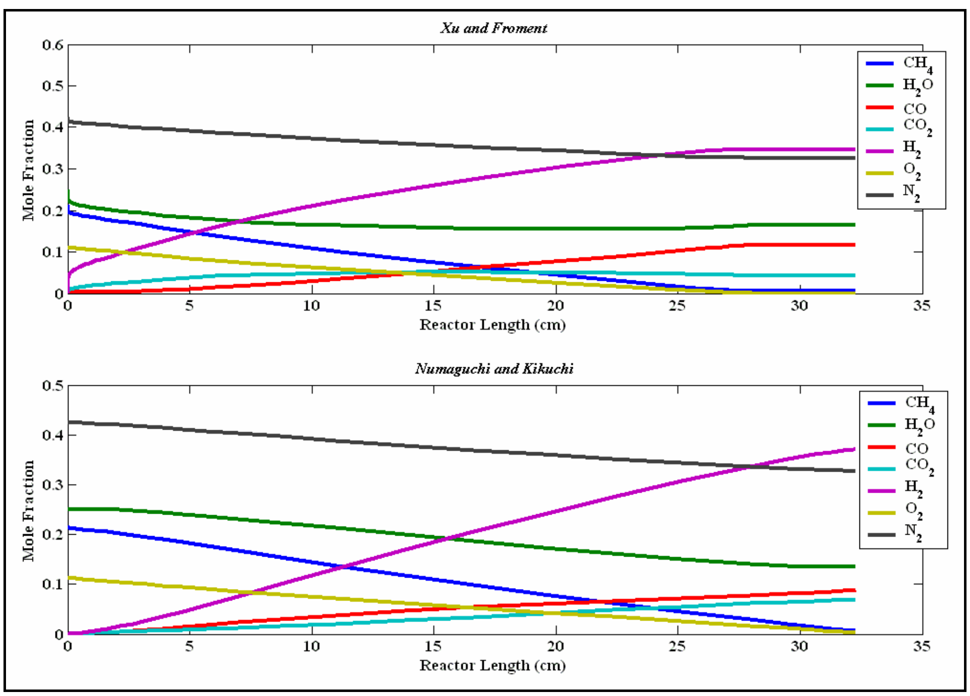

Figure 4.10. Mole fraction profiles ($CH_4/O_2 = 1.89$, $H_2O/CH_4 = 1.17$)

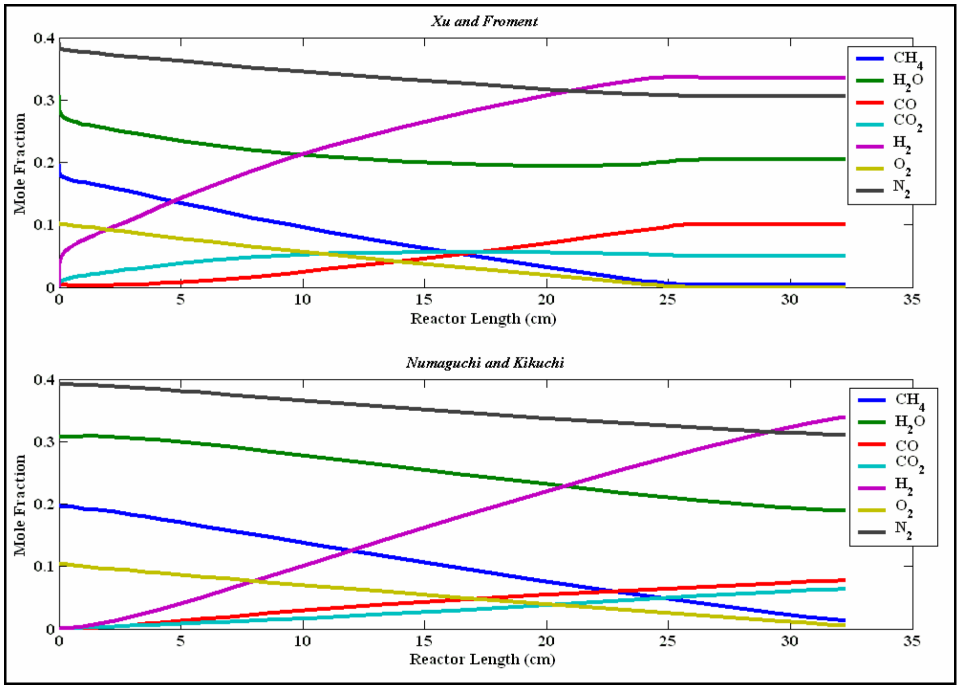

Figure 4.11. Mole fraction profiles ($CH_4/O_2 = 1.89$, $H_2O/CH_4 = 1.56$)

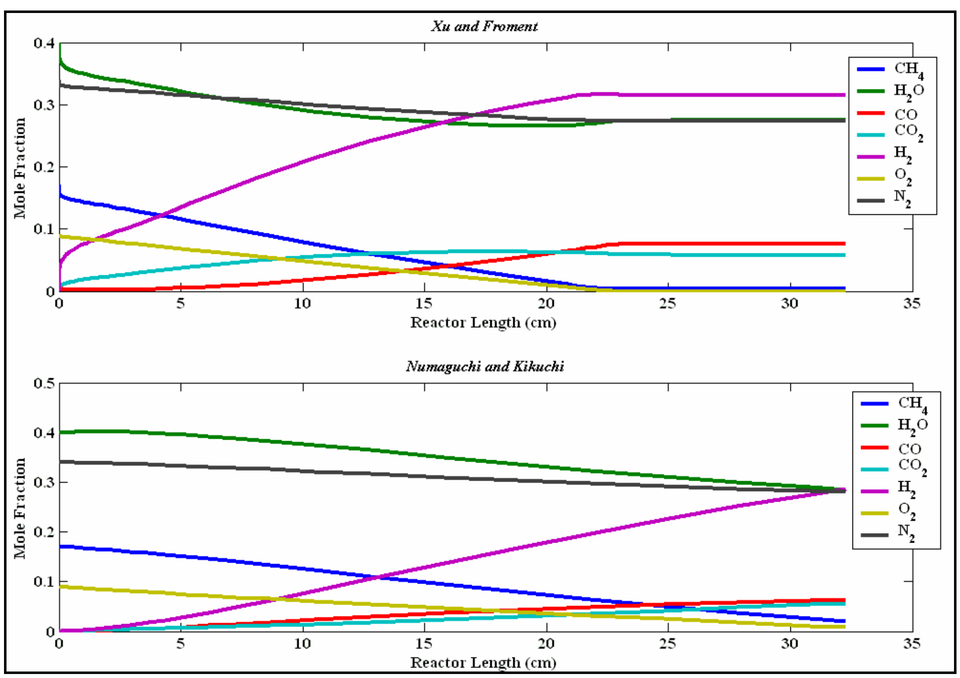

Figure 4.12. Mole fraction profiles ($CH_4/O_2 = 1.89$, $H_2O/CH_4 = 2.34$)

The results also indicate that at constant methane–to–oxygen ratio, an increase in the inlet molar flow rate of steam lowers the maximum bed temperature (Figures 4.2–4.4 and 4.6–4.8). A possible explanation to this phenomenon is that heat transfer between the Pt and Ni sites on the catalysts is facilitated by steam. In addition, methane conversion at constant methane–to–oxygen ratio slightly increases as the inlet steam–to–carbon ratio is increased in the case of simulations with the XF model, whereas a decrease is observed in the case of the NK model (Table 4.2). Also, carbon monoxide yield decreases as the inlet steam flow rate increases, indicating that the water–gas shift equilibrium reaction is shifted by excess steam towards the formation of products (Figures 4.6–4.8). The NK model does not take into account direct steam reforming to carbon dioxide, thus due to the relatively smaller amount of CO_2 in the reactor, equilibrium is further shifted to the right which decreases the carbon monoxide yield.

According to the mole fraction profiles, 30–40 per cent of the product stream is hydrogen. However, steam partial pressure increases as the inlet steam flow rate is increased (Figures 4.10–4.12). The presence also of the inert nitrogen requires downstream processing if the hydrogen is to be used in applications other than a fuel cell.

In Figures 4.1 through 4.4, independent of the feed conditions, a sudden temperature decrease at the reactor entrance is observed with the XF model due to the rapid steam reforming reactions which take place around 800 K, even before the reactor temperature is allowed to rise. As for the profiles with the NK rate law which models the reforming reaction rather slowly, the reforming rate at the reactor entrance is comparably lower. In all simulations with both models, hot spot formation is not a problem, at least at steady state. It can tentatively be said that catalytic operation is not likely to be halted by excessive temperatures, which are, in all cases simulated, less than 1100 K along the reactor. However, this claim must be verified by the results from a dynamical analysis.

<u>4.1.1.2. Start–up Behavior.</u> The temperature profiles obtained by steady–state simulation show that in the case of the model proposed by Xu and Froment, steep gradients exist at the reactor inlet due to the fast reforming rate. In order to ensure accuracy and stability, a very small spatial grid size in the order of 10^{-30} cm should be used within a few centimeters

from the entrance, hence an extremely small time step. Without a method adaptive both in space and time, solution of the model equations is costly due to prolonged computation and computer memory restrictions. The model of Numaguchi and Kikuchi, on the other hand, is easier to handle at a moderate grid size (3.25 cm) and time step (4–5.5 × 10^{-4} s). The product yields and temperature profiles at steady–state show that downstream behavior of each is acceptably close to one another, so the NK model is used to perform the dynamic simulations.

It should be emphasized that start–up of the reactor and start–up of autothermal reforming are considered to be two different phenomena. In the case of reactor start–up, there is no flow in the reactor initially. At t = 0, flow of air (or a nonreactive mixture consisting of air and steam) is allowed at a predetermined rate, the dynamics of which is governed solely by the laws of fluid dynamics. Once the flow rate and temperature settle to a steady–state value, the reactive mixture consisting of methane, air and steam is fed into the reactor. This is called the start–up of autothermal reforming.

For simplicity, it is assumed that the nonreactive mixture (air in this work) is initially flowing at the same GHSV and temperature as the reactive mixture that is to be fed at the start–up of autothermal reforming. The operating conditions and reactor data are presented in Table 4.1. The void fraction of the catalyst bed is also needed, and it is taken to be 0.45 (Hoang and Chan, 2004). The initial and feed conditions are given in Table 4.3. At t = 0 air is flowing at steady state.

Table 4.3. Initial and feed conditions for dynamic reactor simulation

Run	$t = 0$ Nonreactive Flow (Air)		$t > 0$ Reactive Flow (CH_4, H_2O, O_2)			
	GHSV (h^{-1})	Temperature (K)	CH_4/O_2	H_2O/CH_4	GHSV (h^{-1})	T^{in} (K)
1	37,600	800	2.24	1.17	37,600	800
2	41,100	800	1.89	1.17	41,100	800
3	44,500	800	1.89	1.56	44,500	800
4	51,300	800	1.89	2.34	51,300	800

Simulation of the start–up of autothermal reforming subject to different initial and boundary conditions (Table 4.3) shows that temperature increase in the spatial (axial) direction is monotonic, that is, there is no occurrence of either a hotspot or a minimum, which is consistent with the results obtained from steady–state simulations. Likewise, temporal increase in temperature at every point of the reactor is observed until steady state is reached. The duration of transient operation is between 100 and 120 seconds, depending on the initial configuration and feed condition (Figures 4.13–4.16).

The steady–state product or exit temperatures T_{exit}^{SS} at each run, predicted by steady–state and dynamic simulations are presented in Table 4.4 for comparison. The considerable difference in the figures is due to the first–order accuracy of the Lax–Friedrichs finite difference scheme. Yet, the results obtained by dynamic simulation conform to the expectation that a decrease in the methane–to–oxygen ratio leads to higher temperatures, which in turn increases the hydrogen yield (cf. Runs 1 and 2). Also, at constant methane–to–oxygen ratio, an increase in the steam flow rate lowers the bed temperature (cf. Runs 2, 3 and 4). Although catalytic operation is not expected to be adversely affected at these conditions, the exit temperatures in Runs 2 and 3 are critically high, which, in case of a disturbance, may begin increasing indefinitely (run–away situation), hence posing threat to the catalyst.

Table 4.4. Methane conversion, product yields and temperatures at steady state

Run	Steady–State Simulation				Dynamic Simulation			
	$x_{CH_4}^{SS}$ †	$y_{H_2}^{SS}$ ‡	y_{CO}^{SS} ‡	T_{exit}^{SS} (K)	$x_{CH_4}^{SS}$ †	$y_{H_2}^{SS}$ ‡	y_{CO}^{SS} ‡	T_{exit}^{SS} (K)
1	82.60	202.06	44.91	998.56	71.37	219.66	48.86	978.53
2	95.60	225.80	53.71	1069.44	88.80	297.86	73.04	1081.87
3	91.97	218.19	50.49	1046.22	86.28	277.49	66.16	1072.32
4	86.02	203.25	46.00	1024.82	82.82	253.66	58.33	1066.28

† Methane conversion: Moles of methane reacted/100 moles of methane fed
‡ Product yield: Moles of product obtained/100 moles of methane fed

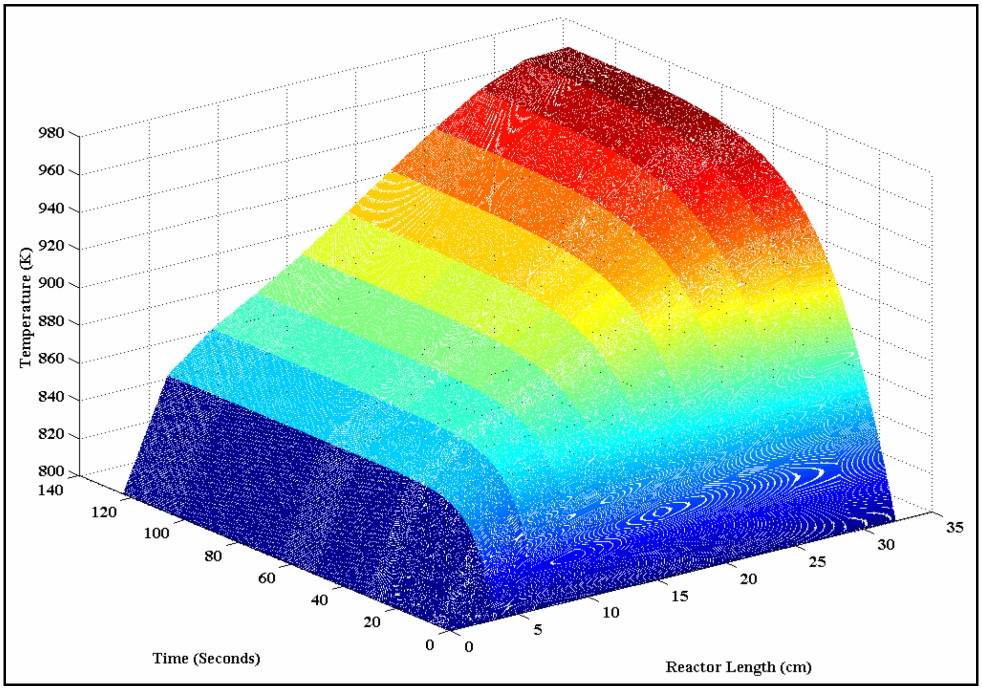

Figure 4.13. Reactor temperature as a function of time and reactor length (CH_4/O_2 = 2.24, H_2O/CH_4 = 1.17)

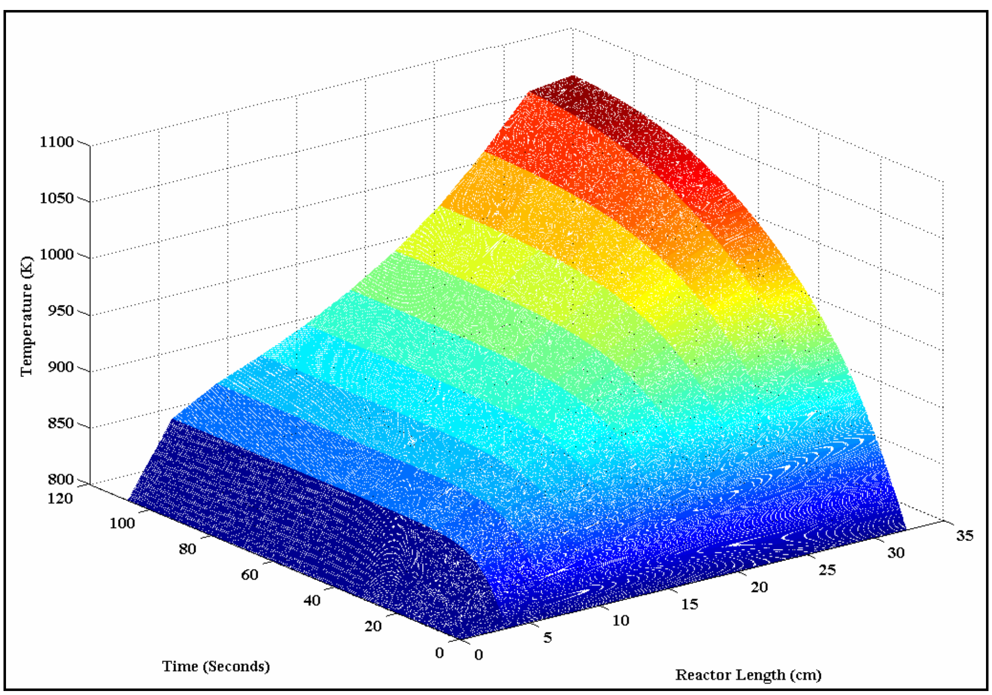

Figure 4.14. Reactor temperature as a function of time and reactor length (CH_4/O_2 = 1.89, H_2O/CH_4 = 1.17)

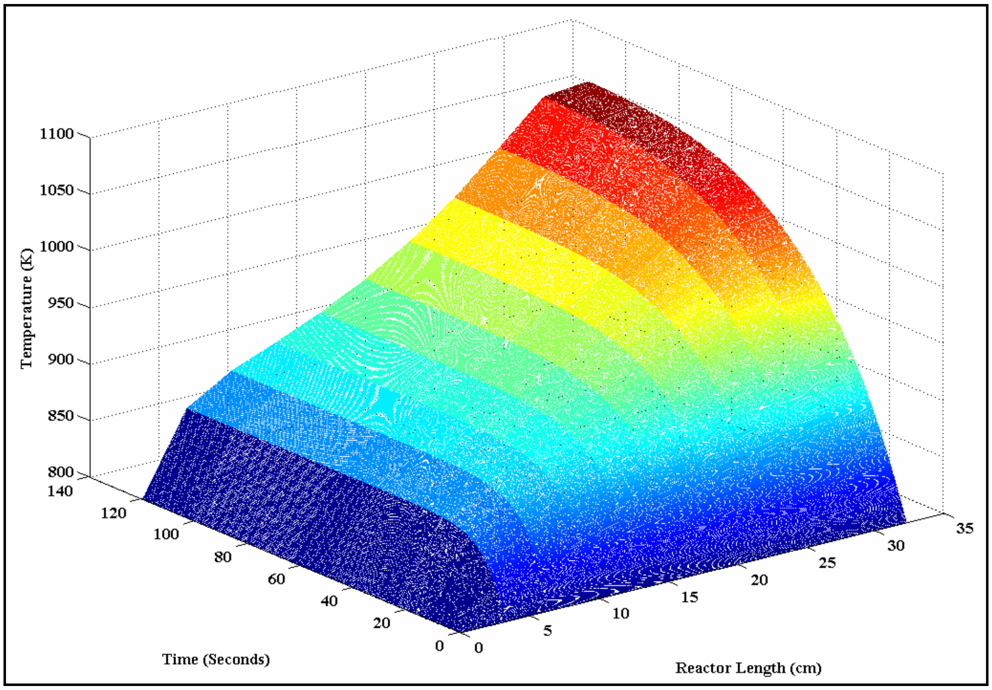

Figure 4.15. Reactor temperature as a function of time and reactor length ($CH_4/O_2 = 1.89$, $H_2O/CH_4 = 1.56$)

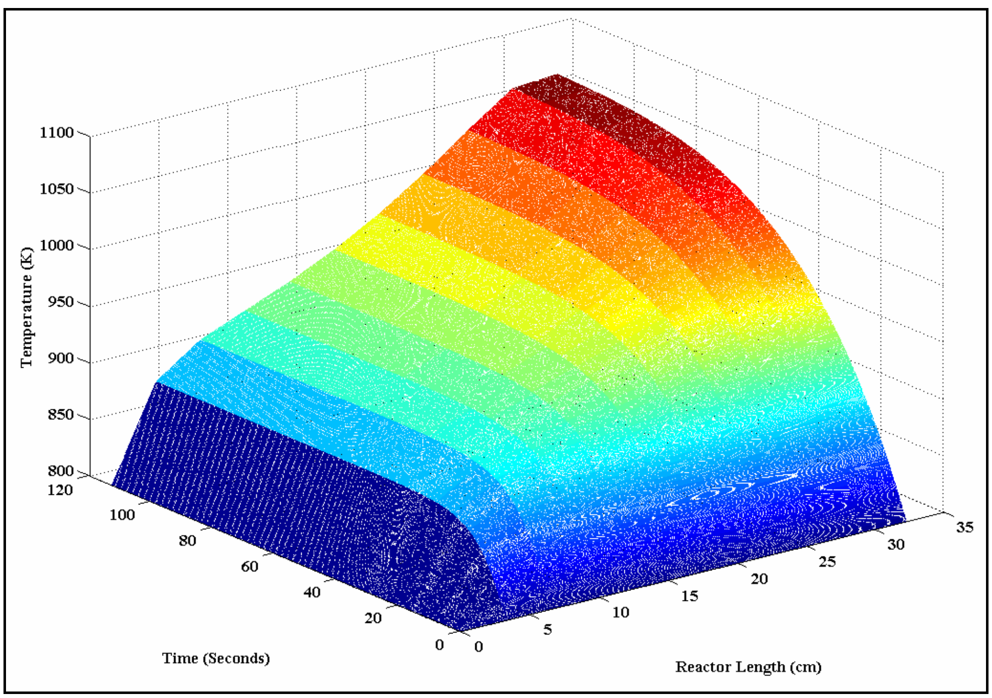

Figure 4.16. Reactor temperature as a function of time and reactor length ($CH_4/O_2 = 1.89$, $H_2O/CH_4 = 2.34$)

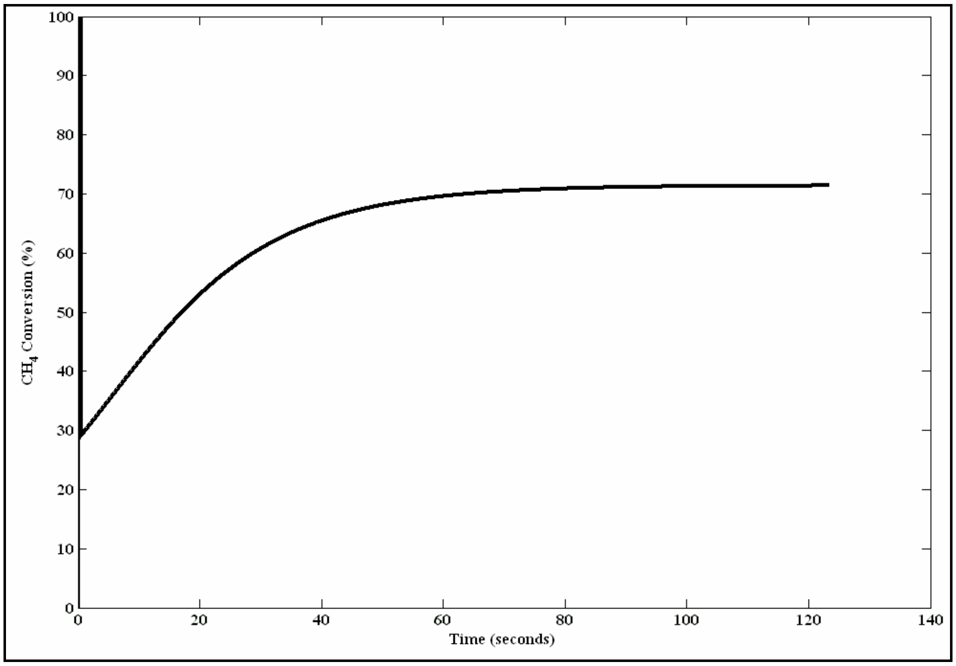

Figure 4.17. Temporal variation of methane conversion

(CH_4/O_2 = 2.24, H_2O/CH_4 = 1.17)

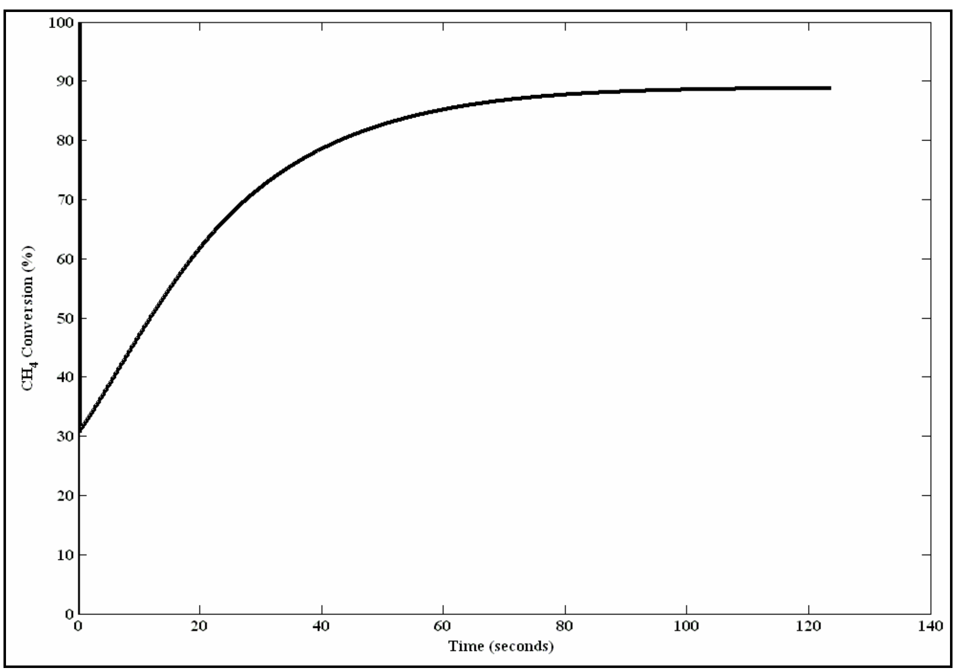

Figure 4.18. Temporal variation of methane conversion

(CH_4/O_2 = 1.89, H_2O/CH_4 = 1.17)

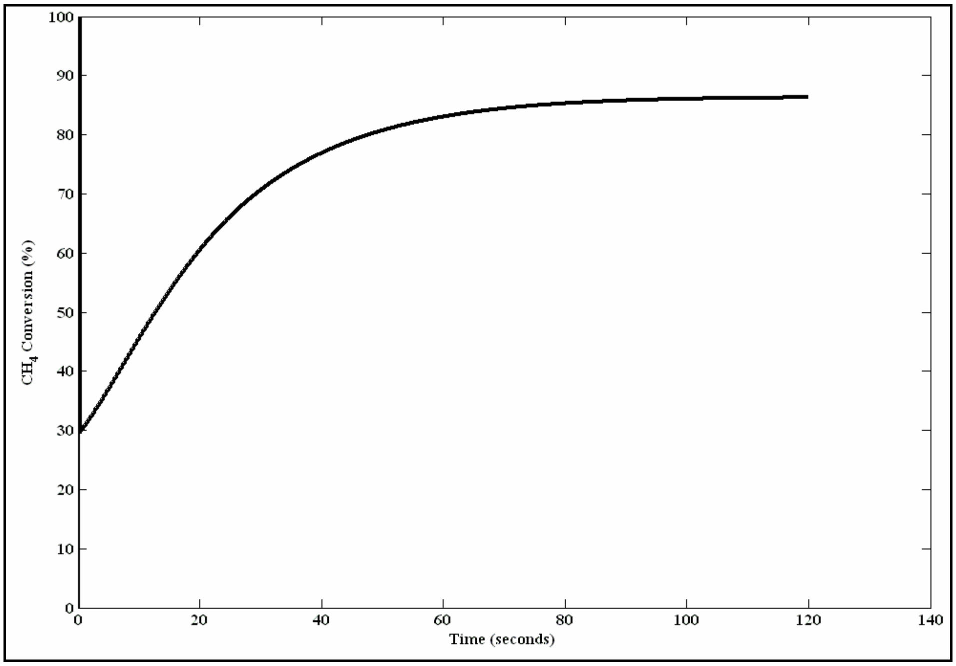

Figure 4.19. Temporal variation of methane conversion
(CH_4/O_2 = 1.89, H_2O/CH_4 = 1.56)

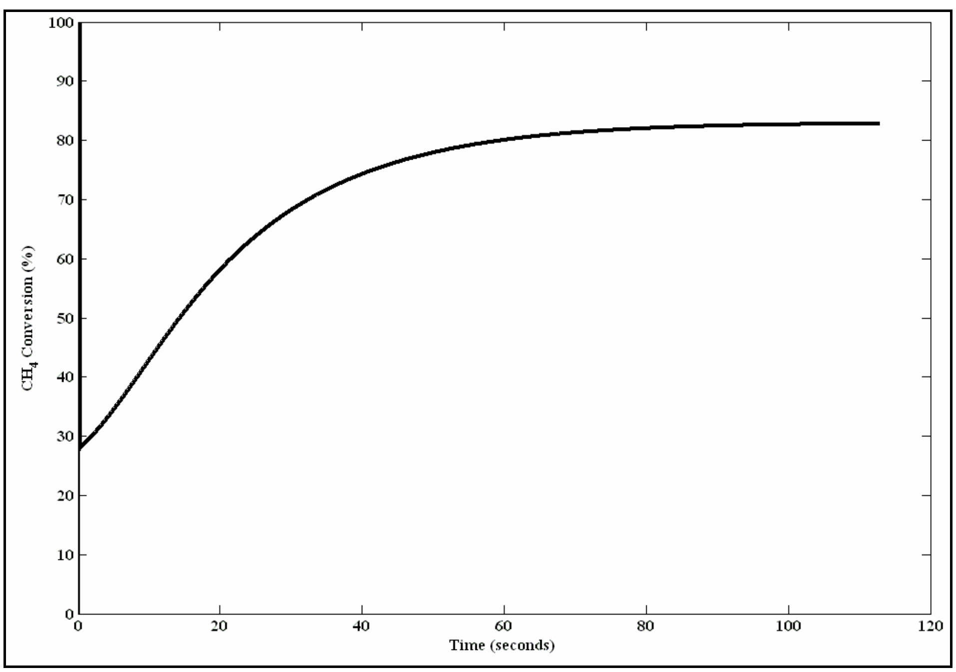

Figure 4.20. Temporal variation of methane conversion
(CH_4/O_2 = 1.89, H_2O/CH_4 = 2.34)

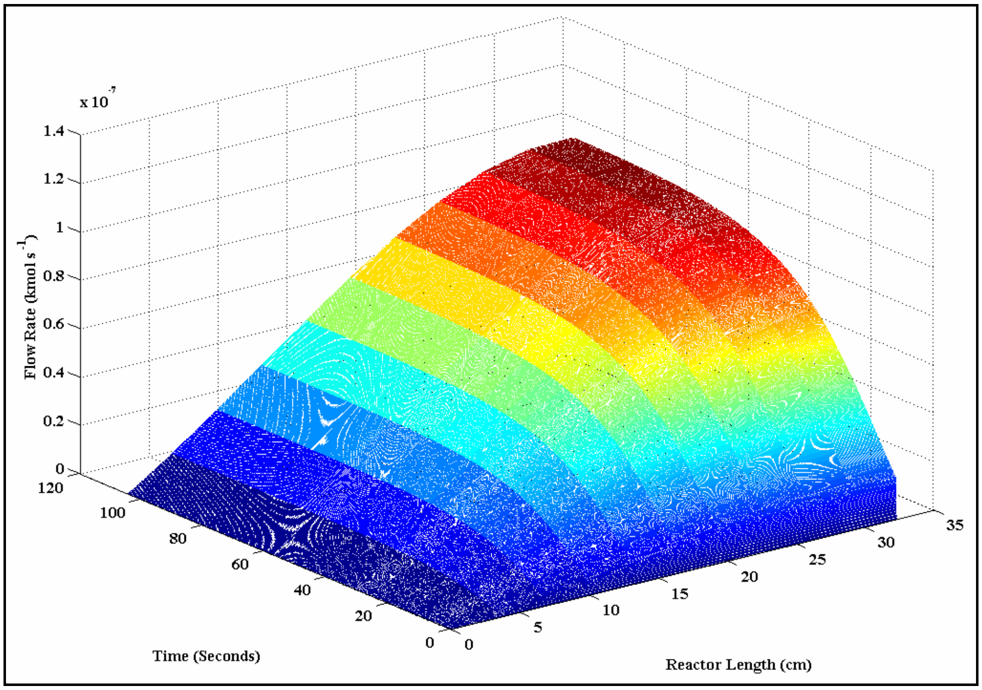

Figure 4.21. Hydrogen flow rate as a function of time and reactor length ($CH_4/O_2 = 2.24$, $H_2O/CH_4 = 1.17$)

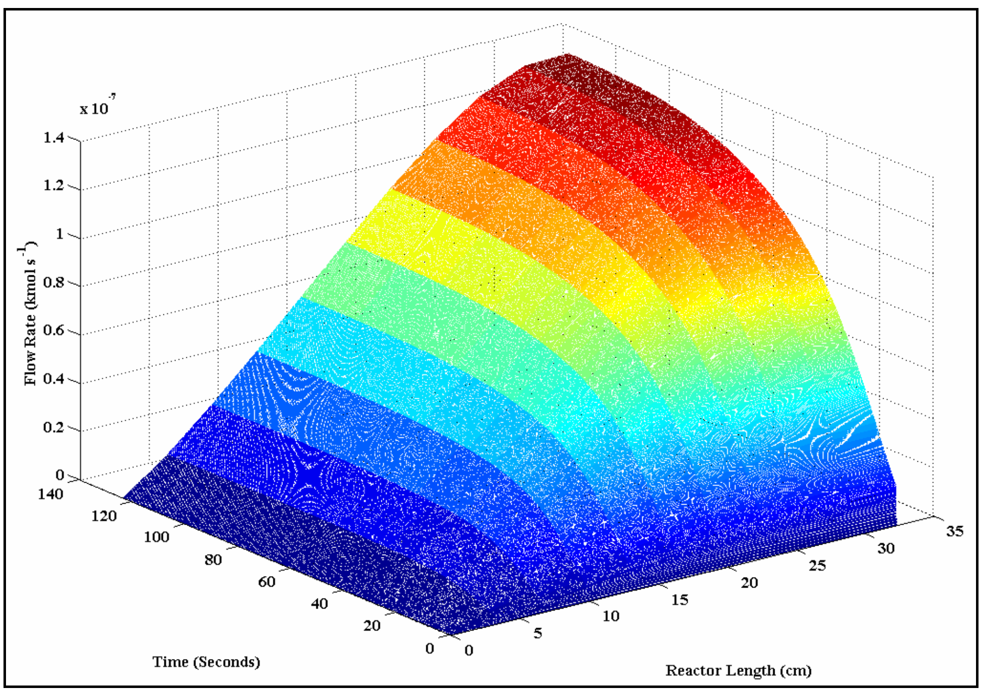

Figure 4.22. Hydrogen flow rate as a function of time and reactor length ($CH_4/O_2 = 1.89$, $H_2O/CH_4 = 1.17$)

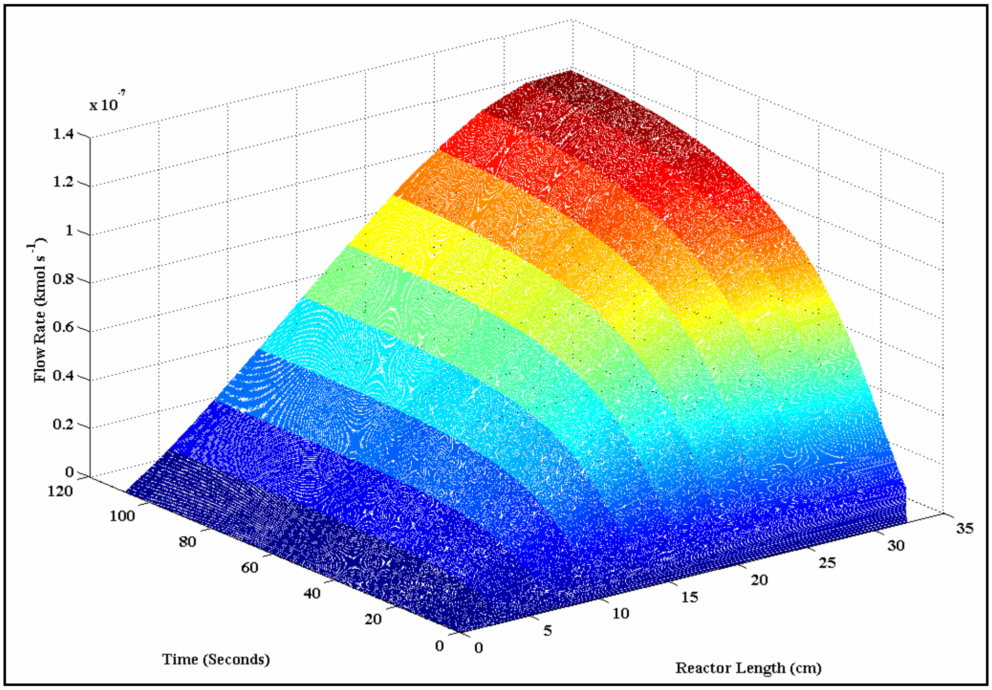

Figure 4.23. Hydrogen flow rate as a function of time and reactor length ($CH_4/O_2 = 1.89$, $H_2O/CH_4 = 1.56$)

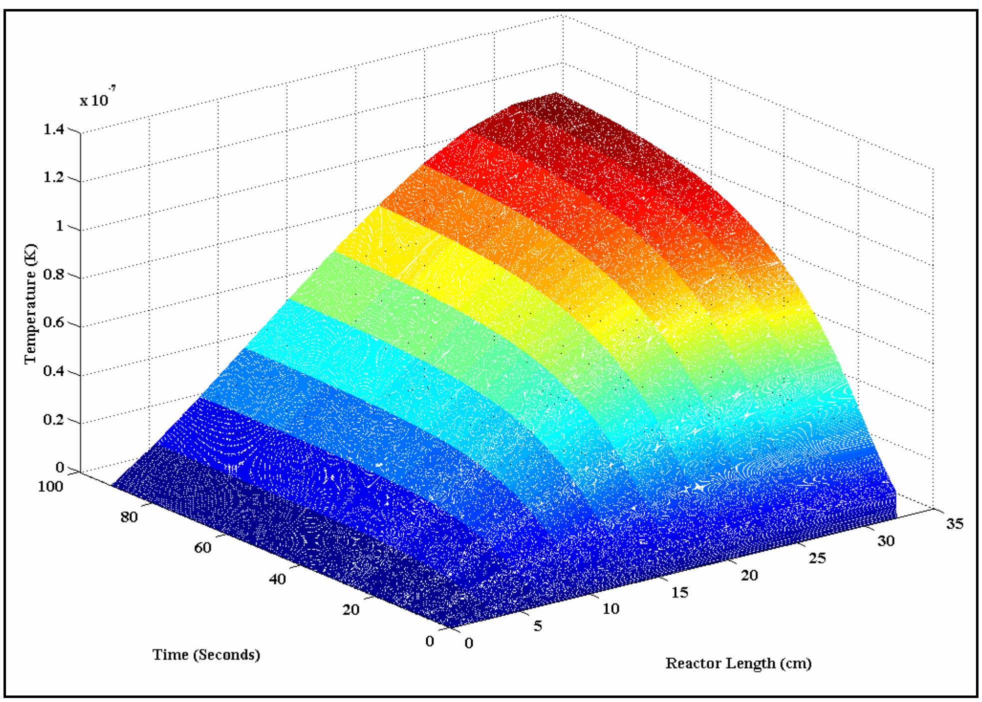

Figure 4.24. Hydrogen flow rate as a function of time and reactor length ($CH_4/O_2 = 1.89$, $H_2O/CH_4 = 2.34$)

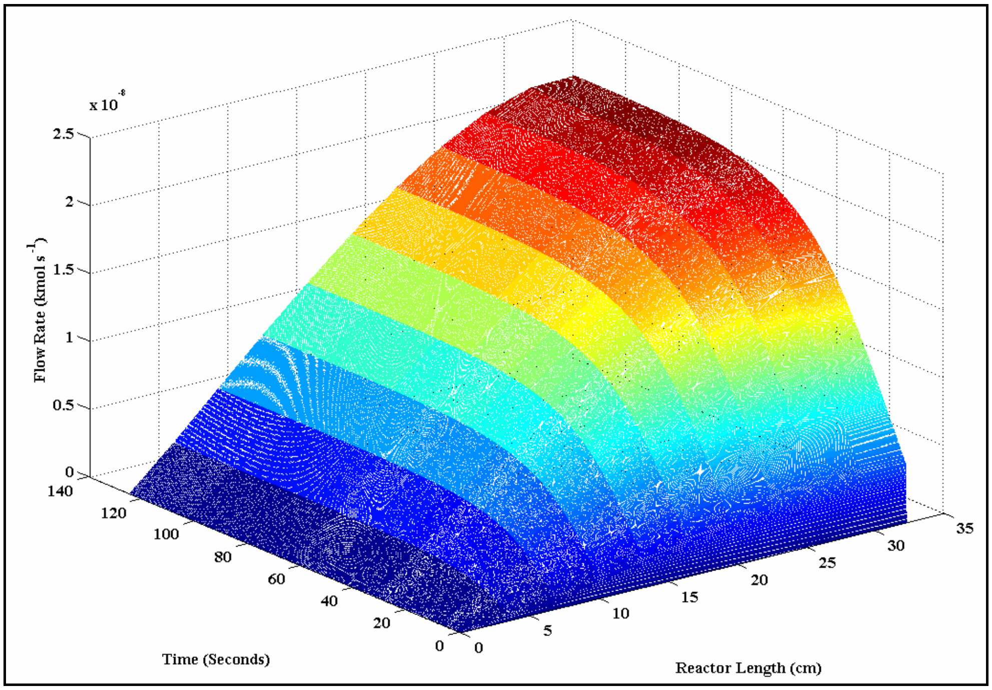

Figure 4.25. Carbon monoxide flow rate as a function of time and reactor length (CH_4/O_2 = 2.24, H_2O/CH_4 = 1.17)

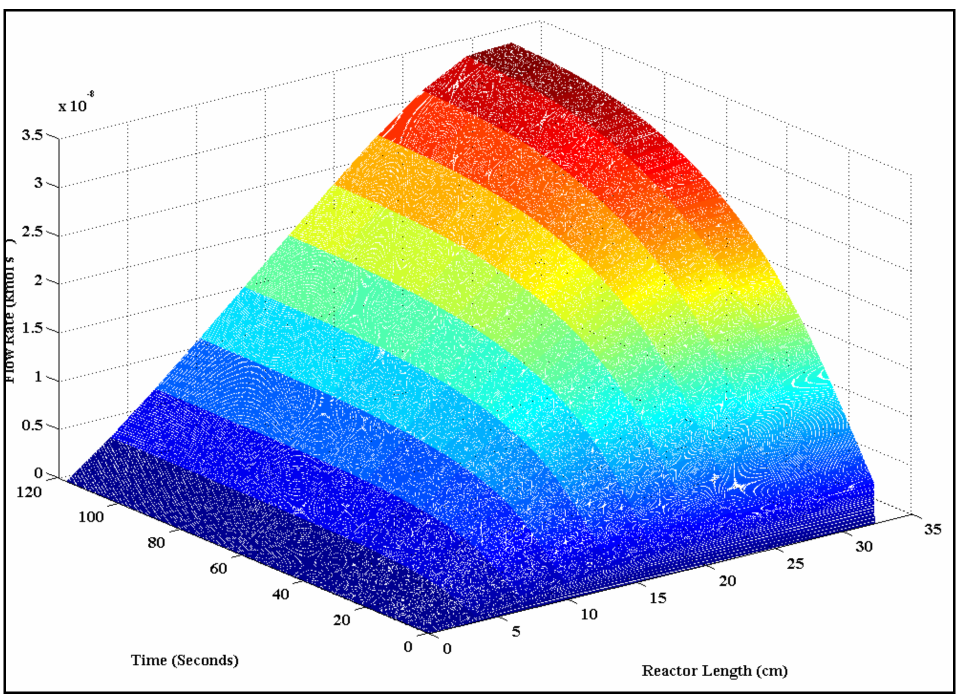

Figure 4.26. Carbon monoxide flow rate as a function of time and reactor length (CH_4/O_2 = 1.89, H_2O/CH_4 = 1.17)

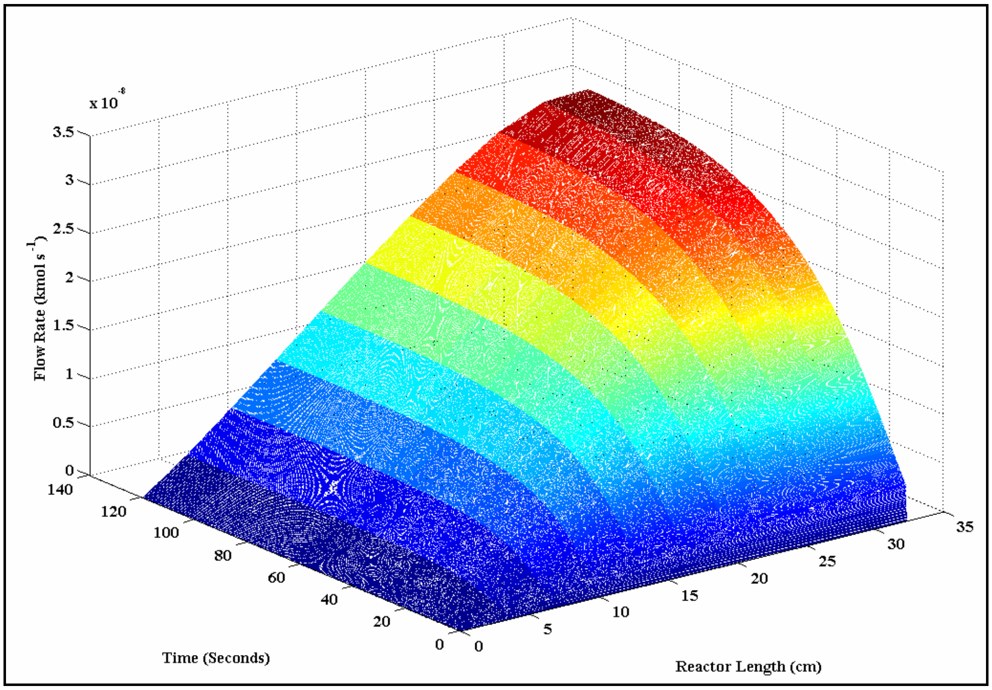

Figure 4.27. Carbon monoxide flow rate as a function of time and reactor length (CH_4/O_2 = 1.89, H_2O/CH_4 = 1.56)

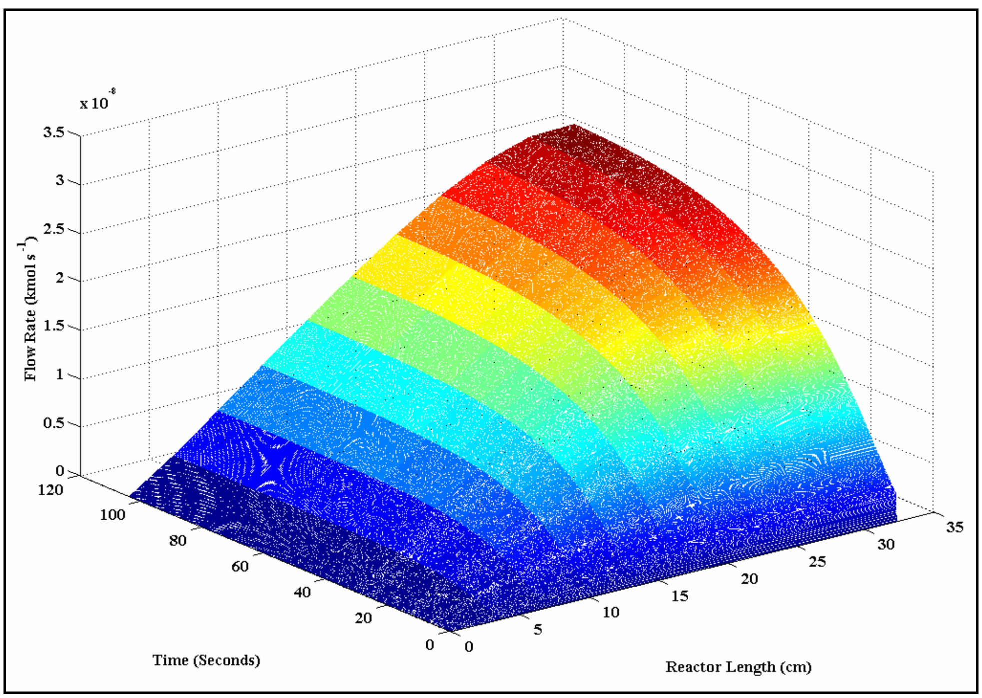

Figure 4.28. Carbon monoxide flow rate as a function of time and reactor length (CH_4/O_2 = 1.89, H_2O/CH_4 = 2.34)

Conversion of a reactant is defined here as the ratio of the amount that has reacted to the amount that had been fed. In Figures 4.17–4.20, immediately after start–up, methane conversion reaches 100 per cent and suddenly decreases to 30 per cent. This behavior can be attributed to the absence of methane downstream in the first few milliseconds of transient operation. Only after enough methane migrates downstream in the reactor can the oxidation and reforming reactions initiate, and this is when kinetics come into play. Hence, consumption of methane dictated by reaction kinetics increases with time until steady state is reached.

Temporal and spatial variation of hydrogen and carbon monoxide flow rates are shown in Figures 4.21–4.28 and the product yields in Table 4.4. The product variation is in accordance with temperature variation, that is, the flow rates increase both in space and time. The hydrogen–to–carbon monoxide ratio in each run varies from 4:1 to 4.5:1 along the reactor during transient operation and at steady state.

4.1.1.3. Response to a Disturbance in the Feed. Two cases are investigated in order to gain insight into the dynamic behavior of the reaction system upon imposition of a change in the feed conditions or a disturbance. The first involves a decrease in the carbon–to–oxygen ratio, and the second an increase in the ratio of steam to carbon. The volumetric flow rate is accordingly adjusted in order to keep the amount of methane fed constant. The steady–state (or initial) values at $t = 0$ are directly taken from the simulation results for the start–up analysis. The inlet temperatures are not altered. For each case the feed conditions before and after the disturbances are imposed are shown in Table 4.5.

Table 4.5. Feed conditions before and after a disturbance

Case	Before				After			
	CH_4/O_2	H_2O/CH_4	GHSV (h^{-1})	T^{in} (K)	CH_4/O_2	H_2O/CH_4	GHSV (h^{-1})	T^{in} (K)
1	2.24	1.17	37,600	800	1.89	1.17	41,100	800
2	1.89	1.17	41,100	800	1.89	1.56	44,500	800

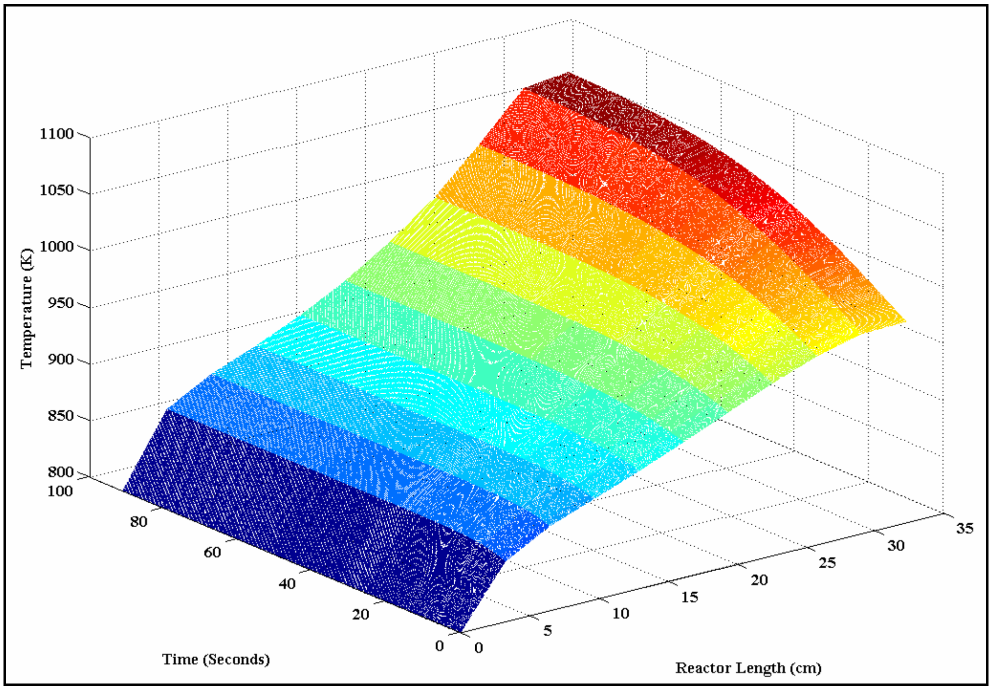

Figure 4.29. Variation of temperature upon the decrease in CH_4/O_2

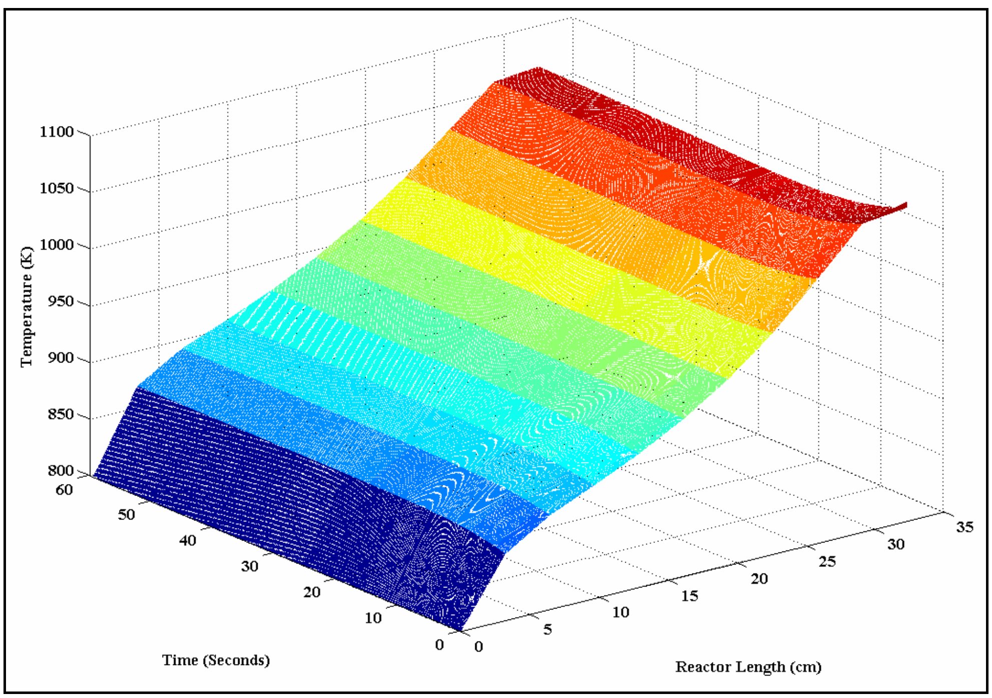

Figure 4.30. Variation of temperature upon the increase in H_2O/CH_4

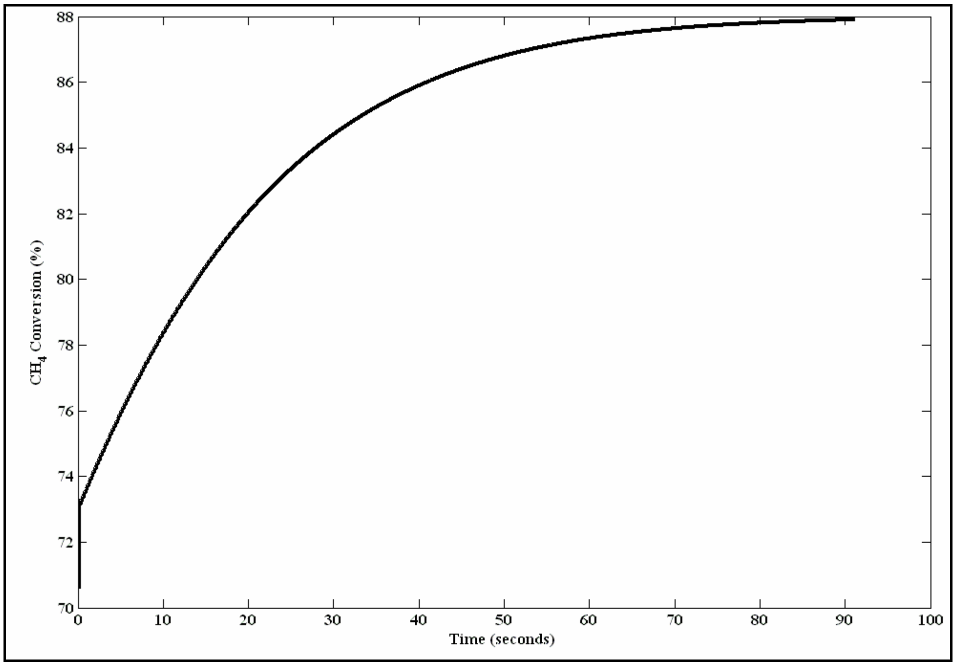

Figure 4.31. Temporal variation of methane conversion upon the decrease in CH_4/O_2

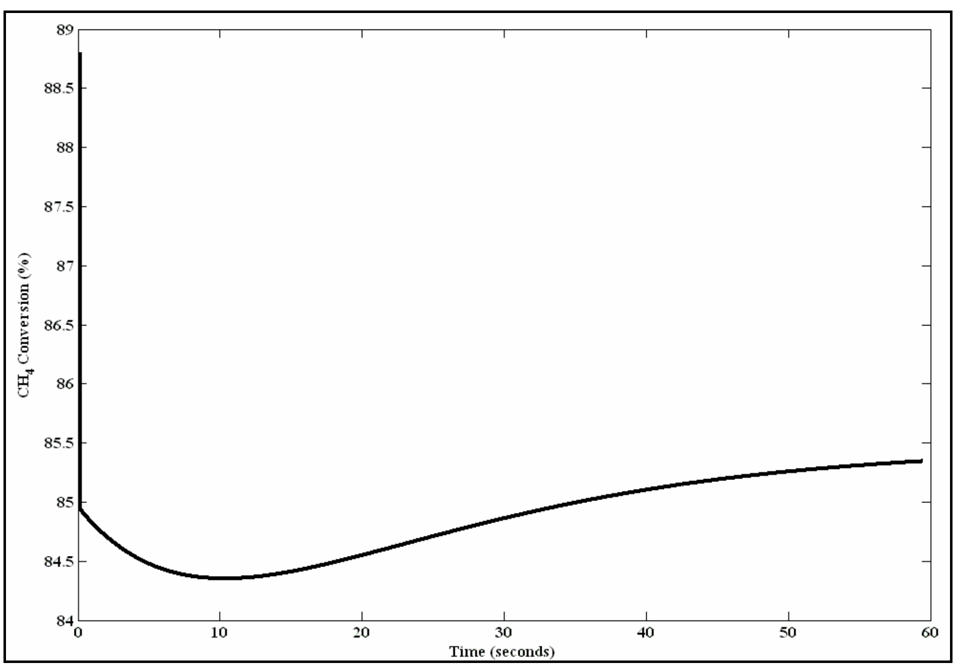

Figure 4.32. Temporal variation of methane conversion upon the increase in H_2O/CH_4

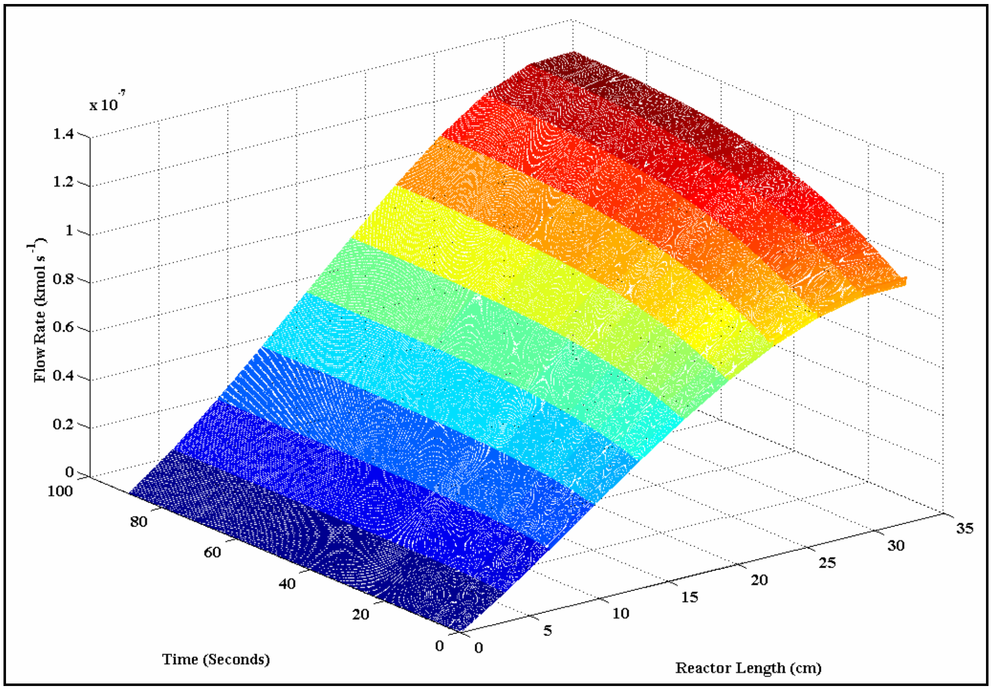

Figure 4.33. Variation of hydrogen flow rate upon the decrease in CH_4/O_2

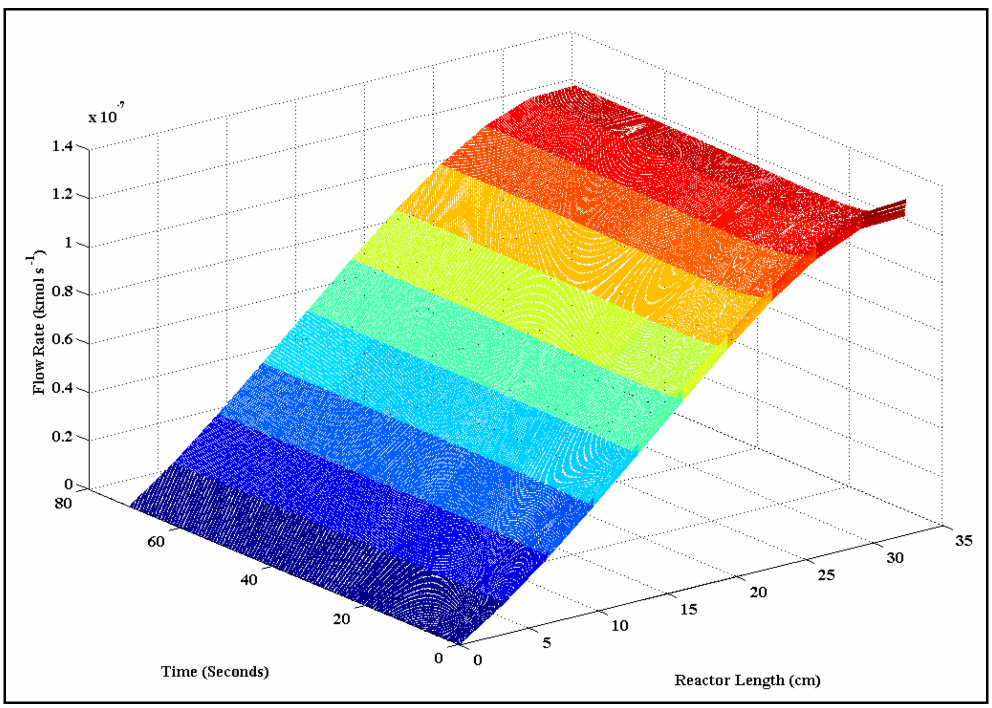

Figure 4.34. Variation of hydrogen flow rate upon the increase in H_2O/CH_4

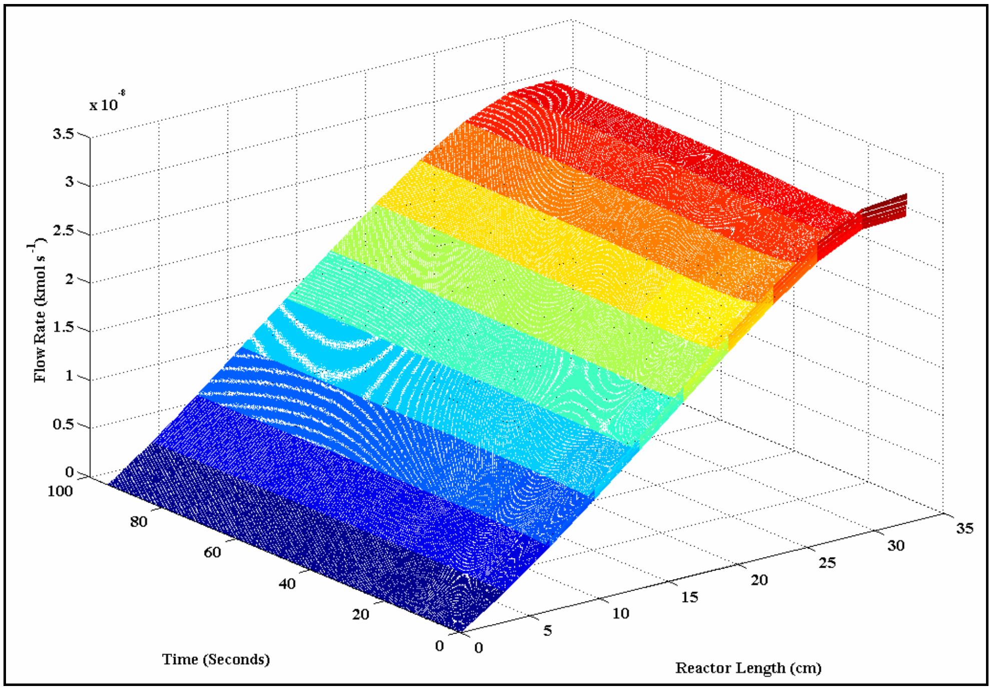

Figure 4.35. Variation of carbon monoxide flow rate upon the decrease in CH_4/O_2

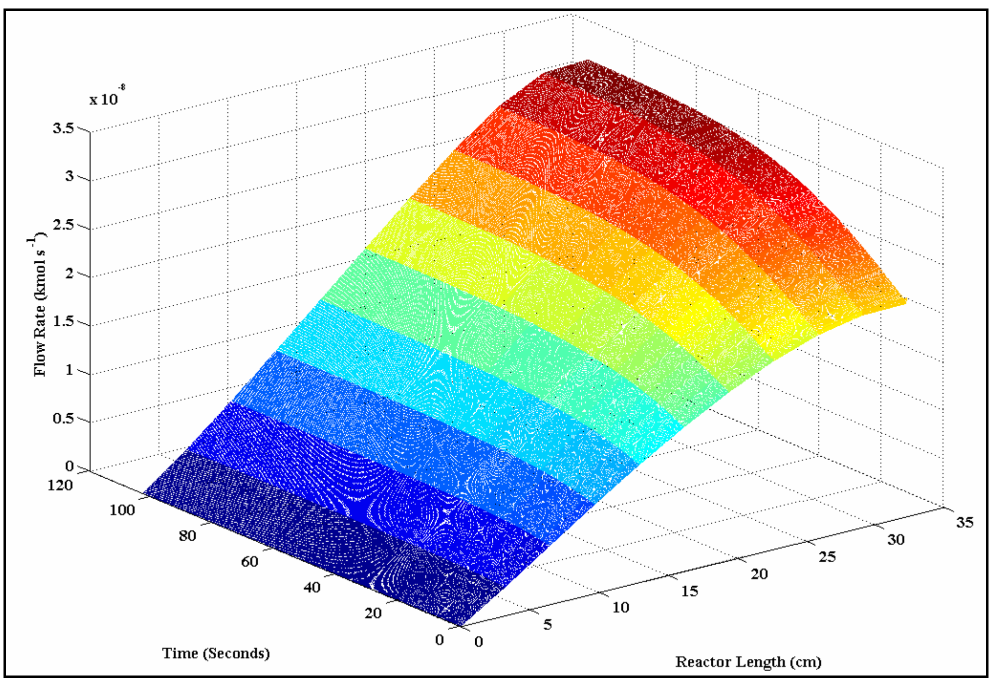

Figure 4.36. Variation of carbon monoxide flow rate upon the increase in H_2O/CH_4

Table 4.6. Steady–state methane conversion, product yields and exit temperatures

Case	Before Disturbance				After Disturbance			
	$x_{CH_4}^{SS}$ †	$y_{H_2}^{SS}$ ‡	y_{CO}^{SS} ‡	T_{exit}^{SS} (K)	$x_{CH_4}^{SS}$ †	$y_{H_2}^{SS}$ ‡	y_{CO}^{SS} ‡	T_{exit}^{SS} (K)
1	71.37	219.66	48.86	978.53	87.90	291.70	70.95	1073.07
2	88.80	297.86	73.04	1081.87	85.34	272.37	64.53	1065.02

† Methane conversion: Moles of methane reacted/100 moles of methane fed
‡ Product yield: Moles of product obtained/100 moles of methane fed

A disturbance that involves a decrease in the carbon–to–oxygen ratio leads to an increased oxygen flow rate, hence more methane is combusted, which results eventually in elevation of the temperature. This is the case illustrated in Figure 4.29. Before the disturbance, the highest temperature attained by the steady autothermal reforming process is 978 K, which, upon the change in the feed condition increases to the steady–state value of 1073 K. Although the temperature limit of 1100 K is near, catalytic operation need not be halted. It takes about 90 seconds for the process to settle down to the new steady state. The temperature, hence the product flow rates increase monotonically between two steady states (Figures 4.31, 4.33 and 4.35). The conversion and yield figures are summarized in Table 4.6.

On the contrary, addition of steam, as verified by steady–state and start–up simulations, lowers the reactor temperature. The same behavior is expected when this addition is made by way of a disturbance that alters the feed condition of the reaction system that is initially at steady–state. Figure 4.30 shows that when the inlet steam–to–carbon ratio is increased, at the same time keeping the amount of methane fed constant, a temporal temperature decrease is observed for about 10 seconds until a minimum is encountered, in this case corresponding to 1059 K. After 10 seconds the temperature begins to rise and settles to the steady–state value of 1065 K in 50 seconds. Likewise, local minima in the temporal conversion profile and hydrogen and carbon monoxide variations are displayed (Figures 4.32, 4.34 and 4.36).

Steam reforming is accountable for the inverse response realized in Figure 4.34. The steam reforming process favors high temperatures, however, upon increasing the steam flow rate, the temperature, hence the reforming rate is lowered, and this situation corresponds to the minimum hydrogen flow rate. At this point, exothermic total oxidation starts to dominate as the heat sink, namely steam reforming is working at its minimum and the temperature begins to rise. Since there is no other exogenous disturbance involved, increase in temperature and product yields is observed until steady state is reached.

4.1.2. Reactor Sizing for Producing Hydrogen Required to Run a 1.5–kW PEMFC

In order for a PEM fuel cell to generate 1.5 kW of power, it has to be fed with 27 L H_2/min at STP (Özşentürk, 2004). At the reaction conditions adapted for this work (800 K and 1 atm), this amounts to 2.4×10^{-5} kmol H_2/s (0.864 kmol H_2/h). Sizing of an IPOX reactor is the major goal, so it is assumed that the product stream is stripped off the contaminants and fed directly to the fuel cell, and that hydrogen is not generated elsewhere, such as in a water–gas shift reactor. However, a stand–alone IPOX reactor is not sufficient for generating fuel–cell–grade hydrogen due to the impurity of the product.

The parameter that is varied is the catalyst weight (reactor length), and all others are held fixed. Hydrogen production is simulated using the four different feed conditions given previously. The results are presented in Table 4.7.

Even though the weight of catalyst or the size of the IPOX reactor required to produce the stated amount of hydrogen is more or less the same at all feed conditions, at higher power demands the sizing issue becomes critical. For instance, the first two rows of Table 4.7 show that the lower the carbon–to–oxygen ratio, the smaller is the reactor volume. However, the drawback of working with this configuration is that the catalyst is prone to sintering at elevated temperatures. On the other hand, increasing the steam flow rate at constant carbon–to–oxygen ratio is advantageous in lowering the temperature and eliminating considerable carbon monoxide, but in this case the product stream is diluted by unreacted steam. The very best solution, it must be concluded, depends on the degree of

Table 4.7. Weight of catalyst required to produce 1.5 kW–fuel–cell–grade hydrogen

	CH_4/O_2	H_2O/CH_4	GHSV (h^{-1})	T^{in} (K)	Catalyst Weight (g)	Reactor Length (cm)*
1	2.24	1.17	37,600	800	118	14.30
2	1.89	1.17	41,100	800	113	13.70
3	1.89	1.56	44,500	800	113	13.70
4	1.89	2.34	51,300	800	113	13.70

* The diameter is 3 cm in each case

integration of the processing units and on the principles regarding the operation of this integrated assembly. Optimal sizing can be achieved only when the assembly is analyzed as a whole.

5. CONCLUSIONS AND RECOMMENDATIONS

5.1. Conclusions

The objective of this study was to develop a simple but representative mathematical model for simulating the steady and dynamic behavior of an indirect partial oxidation reactor for producing hydrogen by autothermal methane reforming. The major conclusions drawn indicate that the objective was satisfied. These conclusions are as follows:

- Autothermal conversion of methane to hydrogen over a physical mixture of $Pt/\delta{-}Al_2O_3$ and $Ni/MgO{-}Al_2O_3$ catalysts was described using a simple pseudohomogeneous reactor model.

- Reaction kinetics of autothermal reforming were expressed by Langmuir–Hinshelwood–Hougen–Watson–type rate laws.

- The steady–state model comprising a set of ordinary differential equations was solved for 4 different feed conditions. Two different rate laws for predicting the rate of steam reforming were incorporated into the model. Increasing the air flow rate was seen to elevate the temperature and lead to higher product yields. Temperature was seen to drop upon an increase in the inlet steam flow rate. Hotspot formation and rigorous conditions were not observed.

- Start–up of autothermal reforming and its response to a disturbance in the feed conditions were analyzed by a series of dynamic simulations. The hyperbolic system of partial differential equations was solved using the Lax–Friedrichs finite difference scheme.

- The duration of transient operation in the case of start–up simulations varied between 100 and 120 seconds. Despite the discrepancies between the results of steady–state and dynamic simulations, the evolution of transients in the spatial direction was consistent with their steady counterparts. The differences were attributed to the low–resolution numerical scheme.

- When the steady process was disturbed by an increase in the inlet oxygen flow rate, it responded by elevating the temperature. In the case simulated, this temperature rise was almost 100 K, which nearly passed beyond the limit of 1100 K. The new steady state upon disturbance was attained in about 90 seconds.

- A temporal temperature decrease was observed when the disturbance involved an increase in the steam flow rate. For the case studied, in 10 seconds a local minimum was encountered, but due to the domination of total oxidation at the minimum temperature begins to rise and settles down in 50 seconds.

- Size of an indirect partial oxidation reactor for producing 1.5 kW–fuel–cell–grade hydrogen was investigated. Steady–state simulations were performed at different feed conditions and with different catalyst weights. A tube approximately 14 cm long with 3 cm diameter and filled with 113 g of catalyst was seen to achieve the conversion. However, stand–alone sizing of the indirect partial oxidation reactor was argued not to be useful.

5.2. Recommendations

The following improvements can be made in order to enhance the ability of the mathematical models to predict accurately the outcome of real–time practical autothermal reforming:

- The total oxidation and steam reforming reaction rates on a bimetallic Pt–NiO/Al_2O_3 catalyst can be expressed by an experimental or theoretical rate law, because the bimetallic catalyst was seen to experimentally exhibit the best performance among other configurations.

- The hierarchy of the model describing the autothermal reforming process has to be increased. Since interfacial and intraparticle diffusional limitations are effective during steam reforming, their omission reduces the accuracy of the model greatly.

- The numerical method has to be replaced by a higher–order one. In addition, it has to be adaptive both in space and time.

- The fuel cell/fuel processor assembly with integrated peripherals has to be modeled and analyzed as a whole in order to assure safe and accurate operation.

APPENDIX A: PHYSICAL PROPERTIES OF THE SPECIES

Table A.1. Constants of the heat capacity equation and standard molar enthalpy of species (Sinnot, 1993)

Species, j	α_j	β_j ($\times 10^2$)	γ_j ($\times 10^5$)	δ_j ($\times 10^9$)	ΔH_{fj}^{0} (kJ gmol^{-1})
CH_4	19.251	5.2126	1.1974	–11.32	–74.86
H_2O	32.243	0.19238	1.0555	–3.596	–242
CO	30.869	–1.285	2.7892	–12.72	–110.62
CO_2	19.795	7.3436	–5.602	17.153	–393.77
H_2	27.143	0.92738	–1.381	7.6451	0
O_2	28.106	–0.00037	1.7459	–10.65	0
N_2	31.15	–1.357	2.6796	–11.68	0

$$c_{pj} = \alpha_j + \beta_j T + \gamma_j T^2 + \delta_j T^3 \quad [\text{J gmol}^{-1}\ \text{K}^{-1}] \tag{A.1}$$

REFERENCES

Aasberg–Petersen K., J. H. Bak Hansen, T. S. Christensen, I. Dybkjaer, P. Seier Christensen, C. Stub Nielsen, S. E. L. Winter Madsen and J. R. Rostrup–Nielsen, 2001, "Technologies for Large–Scale Gas Conversion", *Applied Catalysis A: General*, Vol. 221, pp. 379–387.

Ahmed S. and M. Krumpelt, 2001, "Hydrogen from Hydrocarbon Fuels for Fuel Cells", *International Journal of Hydrogen Energy*, Vol. 26, pp. 291–301.

Amadeo, N. E. and M. A. Laborde, 1995, "Hydrogen Production from the Low–Temperature Water–Gas Shift Reaction: Kinetics and Simulation of the Industrial Reactor", *International Journal of Hydrogen Energy*, Vol. 20, pp. 949–956.

Armor, J. N., 1999, "The Multiple Roles for Catalysis in the Production of H_2", *Applied Catalysis A: General*, Vol. 176, pp. 159–176.

Aryafar, M and F. Zaera, 1997, "Kinetic Study of the Catalytic Oxidation of Alkanes over Nickel, Palladium and Platinum Foils", *Catalysis Letters*, Vol. 48, pp. 173–183.

Avcı A. K., D. L. Trimm and Z. İ. Önsan, 2000, "Simulation of Alternative Catalyst Bed Configurations in Autothermal Hydrogen Production", *Studies in Surface Science and Catalysis*, Vol. 130, pp. 2753–2758.

Avcı, A. K., Z. İ. Önsan and D. L. Trimm, 2001a, "On–board Fuel Conversion for Hydrogen Fuel Cells: Comparison of Different Fuels by Computer Simulations", *Applied Catalysis A: General*, Vol. 216, pp. 243–256.

Avcı, A. K., D. L. Trimm and Z. İ. Önsan, 2001b, "Heterogeneous Reactor Modeling for Simulation of Catalytic Oxidation and Steam Reforming of Methane", *Chemical Engineering Science*, Vol. 56, pp. 641–649.

Avcı, A. K., D. L. Trimm and Z. İ. Önsan, 2002, "Quantitative Investigation of Catalytic Natural Gas Conversion for Hydrogen Fuel Cell Applications", *Chemical Engineering Journal*, Vol. 90, pp. 77−87.

Avcı, A. K., D. L. Trimm and Z. İ. Önsan, 2003, "On−board Hydrogen Generation for Fuel Cell Powered Vehicles: The Use of Methanol and Propane", *Topics in Catalysis*, Vol. 22, pp. 359−367.

Avcı, A. K., 2003, *Computational and Experimental Investigation of Catalytic Hydrocarbon Fuel Processing for Autothermal Hydrogen Production*, Ph.D. Dissertation, Boğaziçi University.

Basile A., S. Fasson, G. Vitulli and E. Drioli, 1998, *Natural Gas Conversion* V, Vol. 119, Elsevier, Amsterdam.

Bharadwaj, S. S. and L. D. Schmidt, 1995, "Catalytic Partial Oxidation of Natural Gas to Syngas", *Fuel Processing Technology*, Vol. 42, pp. 109−127.

Borowiecki, T., A. Golebiowski and B. Stasinska, 1997, "Effects of Small MoO_3 Additions on the Properties of Nickel Catalysts for the Steam Reforming of Hydrocarbons", *Applied Catalysis A: General*, Vol. 153, pp. 141−156.

Boucouvalas, Y., Z. L. Zhang and X. E. Verykios, 1996, "Partial Oxidation of Methane to Synthesis Gas via the Direct Reaction Scheme over Ru/TiO_2 Catalyst", *Catalysis Letters*, Vol. 40, pp. 189−195.

Bradford, M. C. J. and M. A. Vannice, 1996, "Catalytic Reforming of Methane with Carbon Dioxide over Nickel Catalysts II. Reaction Kinetics", *Applied Catalysis A: General*, Vol. 142, pp. 97−122.

Brown, L. F., 2001, “A Comparative Study of Fuels for On–board Hydrogen Production for Fuel–Cell–Powered Automobiles”, *International Journal of Hydrogen Energy*, Vol. 26, pp. 381–397.

Bui, P. A., D. G. Vlachos and P. R. Westmoreland, 1997, “Catalytic Ignition of Methane/Oxygen Mixtures over Platinum Surfaces: Comparison of Detailed Simulations and Experiments”, *Surface Science*, Vol. 385, pp. 1029–1034.

Burch, R., D. J. Crittle and M. J. Hayes, 1999, “C–H Bond Activation in Hydrocarbon Oxidation on Heterogeneous Catalysts”, *Catalysis Today*, Vol. 47, pp. 229–234.

Ciaparu, D and L. Pfefferle, 2001, “Methane Combustion Activity of Supported Palladium Catalysts After Partial Reduction”, *Applied Catalysis A: General*, Vol. 218, pp. 197–209.

Dalla Betta, R. A. and T. Rostrup–Nielsen, 1999, “Application of Catalytic Combustion to a 1.5 MW Industrial Gas Turbine”, *Catalysis Today*, Vol. 47, pp. 369-375.

De Groote, A. M. and G. F. Froment, 1996, “Simulation of the Catalytic Partial Oxidation of Methane to Synthesis Gas”, *Applied Catalysis A: General*, Vol. 138, pp. 245–264.

De Smet, C. R. H., M. H. J. M. de Croon, R. J. Berger, G. B. Marin and J. C. Schouten, 2001, “Design of Adiabatic Fixed–Bed Reactors for the Partial Oxidation of Methane to Synthesis Gas. Application to Production of Methanol and Hydrogen–for–fuel–cells”, *Chemical Engineering Science*, Vol. 56, pp. 4849–4861.

Dhathathreyan, K. S., P. Sridhar, G. Sasikumar, K. K. Ghosh, G. Velayutham, N. Rajalakshmi, C. K. Subramaniam, M. Raja and K. Ramya, 1999, “Development of Polymer Electrolyte Membrane Fuel Cell Stack”, *International Journal of Hydrogen Energy*, Vol. 24, pp. 1107–1115.

Dicks, A. L., 1996, “Hydrogen Generation from Natural Gas for the Fuel Cell Systems of Tomorrow”, *Journal of Power Sources*, Vol. 61, pp. 113–124.

Elnashaie, S. S. E. H, A. M. Adris, A. S. Al−Ubaid and M. A. Soliman, 1990, "On the Non−Monotonic Behaviour of Methane Steam Reforming Kinetics", *Chemical Engineering Science*, Vol. 45, pp. 491−501.

Elnashaie, S. S. E. H, 1996, "Dynamic Modelling, Bifurcation and Chaotic Behaviour of Gas−Solid Catalytic Reactors", in *Topics in Chemical Engineering*, Vol 9., Gordon and Breach Science Publishers, Amsterdam.

Finnerty, C, G. A. Tompsett, K. Kendall and R. M. Ormerod, 2000, "SOFC System with Integrated Catalytic Fuel Processing", *Journal of Power Sources*, Vol. 86, pp. 459−463.

Fogler, H. S., 1999, *Elements of Chemical Reaction Engineering*, Prentice Hall, New Jersey.

Frauhammer, J., G. Eigenberger, L. v. Hippel and D. Arntz, 1999, "A New Reactor Concept for Endothermic High−Temperature Reactions", *Chemical Engineering Science*, Vol. 54, pp. 3661−3670.

Freni S., G. Calogero and S. Cavallaro, 2000, "Hydrogen Production from Methane through Catalytic Partial Oxidation Reactions", *Journal of Power Sources*, Vol. 87, pp. 28−38.

Froment, G. F. and K. B. Bischoff, 1990, *Chemical Reactor Analysis and Design*, Wiley, New York.

Gallucci F., L. Paturzo and A. Basile, 2004, "A Simulation Study of the Steam Reforming of Methane in a Dense Tubular Membrane Reactor", *International Journal of Hydrogen Energy*, Vol. 29, pp. 611–617.

Gamburzev, S., C. Boyer and A. J. Appleby, 1999, "Low Platinum Loading, Lightweight PEM Fuel Cells", *Fuel Cells Bulletin*, Vol. 2, pp. 6–8.

Garcia, E. and M. Laborde, 1991, “Hydrogen Production by the Steam Reforming of Ethanol: Thermodynamic Analysis”, *International Journal of Hydrogen Energy*, Vol. 16, pp. 307–312.

Gasteiger, H. A., J. E. Panels and S. G. Yan, 2004, “Dependence of PEM Fuel Cell Performance on Catalyst Loading”, *Journal of Power Sources*, Vol. 127, pp. 162–171.

Grevskott, S., T. Rusten, M. Hillestad, E. Edwin and O. Olsvik, 2001, “Modeling and Simulation of a Steam Reforming Tube with Furnace”, *Chemical Engineering Science*, Vol. 56, pp. 597–603.

Hickman D. A. and L. D. Schmidt, 1992, “Synthesis Gas Formation by Direct Oxidation of Methane over Pt Monoliths”, *Journal of Catalysis*, Vol. 138, pp. 267–282.

Hickman D. A. and L. D. Schmidt, 1993, “Production of Syngas by Direct Catalytic Oxidation of Methane”, *Science*, Vol. 259, pp. 343–346.

Hoang, D. L and S. H. Chan, 2004, “Modeling of a Catalytic Autothermal Methane Reformer for Fuel Cell Applications”, *Applied Catalysis A: General*, Vol. 268, pp. 207–216.

Horiuchi, T., K. Sakuma, T. Fukui, Y. Kubo, T. Osaki and T. Mori, 1996, “Supression of Carbon Deposition in the CO_2–reforming of CH_4 by Adding Basic Metal Oxides to a Ni/AL_2O_3 Catalyst”, *Applied Catalysis A: General*, Vol. 144, pp. 111–120.

İnce, T., G. Uysal, A. N. Akın and R. Yıldırım, 2005, “Selective Low–Temperature CO Oxidation over $Pt–Co–Ce/Al_2O_3$ in Hydrogen–Rich Streams”, Applied Catalysis A: General, Vol. 292, pp. 171–176.

Ioannides, T., 2001, “Thermodynamic Analysis of Ethanol Processors for Fuel Cell Applications”, *Journal of Power Sources*, Vol. 92, pp. 17–25.

Jamal Y. And M. L. Wyszynski, 1994, "On−board Hydrogen Generation of Hydrogen−Rich Gaseous Fuels – A Review", *International Journal of Hydrogen Energy*, Vol. 19, pp. 557−572.

Jiang, C. 1992, *Studies of the Production of Hydrogen from Methanol Steam Reforming at Low Temperatures*, Ph.D. Dissertation, University of New South Wales.

Jiang, C., D. L. Trimm and M. S. Wainwright, 1995, "New Technology for Hydrogen Production by the Catalytic Oxidation and Steam Reforming of Methanol at Low Temperatures", *Chemical Engineering Technology*, Vol. 18, pp. 1−6.

Jin, R., Y. Chen, W. Li, W. Cui, Y. Ji, C. Yu and Y. Jiang, 2000, "Mechanism for Catalytic Partial Oxidation of Methane to Syngas over a Ni/Al_2O_3 Catalyst", *Applied Catalysis A: General*, Vol. 201, pp. 71−80.

Joensen F. and J. R. Rostrup−Nielsen, 2002, "Conversion of Hydrocarbons and Alcohols for Fuel Cells", *Journal of Power Sources*, Vol. 105, pp. 195−201.

Kolios, G., J. Frauhammer and G. Eigenberger, 2000, "Autothermal Fixed−Bed Reactor Concepts", *Chemical Engineering Science*, Vol. 55, pp. 5945−5967.

Kolios, G., J. Frauhammer and G. Eigenberger, 2001, "A Simplified Procedure for the Optimal Design of Autothermal Reactors for Endothermic High−Temperature Reactions", *Chemical Engineering Science*, Vol. 56, pp. 351−357.

Kolios, G, J. Frauhammer and G. Eigenberger, 2002, "Efficient Reactor Concepts for Coupling of Endothermic and Exothermic Reactions", *Chemical Engineering Science*, Vol. 57, pp. 1505−1510.

Kolios, G., A. Gritsch, B. Glöckler and G. Sorescu, 2004, "Novel Reactor Concepts for Thermally Efficient Methane Steam Reforming: Modeling and Simulation", *Industrial and Engineering Chemistry and Research*, Vol. 43, pp. 4796−4808.

Kusakabe K., S. Fumio, T. Eda, M. Oda and K. Sotowa, 2005, "Hydrogen Production in Zirconia Membrane Reactors for Use in PEM fuel cells", *International Journal of Hydrogen Energy*, Vol. 30., pp. 989–994.

Kvamsdal, H. M., H. F. Svendsen, T. Hertzberg and O. Olsvik, 1999, "Dynamic Simulation and Optimization of a Catalytic Steam Reformer", *Chemical Engineering Sc*ience, Vol. 54, 2697–2706.

Lee, J. H., D. L. Trimm and N. W. Cant, 1999, "The Catalytic Combustion of Methane and Hydrogen Sulphide", *Catalysis Today*, Vol. 47, pp. 353–357.

Lee, D. K., I. H. Baek and W. L. Yoon, 2004, "Modeling and Simulation for the Methane Steam Reforming Enhanced by in situ CO_2 Removal Utilizing the CaO Carbonation for H_2 Production", *Chemical Engineering Science*, Vol. 59, pp. 931–942.

LeVeque, R. J., 2002, *Finite Volume Methods for Hyperbolic Problems*, Cambridge University Press, Cambridge.

Ma, L, 1995, *Hydrogen Production from Steam Reforming of Light Hydrocarbons in an Autothermic System*, Ph.D. Dissertation, University of New South Wales.

Ma, L. and D. L. Trimm, 1996, "Alternative Catalyst Bed Configurations for the Autothermic Conversion of Methane to Hydrogen", *Applied Catalysis A: General*, Vol. 138, pp. 265–273.

Ma, L., D. L. Trimm and C. Jiang, 1996, "The Design and Testing of an Autothermal Reactor for the Conversion of the Light Hydrocarbons to Hydrogen I. The Kinetics of the Catalytic Oxidation of Light Hydrocarbons", *Applied Catalysis A: General*, Vol 138, pp. 275–283.

Mariño, F, M. Boveri, G. Baronetti and M. Laborde, 2001, "Hydrogen Production from Steam Reforming of Bioethanol using Cu/Ni/K/γ-Al_2O_3 Catalysts. Effect of Ni", *International Journal of Hydrogen Energy*, Vol. 26, pp. 665–668.

Numaguchi, T. and K. Kikuchi, 1988, “Intrinsic Kinetics and Design Simulation in a Complex Reaction Network: Steam−Methane Reforming”, *Chemical Engineering Science,* Vol. 43, 2295−2301.

Opoku−Gyamfi, K. and A. A. Adesina, 1999, “Kinetic Studies of CH_4 Oxidation over Pt−NiO/δ−Al_2O_3 in a Fluidised Bed Reactor”, *Applied Catalysis A: General*, Vol. 180, pp. 113−122.

Özkara, S. and A. E. Aksoylu, 2003, “Selective Low Temperature Carbon Monoxide Oxidation in H_2-rich Gas Streams over Activated Carbon Supported Catalysts”, *Applied Catalysis A: General*, Vol. 251, pp. 75−83.

Özşentürk, S., 2004, Private communication.

Pena, M. A., J. P. Gomez and J. L. G. Fierro, 1996, “New Catalytic Routes for Syngas and Hydrogen Production”, *Applied Catalysis A: General*, Vol. 144, pp. 7−57.

Perry, R. H. and D. W. Green, 1997, *Perry’s Chemical Engineers’ Handbook*, 7th ed., McGraw−Hill, USA.

Quinta Ferreira, R. M., M. M. Marques, M. F. Babo and A. E. Rodrigues, 1992, “Modelling of the Methane Steam Reforming Reactor with Large−Pore Catalysts”, *Chemical Engineering Science*, Vol. 47, pp. 2909−2914.

Ralph, T. R., 1999, “Clean Fuel Cell Energy for Today”, *Platinum Metals Review*, Vol. 43, pp. 14–17.

Ralph, T. R. and G. A. Hards, 1998, “Powering the Cars and Homes of Tomorrow”, *Chemistry & Industry*, Vol. 9, pp. 337–342.

Rostrup–Nielsen, J. R., 1984, "Catalytic Steam Reforming", in J. R. Anderson and M. Boudart (Eds.), *Catalysis, Science & Technology*, Vol 5., pp. 1–117, Springer–Verlag, Berlin.

Rostrup–Nielsen, J. R. and L. Alstrup, 1999, "Innovation and Science in the Process Industry. Steam Reforming and Hydrogenolysis", *Catalysis Today*, Vol. 53, pp. 311–316.

Rostrup–Nielsen, J. R. and J. H. Bak Hansen, 1993, "CO_2–reforming of Methane over Transition Metals", *Journal of Catalysis*, Vol. 144, pp. 38–49.

Sasikumar, G., J. W. Ihm and H. Ryu, 2004, "Optimum Nafion Content in PEM Fuel Cell Electrodes", *Electrochimica Acta*, Vol. 50, pp. 601–605.

Seo, Y. S., S. K. Kang, M. H. Han, Y. S. Baek, 1999, "Development of a Catalytic Burner with Pd/NiO Catalysts", *Catalysis Today*, Vol. 47, pp. 421–427.

Sinnot, R. K., 1993, *Coulson's & Richardson's Chemical Engineering*, *Design*, Vol. 6., 2nd ed., Butterworth–Heinemann, London.

Springmann, S, M. Bohnet, M. Sommer, M. Himmen and G. Eigenberger, 2003, "Steady–State and Dynamic Simulation of an Autothermal Gasoline Reformer", *Chemical Engineering Technology*, Vol. 26, pp. 790–796.

Springmann, S., M. Bohnet, A. Docter, A. Lamm and G. Eigenberger, 2004, "Cold Start Simulations of a Gasoline Based Fuel Processor for Mobile Fuel Cell Applications", *Journal of Power Sources*, Vol. 128, pp. 13–24.

Starz, K. A., E. Auer, T. Lehmann and R. Zuber, 1999, "Characteristics of Platinum–Based Electrocatalysts for Mobile PEMFC Applications", *Journal of Power Sources*, Vol. 84, pp. 167–172.

Stevens, D. A., S. Zhang, Z. Chen and J. R. Dahn, 2003, "On the Determination of Platinum Particle Size in Carbon–Supported Platinum Electrocatalysts for Fuel Cell Applications", *Carbon*, Vol. 41, pp. 2769–2777.

Strikwerda, J. C., 1989, *Finite Difference Schemes and Partial Differential Equations*, Wadsworth & Brooks/Cole, California.

Takano, A., T. Tagawa and S. Goto, 1994, "Carbon Dioxide Reforming of Methane on Supported Nickel Catalysts", *Journal of Chemical Engineering of Japan*, Vol. 27, pp. 727−731.

Thomas C. E., B. D. James, F. D. Lomax Jr and I. F. Kuhn Jr., 2000, "Fuel Options for the Fuel Cell Vehicle: Hydrogen, Methanol or Gasoline?", *International Journal of Hydrogen Energy*, Vol. 25, pp. 551−567.

Trimm, D. L. and C. W. Lam, 1980, "The Combustion of Methane on Platinum−Alumina Fibre Catalysts", *Chemical Engineering Science*, Vol. 35, pp. 1405−1413.

Trimm, D. L., 1983, "Catalytic Combustion", *Applied Catalysis*, Vol. 7, pp. 249−282.

Trimm, D. L., 1999, "Catalysts for the Control of Coking During Steam Reforming", *Catalysis Today*, Vol. 49, pp. 3−10.

Trimm, D. L. and Z. İ. Önsan, 2001, "Onboard Fuel Conversion for Hydrogen−Fuel−Cell−Driven Vehicles", *Catalysis Reviews: Science and Engineering*, Vol. 43, pp 31−84.

Urban, P. M., A. Funke, J .T. Müller, M. Himmen and A. Docter, 2001, "Catalytic Processes in Solid Polymer Electrolyte Fuel Cell Systems", *Applied Catalysis A: General*, Vol. 221, pp. 459–470.

Utaka, T. K., K. Sekizawa and K. Eguchi, 2000, “CO Removal by Oxygen−Assisted Water Gas Shift Reaction over Supported Cu Catalysts”, *Applied Catalysis A: General*, Vol. 194−195, pp. 21−26.

Veser, G. and L. D. Schmidt, 1996, “Ignition and Extinction in the Catalytic Oxidation of Hydrocarbons over Platinum”, *AIChE Journal*, Vol. 42, pp. 1077−1087.

Veser, G, M. Ziauddin and L. D. Schmidt, 1999, “Ignition in Alkane Oxidation on Noble−Metal Catalysts”, *Catalysis Today*, Vol. 47, pp. 219−228.

Vielstich, W. and T. Iwasita, 1997, in G. Ertl, H. Knozinger, J. Weitkamp (Eds.), Handbook of Heterogeneous Catalysis, Wiley–VCH, New York.

Xiu, G, P. Li and A. E. Rodrigues, 2003, “Adsorption−Enhanced Steam−Methane Reforming with Intraparticle−Diffusion Limitations”, *Chemical Engineering Journal*, Vol. 95, pp. 83−93.

Veser, G. and J. Frauhammer, 2000, “Modeling Steady State Ignition During Catalytic Methane Oxidation in a Monolith Reactor”, *Chemical Engineering Science*, Vol. 55, 2271−2286.

Veser, G., J. Frauhammer and U. Friedle, 2000, “Syngas Formation by Direct Oxidation of Methane: Reaction Mechanisms and New Reactor Concepts”, Catalysis Today, Vol. 61, 55−64.

Xu, J. and G. F. Froment, 1989a, “Methane Steam Reforming, Methanation and Water−Gas Shift: I. Intrinsic Kinetics”, *AIChE Journal*, Vol. 35, pp. 88−96.

Xu, J. and G. F. Froment, 1989b, “Methane Steam Reforming: II. Diffusional Limitations and Reactor Simulation”, *AIChE Journal*, Vol. 35, pp. 97−103.

Witt, P. M. and L. D. Schmidt, 1996, "Effect of Flow Rate on the Partial Oxidation of Methane and Ethane", *Journal of Catalysis*, Vol. 163, pp. 465−475.

Yamazaki, O., K. Tomishige and K. Fujimoto, 1996, "Development of Highly Stable Nickel Catalyst for Methane−Steam Reaction under Low Steam to Carbon Ratio", *Applied Catalysis A: General*, Vol. 136, pp. 49−56.

Yu, W., T. Ohmori, T. Yamamoto, A. Endo, M. Nakaiwa, T. Hayakawa and N. Itoh, 2005, "Simulation of a Porous Ceramic Membrane Reactor for Hydrogen Production", *International Journal of Hydrogen Energy*, Vol. 30, pp. 1071–1079.